論文 / 著書情報
Article / Book Information

題目(和文)	流動床炉型一般廃棄物焼却飛灰の不均一性および粒子特性の解明
Title(English)	Geochemical Heterogeneity and Characterization of Fly Ash Generated from A Fluidized Bed Incineration of Municipal Solid Wastes
著者(和文)	DAHLAN ASTRYD VIANDILA
Author(English)	Astryd Viandila Dahlan
出典(和文)	学位:博士(工学), 学位授与機関:東京工業大学, 報告番号:甲第11631号, 授与年月日:2020年9月25日, 学位の種別:課程博士, 審査員:高橋 史武,中﨑 清彦,竹下 健二,江頭 竜一,時松 宏治
Citation(English)	Degree:Doctor (Engineering), Conferring organization: Tokyo Institute of Technology, Report number:甲第11631号, Conferred date:2020/9/25, Degree Type:Course doctor, Examiner:,,,,
学位種別(和文)	博士論文
Type(English)	Doctoral Thesis

Geochemical Heterogeneity and Characterization of Fly Ash Generated from A Fluidized Bed Incineration of Municipal Solid Wastes

Doctoral Dissertation

Astryd Viandila Dahlan

Supervisor: Associate Professor Fumitake Takahashi

Global Engineering course for Development, Environment and Society

Department of Transdisciplinary Science and Engineering

Tokyo Institute of Technology

September 2020

流動床炉型一般廃棄物焼却飛灰の不均一性および粒子特性の解明

博士論文

Astryd Viandila Dahlan

指導教員:高橋　史武　准教授

地球環境共創コース

環境・社会理工学院 融合理工学系

東京工業大学

令和２年度

Acknowledgment

In the name of Allah, the Most Gracious and the Most Merciful.

All praises to Allah on whom ultimately, I depend on the strengths and His guidance in completing this doctoral thesis. This doctoral thesis is a requirement for graduation from the Global Engineering course for Development, Environment and Society, Department of Transdisciplinary Science and Engineering, Tokyo Institute of Technology.

I would like to express my sincere appreciation goes to my supervisor, Associate Professor Fumitake Takahashi, whose guidance and constant support. His invaluable help, guidance, and constructive comment throughout my research during my master's and doctoral program. I was able to have many experiences throughout attendance domestic and international conferences and have the opportunity to visit incinerator plant.

I have not forgotten my appreciation to Associate Professor Koji Tokimatsu for constructive comments and meaningful discussion for my research during seminar. I am thankful for your kind consideration. Assoc. Prof. H. B Gonzalez for her support and valuable discussion for my better manuscript writing. My acknowledgment also to Mrs. Eriko Ohno and Mrs. A Takahashi, for their co-operation and great support.

Sincere thanks to all my peers and lab mates for their kindness and support during my study. Especially for Indonesia lab mates and my Indonesian friends whom I get all my mental support during my study in Japan. Thanks for the friendship and memories so I could enjoy my life in Japan.

I also gratefully acknowledge the funding received towards my study from the Japanese Government (Monbukagakusho: MEXT) from my master and doctoral program at the Tokyo Institute of Technology.

Finally, my deepest gratitude goes to my beloved parents and my sister for their endless love, prayers, and encouragement to complete my study in Japan.

July 2020

Astryd Viandila Dahlan

Table of Content

List of Figures

List of Tables

Chapter 1

Introduction

Abstract: This chapter presents the background and objective of this study. Overview of municipal solid waste management in Japan is firstly explained. The treatment of municipal solid waste that has been majorly adopting in Japan is the incinerator. The incinerator and type of incinerator are presented. Municipal solid waste incineration residue is mentioned, and one of MSWI residue is fly ash is explained. Moreover, fly ash characterization and fly ash treatments are presented. Finally, the objectives and the originality of this research are stated.

1.1 Overview of waste management in Japan

Before having a stable system of waste management as a present, Japan also experienced similar waste problems as developing countries today. Waste was often piled up on roadsides or vacant lots in unsanitary conditions. Moreover, rapid economic growth causing a rapid increase in the amount and diversity of municipal solid waste. In order to specify and standards for the management of all waste, including industrial waste, and to develop a basic system for waste management, the Japanese government enacted the Waste Management Act. It established the responsibility of municipalities to manage municipal waste, while the responsibility of waste-generating business operators to manage industrial waste [1].

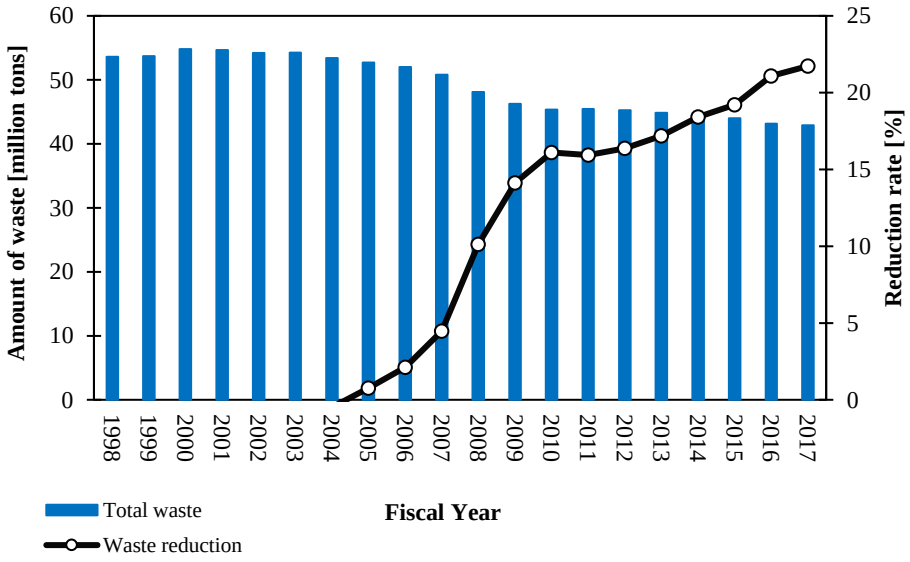

Figure 1.1 Amount of waste generated from FY 1998 to 2017

However, some issues needed to be resolved. It including the continuing increase in waste generation and the resulting shortage of landfills. Therefore, the Japanese government established the Basic Act for Establishing a Sound Material-Cycle Society (Basic Recycling Act) in 2000 to ensure the implementation of the 3R (Reduce, Reuse, Recycle) and proper waste management. This law presents basic principles for the establishment of a sound material-cycle society: generation reduction, reuse, recycling, thermal recovery, and proper disposal. The impact of the Japanese government's effort to reduce the growing amount of waste through incineration and recycling waste was clearly shown in

Figure 1.1. The amount of municipal solid waste (MSW) generated from 1998 to 2017 is shown in the above graph [2, 3].

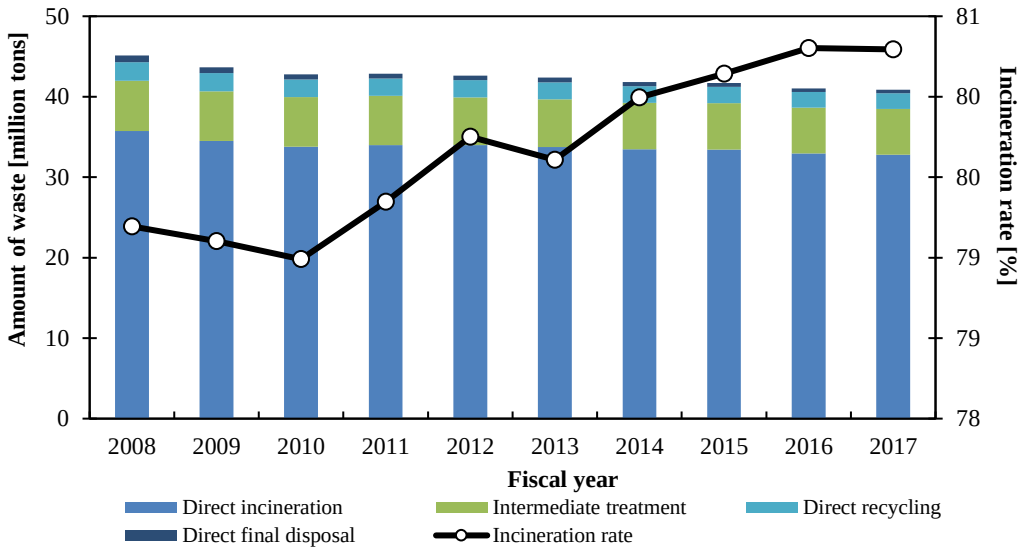

Figure 1.2 Amount of waste treated from FY 2008 to 2017

Even though the government has attempted to minimize the amount of waste generation, there is still a significant amount of waste necessary to treat given the activities of modern society. There are four methods of treatment MSW in Japan: direct recycling refers to waste that is received directly by reclaiming operators and not through recycling facilities; direct incineration; intermediate treatment refers to the treatment of waste other than incineration such as recycling facility, compost facility, refused-derived fuel plant, and other facilities; and direct final disposal. In 2017, 80.3% of MSW treatment by using direct incineration was shown in **Figure 1.2** [3]. Incineration has been the primary treatment method of MSW due to its merit to reduce 90% of the volume and 70% of the weight and concern to construct new landfills owing to public acceptance [4].

1.2 Municipal solid waste incineration (MSWI)

Reducing the amount of waste was the strong point of incineration used to treat MSW. Besides that, there are several main objectives of incinerator: to reduce the total organic content, to destroy organic contaminants, to concentrate inorganic contaminants, to recover the energy content of the waste,

and to preserve raw materials and resources [5–7]. However, incineration does have its issues due to their by-products may give harmful impact to the environment; emission emits from incinerator containing highly toxic dioxins and furans, some materials still have more value for recycling; and high capital cost and trained operators created high operating cost [8].

Incinerator technologies have several types, such as grate or stoker combustor, fluidized bed combustor, and rotary kiln combustor. Stoker combustor is using a movable and mechanical grate to proceed with the waste through the furnace and to let burn completely [9]. The fluidized bed is using the bed of sand or other sand-like materials in upward flowing airstream. Moreover, the fluidized bed has high turbulence to enhance combustion, provide uniform mixing between waste and bed materials, and develop better heat transfer efficiency [10]. About 74% of incinerators in Japan is the stoker type, and 17% is the fluidized bed type [11].

1.2.1 Stoker combustor

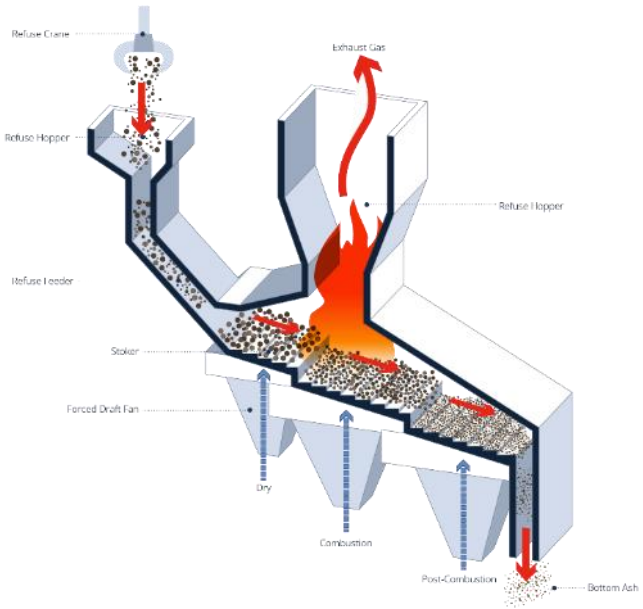

Figure 1.3 Stoker combustor diagram

Stoker combustor or mostly named as grate combustor is shown in **Figure 1.3**. The temperature was controlled at 1000ºC during the combustion process. The grate forms the bottom of the furnace and

supports the burning bed of waste as it moves through the furnace. The grate will cause sifting of the lighter materials to downwards. The crucial factor in the combustion process is the mixing of the waste on the grate and controlling the distribution of air. It is also essential to surpass trace organic in emission. The design of mechanical grate has aimed to allow the waste to have better mixing through the furnace and provide complete combustion [9].

Moreover, the path of combustion gases after burning waste is critical in ensuring uniform and complete combustion. Additionally, 60 to 80% of the air must be added to the furnace to complete the combustion process. Proper design of the furnace and the air injection system ensures proper air mixing and leads to the control of organic contaminants in the flue gas and the APC residues [12].

1.2.2 Fluidized bed combustor

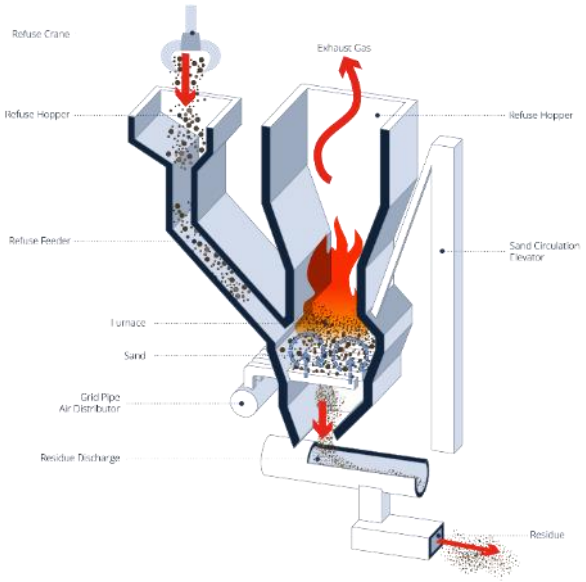

Figure 1.4 Fluidized bed combustor diagram

Fluidized bed combustor, as shown in **Figure 1.4,** has a lower temperature than stoker combustor around 750 – 900ºC. A fluidized bed combustor is containing a bed of granular material such as silica sand, limestone, alumina, or ceramic materials. The bed material is supported by a refractory lined grid with hollow to allow air to be injected. The air passing through the grid expands the bed,

causing it to become fluidized. The constant moving of the fluidized bed increases the contact between waste, the combustion air, and the hot sand bed, thus facilitating complete combustion and relatively high heat transfer rates [13].

Furthermore, the movement in the bed and its inherent thermal storage capacity increases the burnout of material and minimizes bottom ash generation. The movement and generation of fine particles in the bed lead to substantial quantities of fine ash being carried out of the bed by the air movement in the furnace. Thus, these systems generally require additional particulate removal devices in the gas stream ahead of boilers and air pollution control systems [12].

1.3 Municipal solid waste residue

Although there are several types of incinerators, all incinerators generate residues. Solids retained on furnace grates following combustion and solids passing through the grates are generally referred to as bottom ash. Entrained particulates that are trapped and residues generated by acid gas scrubbers and subsequently removed by fabric filters and/or electrostatic precipitators are generally referred to as fly ash. Stoker combustors produce both bottom ash and fly ash. On the other hand, fluidized bed combustors produce only fly ash, excluding metal aggregates collected from the bed. The type of incinerators and the operation condition – i.e., temperature, residence time, and disturbance time can be factors affecting the quality of ashes [14].

Approximately 80% of the residues generated from incinerators are bottom ash. Bottom ash is a heterogeneous mixture of slag, metals, ceramics, glass, other non-combustibles, and uncombusted organic. The fly ash is fine particulate mixtures of residues from air pollution control systems consisting of reaction products of primarily calcium chloride and unreacted lime used for acid gas emission controls [15]. Fly ash of MSWI contains leachable toxic metals and hazardous organic compounds, which cause a potential hazard to the environment [16]. Therefore, fly ash should be treated before its final disposal in a landfill or its utilization.

When considering ash treatment, it is essential to accomplish both decompositions of persistent organic pollutants such as dioxins and the removal of heavy metals. In Japan, there are several methods

used to treat fly ash before disposal, and these include melting, cement solidification, chemical immobilization, and acid extraction [17].

1.3.1 Melting

Melting of MSWI ash has three primary objectives: metal treatment, destruction of dioxins, and volume reduction. The melting point of bottom ash and fly ash is at about 1200 and 1400ºC, respectively. Metal separation can be achieved by evaporation in the melting furnace and physical separation after cooling [18]. Besides, MSWI ash is converted into molten materials, while hazardous material encapsulated into the slag matrix. Therefore, the molten slag expected can be used as environmentally friendly for the fabrication of precast concrete, roadbed construction, asphalt pavements, permeable bricks, interlocking blocks, and others [19].

1.3.2 Cement solidification

Solidification treatments are among the most widespread processes used for waste incineration residues. The primary purpose of solidification is to produce a material whose physical (specific surface area, porosity, and others), mechanical (durability, mechanical strength, and others) and chemical properties are more favorable concerning reducing the leachability of contaminants out of the waste matrix [20]. Mixing cement with fly ash can encapsulate heavy metals in the cement-based solidification product and immobilize heavy metals to leach out. This method decreases the treatment cost and minimizes the volume of products to landfill, providing the technical-economical possibility for industrial treatment of fly ash [21].

1.3.3 Acid extraction

Acid extraction treatment is a method by adding acidic agent and sodium sulfide into slurry fly ash in order to extract soluble heavy metal and immobilize the remaining heavy metals. Acid extraction has advantages, including can recover soluble salts in the fly ash outside the system; can easily control stabilization by changing pH setting; weight and volume of fly ash become comparably small, and the

initial and operation cost is comparatively low. In summary, acid extraction can recover and recycle salts and heavy metals to minimize the disposal volume in the future, in addition to stabilizing and controlling heavy metals in fly ash [22].

1.3.4 Chemical immobilization

Chemical immobilization is one method of reducing the leachability of heavy metals in the ash residues. The principal objective of immobilization is to form new, less soluble mineral phases that are more geochemically stable in leaching environments [23]. Chemical immobilization using a chelate reagent solution has been a significant method because of its simplicity. The heavy metal stabilization effects for fly ash using the chelating agent expected that the heavy metal chelating agent would enhance the long-term stabilization of the heavy metals in treated fly ash so that the risk for environmental pollution may be reduced. [24].

1.4 Fly ash characterization

Physical and chemical characterization of MSWI fly ash was influenced by the incineration process that has a significant effect on the enrichment of the elements. It is probably due to the high combustion temperature and excellent combustion during the process. Volatile elements from waste come into the flue gases, with a decrease in flue gas temperature, the volatile elements condense onto the fly ashes. Then fly ashes captured by the filter, which causes the enrichment of volatile elements. Meanwhile, lime addition into the flue gas scrubber removes the acid gases, such as HCl and SO_2. That is the reason for the high concentration of Ca, Cl, and S in the fly ash [25].

1.4.1 Physical characterization

The particle size distribution of fly ash has probably ranged between 2 and 1000 µm. Fly ash from stoker combustor has particle size distribution between 53 – 250 µm. However, the fly ash particles from the fluidized bed have larger than the 250 µm size. It may result from silica bed materials from the fluidized bed also collected in the exhaust gas [26].

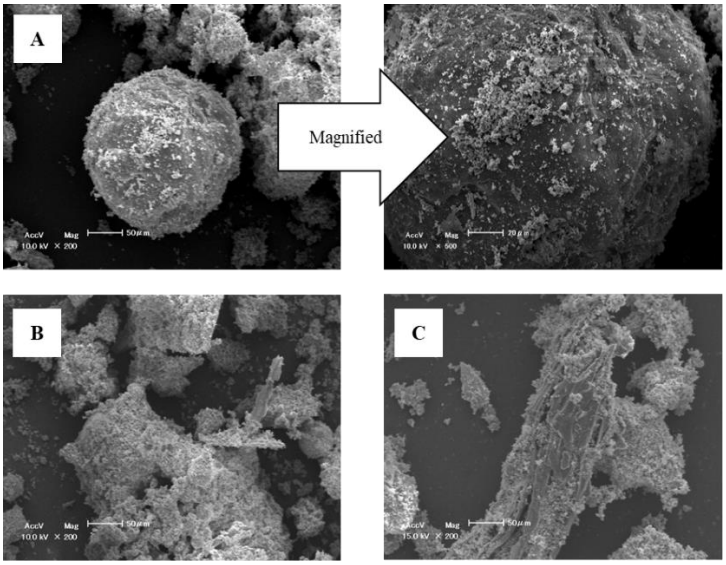

Figure 1.5 SEM images of MSWI fly ash particles (A; large sphere particles attaching smaller particles, B; aggregates of smaller particles, C; fibrous particles [27]

According to SEM observations, the MSWI fly ash particles could be categorized into four types based on their morphological characteristics; large particles (LP), small particles (SP), aggregates of small particles (ASP), and fibrous particles (FP) (as shown in **Figure 1.5**). Among the four-particle types, LP, SP, and ASP were found at a substantially higher frequency than FP. Large sphere particles were always attached to small particles on their surface [27].

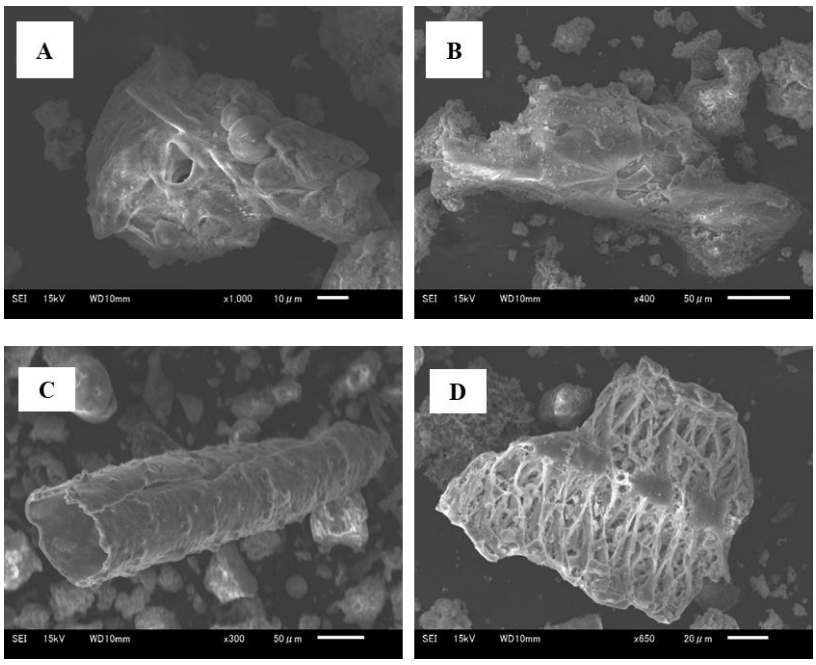

Figure 1.6 SEM images of insoluble residues after TCLP (A and B), and JLT19 (C and D) [27]

MSWI fly ash has a complicated structure inside their bodies. To observe the structure of the MSWI fly ash, Kitamura et al. investigate the insoluble residues after leaching experiments [27]. The solid residue after TCLP experiments, the surface of the residual materials are smooth and consisted mainly of Al, Ca, and Si (see **Figure 1.6 A** and **B**). The soluble component, such as KCl and NaCl, was removed sufficiently from the surface. The residual after JLT 19 likely consisted mainly of Al/Ca/Si-based core. The Si-based residue had a simple structure like tubes, shells, and porous shells (see **Figure 1.6 C**) and complicated three-dimensional structures like skeleton (see **Figure 1.6 D**). According to these results, they suggested MSWI fly ash likely consists of an insoluble core, Al/Ca/Si-based matrices, and soluble aggregates on the surface, as shown in **Figure 1.7**.

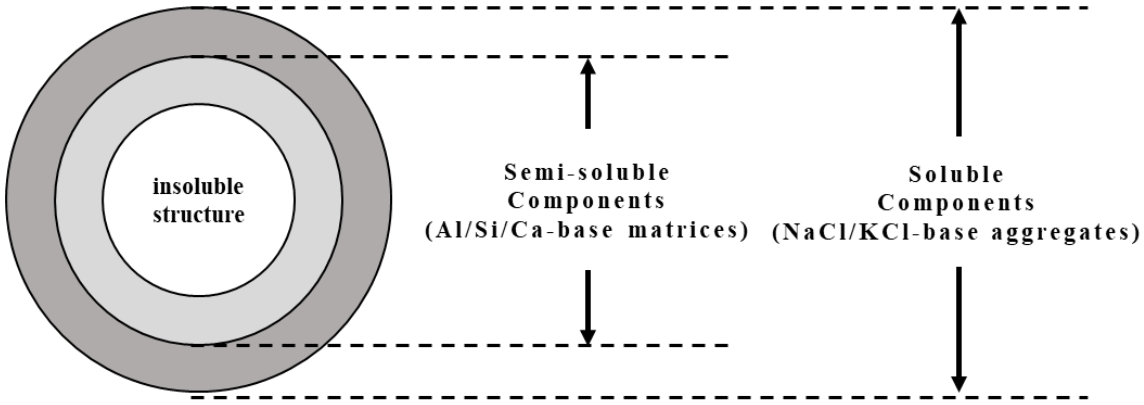

Figure 1.7 Model diagram of MSWI fly ash particle component [27]

1.4.2 Chemical characterization

The most abundant element in fly ash was calcium, followed by soluble chloride ions. The results revealed the presence of traces of several metals (Pb, Zn, Ba, Sb, Cu, Cr, and others) classified as hazardous, and whose content should be taken into account for the disposal of waste in a landfill. The calcium mainly comes from the lime added as an alkaline reagent in the flue gas cleaning system to neutralize acid gases. The chloride ions correspond to the hydrochloric acid present in the flue gas from MSWI plants where this acid is produced during the burning of plastic materials such as polyvinyl chloride. Many heavy metals are transported as volatile chlorides and then condensate in the fly ash particles [28].

The XRD analysis shows that the fly ash sample contains about 40wt.% amorphous and 60wt.% crystalline phases. This calculated mass percentage of amorphous content may also involve the minor crystalline phases, which could not be identified by XRD (below detection limit). In the fly ash sample, the crystalline phases potassium tetra-chlorozincate (K_2ZnCl_4), anhydride ($CaSO_4$), halite (NaCl), calcite ($CaCO_3$), hematite (Fe_2O_3), quartz (SiO_2), and rutile (TiO_2) can be readily identified [29].

1.5 A previous study on MSWI fly ash

Proper and comprehensive characterization by analytical techniques has been implemented to reveal both qualitative and quantitative characterization of fly ash residues [30, 31]. According to previous researches, comparative analysis of fly ash particles from stoker and fluidized bed combustors showed different characteristics of their fly ash. [14, 25, 26, 32, 33]. Heavy metal leaching behavior in fly ash particles that ash characterization, such as chemical speciation, size distribution, have a significant influence on leaching behavior [34]. Another researcher stated that fly ash particles have the heterogenous characterization of mineral composition and major elements in bulk samples [35–38]. The further study described the heterogeneous concentration distribution of major and trace elements in microscopic fly ash particles. They found a possibility to explain the apparent contradiction between the leaching characteristics of Cd in bulk samples and the possible Cd compounds found in a single particle [39]. Heterogeneity in a single fly ash particle not yet investigated. Moreover, heterogeneity characterization not yet explained between different types of combustors.

Inconsistency between geochemical simulation and experimental data of incinerator residue had been clarified in another study. They found the significant gaps in the geochemical model and measured value correlate with pH value in the alkaline range. Overestimation by models dominated the behaviors of most metal in the alkaline pH range [40]. If external matrices around toxic metals also control metal leaching behaviors, their heterogeneities might be necessarily considered. It might explain gaps between experimental leaching concentrations of metals and geochemical model predictions. The impact of intra- and inter-particle heterogeneities on metal leachabilities have not investigated yet.

1.6 Research objectives

As described in the previous section, fly ash stated in a few research as the heterogeneous matrix in the bulk samples of fly ash. Different types of combustors also affecting ash characterization. Individual heterogeneous particle analysis is necessary to provide more insight into fly ash characterization, fly ash formation, and association with heavy metal leaching behavior. Therefore, further quantitative elemental heterogeneity analysis of MSWI fly ash particles at a micro-scale level was needed. This current study aims to investigate heterogeneity in all components of fly ash generated from a fluidized bed combustor and to compare its heterogeneity between fly ash from a stoker combustor and fluidized bed incinerator. Moreover, this study aims to evaluate the impact of heterogeneity on heavy metal leachability by using geochemical modeling.

1.7 Outline of the thesis

The contents of this thesis have been divided into six chapters as follows

Chapter 1: Introduction

In this chapter, the background and objectives of heterogeneity analysis and chemical speciation of municipal solid waste incineration fly ash are explained. Overview of municipal solid waste management in Japan is firstly explained. The treatment of municipal solid waste that has been majorly adopting in Japan is an incinerator. The incinerator and type of incinerator are presented. Municipal solid waste incineration residue is mentioned, and one of MSWI residue is fly ash is explained. Moreover, fly ash characterization and fly ash treatments are presented. Finally, the previous research and the objectives of this research are stated.

Chapter 2: Heterogeneity analysis of fly ash particles generated from fluidized bed incinerator

In Chapter 2, quantitatively investigated two categories of heterogeneity of fly ash produced from a fluidized bed combustor. They are the heterogeneity of a single fly ash particle body (intra-particle heterogeneity) and heterogeneity among fly ash particles (inter-particle heterogeneity). All major elements, excluding Fe and Ti, are 3-66 % higher inter-particle heterogeneities on the surface

than semi-soluble and insoluble core components. It shows that the surface component of the fly ash is more heterogeneous than other components of fly ash particles. Fly ash from fluidized bed combustor has intra- and inter-particle heterogeneity. Besides, heterogeneity analysis can explain the fly ash formation process. Heterogeneity analysis suggests that Si plays more critical roles in the fly ash formation process of the fluidized bed combustor. Fly ash has various bodies, and it might give non-negligible impacts on the leaching of metals included in fly ash components.

Chapter 3: Comparison heterogeneities of fly ash particles generated from a fluidized bed combustor and a stoker combustor of municipal solid waste incineration

In Chapter 3, heterogeneity of fly ash produced from a stoker and a fluidized bed combustor are investigated. In all particle components (surface, semi-soluble, and insoluble core matrices), the fluidized bed combustor fly ash has 4-760 % larger intra-particle heterogeneities than the stoker combustor fly ash. In the surface and semi-soluble components, the fluidized bed combustor fly ash has 14-177 % larger inter-particle heterogeneities of Al, Ca, and Si than the stoker combustor fly ash. On the other hand, in the insoluble core component, the fluidized bed combustor fly ash has larger Ca inter-particle heterogeneity but smaller Al and Si heterogeneities than the stoker combustor fly ash. Heterogeneity analysis suggests that Si plays more critical roles in the fly ash formation process of the fluidized bed combustor than that of the stoker combustor. Fly ash has various bodies, and it might give non-negligible impacts on the leaching of metals included in fly ash matrices.

Chapter 4: Micro-scale correlation of heavy metals speciation within single fly ash particles of municipal solid waste incineration

In Chapter 4, heavy metal speciation in all components of MSWI fly ash is investigated. Heavy metal associations can determine the leachability of metals during leaching processes and have been observed heavy metals in fly ash particles and also their leachability by using several methods. This study aims to propose new possible metal speciation in all components of the fly ash particle by using micro-scale correlation analysis. Micro-scale correlation analysis can estimate possible metal speciation at individual particle levels. New possible metal speciation was observed in this study that might be

formed in the fly ash particle. Heavy metals, such as Cr and Cu, might be trapped into spinel structure and formed onto $MgCr_2O_4$, $CuAl_2O_4$, and $CuFe_2O_4$ in the insoluble core of fly ash. Other heavy metals, Fe and Zn, can host other heavy metals and presented into mineral complexation in semi-soluble component and/or insoluble core of fly ash. Correlation analysis at the micro-scale suggested that heavy metal speciation is different in the individual fly ash particle. Further metal speciation analysis is needed to improve the comprehensive analysis of metal speciation. Heavy metal leachability might be controlled by the leachability of metal speciation and Al/Ca/Si-based matrix around metal speciation.

Chapter 5: Impact of heterogeneity characterization on heavy metal leachability by geochemical modeling

In Chapter 5, geochemical simulation, PHREEQC, is used to investigate the impact of heterogeneity on elemental leachability. Heterogeneity characterization was included in the geochemical modeling of the leaching behavior of major elements and heavy metals. This study aims to evaluate the impact of elemental heterogeneities on their leachabilities. Elemental heterogeneity proposed local pH in the individual level of fly ash particle; pH after leaching is in the range 11- 13, in the high alkaline pH range. Alkaline pH in most of the scenarios might be due to dissolution CaO as the main factor of alkalinity in the fly ash. Heterogeneity affecting solid-phase concentration that is formed after leaching. Major elements are precipitated into the solid phase, which has dispersed concentration. It suggested elemental heterogeneity can be affected by the formation of elements in their solid phase. Elemental heterogeneity might have a negligible effect on heavy metal leachability.

Chapter 6: Conclusion and recommendation

In this chapter, the significant results and findings of the study are summarized. Following the conclusion, recommendations for further work are suggested.

1.8 References

1. Ministry of the Environment (2014) History and the Current State of WM in Japan
2. MOE (Ministry of Environment Japan) (2018) Annual Report on Environmental Statistics. 344
3. MOE (Ministry of Environment Japan) (2019) Annual report of waste management in Japan ("Nihon no Haikibutu Shori") 2017
4. Akiyama T, Harashina S, Osako M (2005) How Public Opposition and Distance Affect Waste Management Facility Siting. J. Japan Soc. Waste Manag. Expert. 16:429–440
5. Tong L, Tang Y, Wang F, et al. (2019) Investigation of controlling factors on toxic metal leaching behavior in municipal solid wastes incineration fly ash. Environ Sci Pollut Res 26:29316–29326. doi: 10.1007/s11356-019-06123-9
6. Silva R V., de Brito J, Lynn CJ, Dhir RK (2019) Environmental impacts of the use of bottom ashes from municipal solid waste incineration: A review. Resour. Conserv. Recycle. 140:23–35
7. Czop M, Łázniewska-Piekarczyk B (2019) Evaluation of the leachability of contaminations of fly ash and bottom ash from the combustion of solid municipal waste before and after stabilization process. Sustain 11:1–16. doi: 10.3390/su11195384
8. McKay G (2002) Dioxin characterization, formation, and minimization during municipal solid waste (MSW) incineration: Review. Chem Eng J 86:343–368. doi: 10.1016/S1385-8947(01)00228-5
9. Lim CN, Goh YR, Nasserzadeh V, et al. (2001) The modeling of solid mixing in municipal waste incinerators. Powder Technol 114:89–95. doi: 10.1016/S0032-5910(00)00273-4
10. Van Caneghem J, Brems A, Lievens P, et al. (2012) Fluidized bed waste incinerators: Design, operational and environmental issues. Prog Energy Combust Sci 38:551–582. doi: 10.1016/j.pecs.2012.03.001
11. Ministry of the Environment (2018) Annual report of waste management in Japan ("Nihon no Haikibutu Shori") 2016
12. Chandler AJ, Eighmy TT, Hjelmar O, et al. (1997) Chapter 3 - Municipal solid waste incineration technologies. In: Studies in Environmental Science. Elsevier, pp 59–95

13. Ning SK, Chang N Bin, Hung MC (2013) Comparative streamlined life cycle assessment for two types of a municipal solid waste incinerator. J Clean Prod 53:56–66. doi: 10.1016/j.jclepro.2012.09.007

14. Lu C-H, Chuang K-H (2015) Effect of municipal solid waste incinerator types on characteristics of ashes from different air pollution control devices. Environ Technol 3330:1–8. doi: 10.1080/09593330.2015.1070919

15. Wiles CC (1996) Municipal solid waste combustion ash: State-of-the-knowledge. J Hazard Mater 47:325–344. doi: 10.1016/0304-3894(95)00120-4

16. Fujimori E, Shiozawa R, Iwata S, et al. (2002) Multielement and morphological characterization of industrial waste incineration fly ash as studied by ICP-AES/ICP-MS and SEM-EDS. Bull Chem Soc Jpn 75:1205–1213. doi: 10.1246/bcsj.75.1205

17. Sakai S (1996) Municipal solid waste management in Japan. Waste Manag 16:395–405. doi: 10.1016/S0956-053X(96)00107-9

18. Ecke H, Sakanakura H, Matsuto T, et al. (2000) State-of-the-art treatment processes for municipal solid waste incineration residues in Japan. Waste Manag Res 18:41–51. doi: 10.1177/0734242X0001800106

19. Sekito T, Dote Y, Onoue K, et al. (2014) Characteristics of element distributions in an MSW ash melting treatment system. Waste Manag 34:1637–1643. doi: 10.1016/j.wasman.2014.04.009

20. Sabbas T, Polettini A, Pomi R, et al. (2003) Management of municipal solid waste incineration residues. Waste Manag 23:61–88. doi: 10.1016/S0956-053X(02)00161-7

21. Ma W, Chen D, Pan M, et al. (2019) Performance of chemical chelating agent stabilization and cement solidification on heavy metals in MSWI fly ash: A comparative study. J Environ Manage 247:169–177. doi: 10.1016/j.jenvman.2019.06.089

22. Katsuura H, Inoue T, Hiraoka M, Sakai S (1996) Full-scale plant study on fly ash treatment by the acid extraction process. Waste Manag 16:491–499. doi: 10.1016/S0956-053X(96)00091-8

23. Crannell BS, Eighmy TT, Krzanowski JE, et al. (2000) Heavy metal stabilization in municipal solid waste combustion bottom ash using soluble phosphate. Waste Manag 20:135–148. doi:

10.1016/S0956-053X(99)00312-8

24. Jianguo J, Jun W, Xin X, et al. (2004) Heavy metal stabilization in municipal solid waste incineration fly ash using heavy metal chelating agents. J Hazard Mater 113:141–146. doi: 10.1016/j.jhazmat.2004.05.030

25. Li M, Xiang J, Hu S, et al. (2004) Characterization of solid residues from municipal solid waste incinerator. Fuel 83:1397–1405. doi: 10.1016/j.fuel.2004.01.005

26. Chang FY, Wey MY (2006) Comparison of the characteristics of bottom and fly ashes generated from various incineration processes. J Hazard Mater 138:594–603. doi: 10.1016/j.jhazmat.2006.05.099

27. Kitamura H, Sawada T, Shimaoka T, Takahashi F (2016) Geochemically structural characteristics of municipal solid waste incineration fly ash particles and mineralogical surface conversions by chelate treatment. Environ Sci Pollut Res 23:734–743. doi: 10.1007/s11356-015-5229-5

28. Atanes E, Cuesta-García B, Nieto-Márquez A, Fernández-Martínez F (2019) A mixed separation-immobilization method for soluble salts removal and stabilization of heavy metals in municipal solid waste incineration fly ash. J Environ Manage 240:359–367. doi: 10.1016/j.jenvman.2019.03.122

29. Bayuseno AP, Schmahl WW (2011) Characterization of MSWI fly ash through mineralogy and water extraction. Resour Conserv Recycl 55:524–534. doi: 10.1016/j.resconrec.2011.01.002

30. Weibel G, Eggenberger U, Kulik DA, et al. (2018) Extraction of heavy metals from MSWI fly ash using hydrochloric acid and sodium chloride solution. Waste Manag. 76:457–471

31. Phua Z, Giannis A, Dong ZL, et al. (2019) Characteristics of incineration ash for sustainable treatment and reutilization. Environ Sci Pollut Res 26:16974–16997. doi: 10.1007/s11356-019-05217-8

32. Hu HY, Liu H, Shen WQ, et al. (2013) Comparison of CaO's effect on the fate of heavy metals during thermal treatment of two typical types of MSWI fly ashes in China. Chemosphere 93:590–596. doi: 10.1016/j.chemosphere.2013.05.077

33. Jung CH, Matsuto T, Tanaka N, Okada T (2004) Metal distribution in incineration residues of municipal solid waste (MSW) in Japan. Waste Manag 24:381–391. doi: 10.1016/S0956-053X(03)00137-5

34. Luo H, Cheng Y, He D, Yang EH (2019) Review of leaching behavior of municipal solid waste incineration (MSWI) ash. Sci. Total Environ. 668:90–103

35. Fermo P, Cariati F, Pozzi A, et al. (2000) Analytical characterization of municipal solid waste incinerator fly ash. Part II. Fresenius J Anal Chem 366:267–72

36. Rémond S, Pimienta P, Bentz D. (2002) Effects of the incorporation of Municipal Solid Waste Incineration fly ash in cement pastes and mortars. Cem Concr Res 32:303–311. doi: 10.1016/S0008-8846(01)00674-3

37. Mahieux PY, Aubert JE, Cyr M, et al. (2010) Quantitative mineralogical composition of complex mineral wastes - Contribution of the Rietveld method. Waste Manag 30:378–388. doi: 10.1016/j.wasman.2009.10.023

38. Ha J, Chae S, Chou KW, et al. (2016) Characterization of Class F Fly Ash Using STXM: Identifying Intraparticle Heterogeneity at Nanometer Scale. J Nanomater 2016. doi: 10.1155/2016/8072518

39. Camerani MC, Golosio B, Somogyi A, et al. (2004) X-ray Fluorescence Tomography of Individual Municipal Solid Waste and Biomass Fly Ash Particles. Anal Chem 76:1586–1595. doi: 10.1021/ac030282w

40. Yin K, Chan WP, Dou X, et al. (2018) Co-complexation effects during incineration bottom ash leaching via comparison of measurements and geochemical modeling. J Clean Prod 189:155–168. doi: 10.1016/j.jclepro.2018.03.320

Chapter 2

Heterogeneity analysis of fly ash particles generated from fluidized bed incinerator

Abstract: Although municipal solid waste incineration fly ashes are fine particles and a priori considered as homogeneous, they have complicated structures inside their bodies. This study quantitatively investigated two categories of heterogeneity of fly ash produced from a fluidized bed combustor. They are the heterogeneity of a single fly ash particle body (intra-particle heterogeneity) and heterogeneity among fly ash particles (inter-particle heterogeneity). Fly ash from fluidized bed combustor has intra- and inter-particle heterogeneity similar to stoker combustor. Besides, heterogeneity analysis can explain the fly ash formation process. Heterogeneity analysis suggests that Si plays more critical roles in the fly ash formation process of the fluidized bed combustor than that of the stoker combustor. Fly ash has heterogeneous bodies, and it might give non-negligible impacts on the leaching of metals included in fly ash components.

2.1 Introduction

The critical factor of fly ash management is comprehensive of its characterization. It becomes necessary for the assessment of fly ash disposal in a short and long-term period and under various environmental situations [1]. Proper and comprehensive characterization by analytical techniques has been implemented to reveal both qualitative and quantitative characterization of fly ash residues [2, 3]. Luo et al. reviewed heavy metal leaching behavior in fly ash particles that ash characterization, such as chemical speciation, size distribution, have a significant influence on leaching behavior [4]. Fly ash had been identified as compositional heterogeneity from the spherical glass phase and crystalline phase. They reported the heterogeneous spatial distribution of elements in the coal fly ash particle [5]. Another researcher stated that fly ash particles have the heterogenous characterization of mineral composition and major elements in bulk samples [6–8]. It is shown from XRF analysis result that MSWI fly ash having a heterogenous elemental composition such as Ca, Cl, K, Si, Al, S, Mg, including heavy metal such as Zn, Ti, Fe, Pb, Br, Sb, Cu, Sn, Ba, Mn, Cr, Sr, Cd, Zr in our previous study [9]. The further study described the heterogeneous concentration distribution of major and trace elements in microscopic fly ash particles. They found a possibility to explain the apparent contradiction between the leaching characteristics of Cd in bulk samples and the possible Cd compounds found in a single particle [10]. Kitamura et al. reported that fly ash particles had different geochemical components that consist of soluble KCl/NaCl-based aggregates on the surface, Al/Ca/Si-based semi-soluble components and Si-based insoluble core components [11]. Moreover, fly ash had an active mineralogical surface on which secondary minerals could be generated under wet conditions. Although secondary mineral formation can immobilize leachable elements, its effect is limited [12].

Therefore, further quantitative elemental heterogeneity analysis of MSWI fly ash particles at the microscale level was needed. Individual heterogeneous particle analysis is necessary to provide more insight into fly ash characterization, fly ash formation, and association with heavy metal leaching behavior. Quantitative heterogeneity analysis of fly ash generated from stoker-type on each body component had been discussed in a previous study [9]. This chapter aims to investigate heterogeneity in all components of fly ash generated from a fluidized bed combustor.

2.2 Materials and methods

2.2.1 Fly ash samples

Fly ash samples were obtained from fluidized bed type MSW incineration plants in Japan. The capacities of the incinerator plants were 250 Mg/day. In the incinerator, $Ca(OH)_2$ slurry and pulverized activated carbon were injected into flue gas for acidic gas neutralization and dioxin control. Fly ash was trapped by fabric filter, then transferred to a storage tank by an air pressure feeder or a mechanical feeder. After that, MSWI fly ash was conveyed from the storage tank to the chelate treatment apparatus. Fly ash samples were collected from the chelate treatment apparatus. All sample was dried under room condition for one week or longer. After drying, the fly ash sample was observed and analyzed.

2.2.2 Leaching tests for the removal of surface and semi-soluble components

Table 2.1 Experimental conditions of each leaching experiment

	JLT46	**TCLP**	**JLT19**
Extractant	Water (H_2O)	Acetic acid (CH_3COOH)	Hydrochloric acid (HCl)
L/S [mL/g]	10	20	33.3
Shaking speed [rpm]	200	30	200
Shaking time [hour]	6	18	2
Filtration paper [μm]	0.45 MF	0.6-0.8 GF	0.45 MF

MF：Membrane Filter, GF：Glass fiber Filter

Three kinds of leaching methods were used: Japan leaching test 46 (JLT 46), toxicity characteristic leaching procedure (TCLP), and Japan leaching test 19 (JLT 19). Leaching test residues were filtrated, recovered, and then dried under room condition for more than 24 hours before analysis.

JLT 46 was carried out to remove the surface component by pure water. The upper semi-soluble structure could be analyzed. The TCLP methods using an acetic acid solution were used to remove the soluble component. It enabled observations of the lower semi-soluble components. JLT 19 was used to remove surface and semi-soluble components altogether by hydrochloric acid. Insoluble core components of fly ash particles were recovered after JLT 19, and then they were analyzed. The experimental conditions of each leaching experiment are summarized in **Table 2.1**. Leaching experiments have been usually used to investigate the leachability of heavy metals included in fly ash. However, this research used them to group fly ash components into the surface, semi-soluble Al/Ca/Si-based, and insoluble core components of fly ash particles, which have been studied by Kitamura et al., as shown in **Figure 2.1** [11].

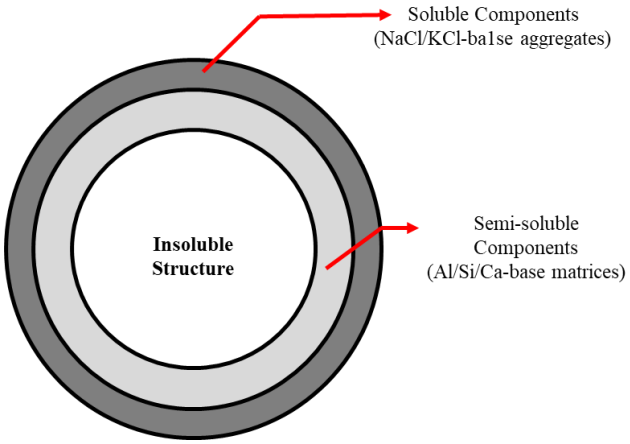

Figure 2.1 Component model of an MSWI fly ash particle referred from Kitamura et al. (2016)

2.2.3 Mineralogical and elemental composition analysis

The mineral composition of fly ash particles is analyzed using x-ray diffraction (XRD; MultiFlex, Rigaku Co., Japan). The measured fly ash samples were conducted using CuKα radiation (λ = 1.5418 Å, U=40keV, I=25mA) to identify the crystal phase on the samples. XRD analysis was conducted from 5° to 75° of 2θ at a rate of 1° min^{-1}. Elemental compositions of fly ash samples were analyzed by energy dispersive X-ray fluorescence spectrometer (EDXRF: S2 RANGER/LE, BRUKER AXS).

2.2.4 Microscopic observation of fly ash particles

The morphological surface of MSWI fly ash particles was observed using a scanning electron microscope (SEM; JSM-6610LA, JEOL Ltd., Japan). The fly ash samples were fixed on the carbon tape on the observation stage. Because it might cause overestimation of carbon content, carbon content would not be presented in this research. The samples were observed after Pt-Pd sputtering for 30 seconds using a sputter coating device (MSP-1S, Vacuum device Ltd., Japan). The elemental composition of fly ash particles was analyzed using energy-dispersive x-ray spectroscopy (EDX) attached to SEM (SEM-EDX JSM-6610 LA, JEOL, Ltd., Japan). Elemental mapping of fly ash particle surfaces was carried out to analyze elemental distribution. In this study, one hundred particles of original fly ash and leaching test residues were analyzed by SEM-EDX. In total, 400 particles were observed in this study.

2.2.5 Elemental heterogeneity analysis based on the surface elemental concentration

Surface elemental concentrations of each fly ash particle, measured by SEM-EDX as described above, were used to analyze elemental heterogeneity of fly ash particles. In this chapter, we investigated two types of heterogeneity. The first is intra-particle heterogeneity, and the other is inter-particle heterogeneity. Intra-particle heterogeneity means heterogeneity of individual fly ash particles. After the elemental distribution of 100 particles of the original fly ash and leaching test residues were measured (called elemental mapping), each single-particle was divided into five sections equally (see **Figure 2.2**).

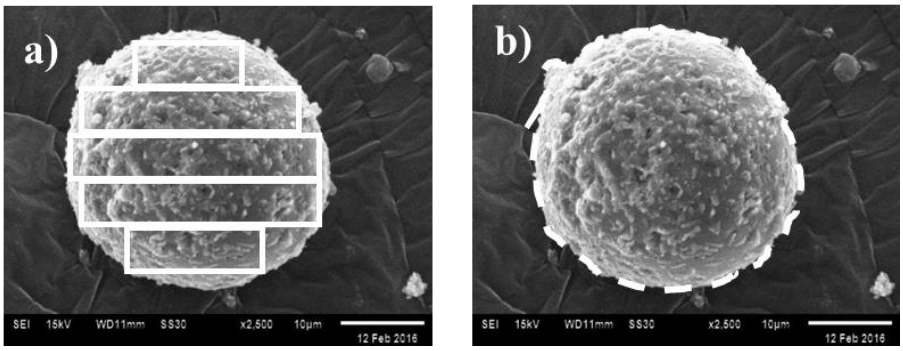

Figure 2.2 Elemental heterogeneity analysis: a) line profile analysis and b) area analysis

It should be noted that the area size of each section in all measured particles was different depending on particle size. In the line profile analysis, all intensity data, which directly correlated to element concentrations, were extracted from 5 sections of each particle and then integrated. Owing to the different size of section areas, the quantity of intensity data was correspondingly different for each particle. The coefficient of variation (CV value = standard deviation/average) was calculated for each element, and each particle using intensity data. The CV values were plotted in the histogram to visualize the distribution of CV values for each element. The quantity of intensity data is calculated into a weighted average of CV values. In this analysis, the weighted average of CV values was used as a quantitative indicator of the intra-particle heterogeneity.

On the other hand, inter-particle heterogeneity means heterogeneity among fly ash particles. According to elemental mapping data, average elemental concentrations of each particle were calculated as weight percent [wt%] (see **Figure 2.2**). They were plotted in the histogram to visualize the distribution of average elemental concentrations. CV values of average elemental concentrations were calculated and used as a quantitative indicator of inter-particle heterogeneity. It is noted again that the weighted average of CV values of 100 particles was used to evaluate intra-particle heterogeneity.

On the other hand, the CV values of 100 average elemental concentrations (100 particles) were used to evaluate inter-particle heterogeneity. It should be noted that 100 particle analysis might still be insufficient. Therefore, this analysis offers limited specific results and conclusions. Uncertainty owing to limited observations should be taken into account (see **Figure S.2-1 and S.2-2**). In this chapter, both heterogeneities were investigated, focusing on the surface components, semi-soluble components, and insoluble core components of fly ash particles.

2.2.6 Element association analysis based on elemental heterogeneity

Visualization of elemental heterogeneity can be acquired by not only the histogram but also the ternary diagram. In this study, a ternary diagram was used to visualize inter-particle heterogeneity and element association of fly ash particles. The average elemental concentration [wt%] of each particle was plot directly to the ternary diagram, and their dispersion describes the elemental inter-particle heterogeneity of fly ash particles. However, different concentrations of each element caused

considerable difficulty in analyzing the priority of element associations. For example, we need to confirm whether Cl would be associated with higher priority, Na or K. Therefore, element concentrations [wt%] of each fly ash particle were transformed to molar concentrations and then standardized by molar-based elemental contents of whole fly ash samples measured by XRF (listed in **Table 2.2**). Plotted molar-based ternary diagrams visualize prior associations of tested elements. The XRD can observe the crystalline phase but is not appropriate to analyze the amorphous phase. In this analysis, the molar-based ternary diagram can clarify the crystalline phase based on XRD analysis and further description of element interrelation on the amorphous phase.

2.3 Results and discussion

2.3.1 Micro-characteristics of fly ash

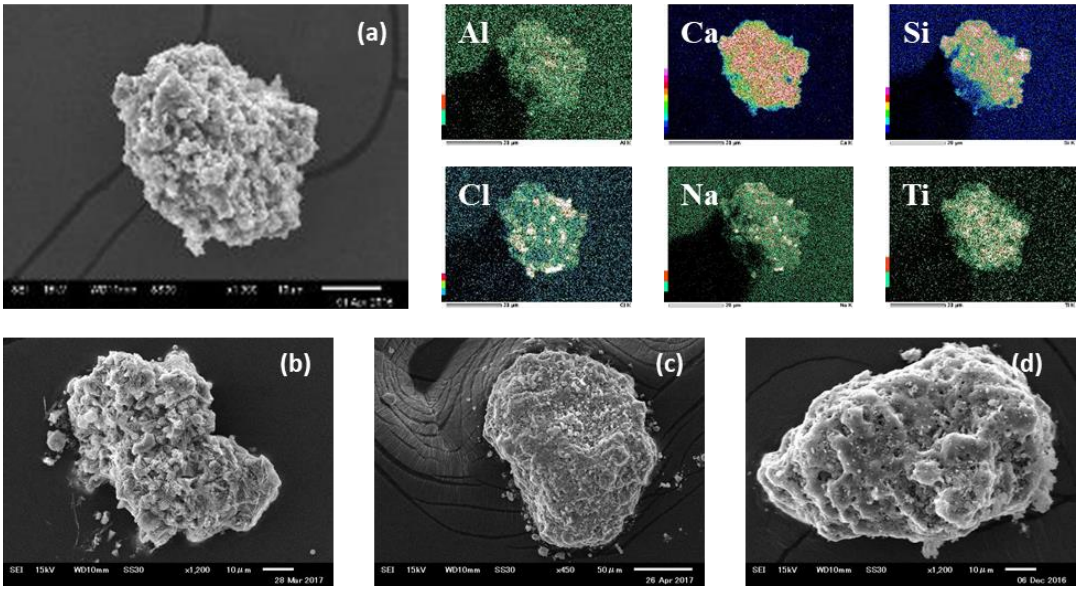

Figure 2.3 Morphological characteristics of a) surface, b) upper semi-soluble, c) lower semi-soluble, and d) insoluble core components of fly ash particles

The fluidized bed combustor fly ash could be categorized into two types: sphere particles and aggregates of small particles. Compared with the authors' previous results [11], the fluidized bed combustor fly ash had similar shapes with the stoker combustor fly ash, as shown in **Figure 2.3**. The

chelate reagent had been used to treat the fluidized bed combustor fly ash. However, secondary mineral crystals like cubic and spicular shapes were not found, although they were observed in the stoker combustor fly ash [11].

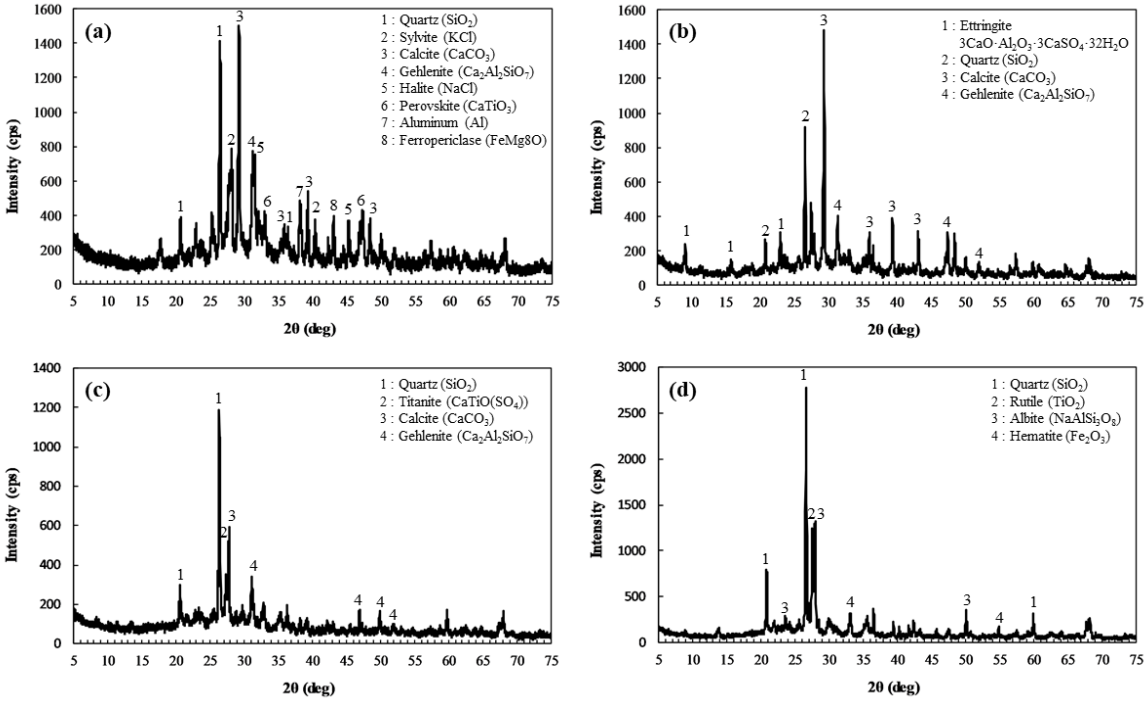

Figure 2.4 XRD patterns of a) surface, b) upper semi-soluble, c) lower semi-soluble, and d) insoluble core components of fly ash particles

After leaching tests, leaching residues of both two types of fly ash have similar shapes, as shown in **Figure 2.3**. The upper semi-soluble component of fly ash particles, shown by the JLT 46 leaching test, has spicular shapes regardless of the combustor type. According to Kitamura et al., spicular shape minerals are considered as ettringite or gypsum [11]. The shape of lower semi-soluble components of the fluidized bed combustor fly ash, shown by the TCLP leaching test, had more aggregates on the surface compared with the stoker combustor fly ash that had a relatively smoother surface. This difference could be derived from Na and K remaining on the surface of the lower semi-soluble component of the fluidized bed combustor fly ash. Upper and lower semi soluble component shows different in the shape and crystalline phase. Fly ash from a fluidized bed shows ettringite is not present in the lower semi-soluble component. Therefore, spicular shapes not found in the lower semi-soluble

component, which is considered as ettringite crystals. In contrast, upper semi-soluble shows spicular shapes attaching to aggregates particles (see **Figure 2.3 b)** and **c)**).

Soluble and semi-soluble components were removed entirely throughout the JLT 19 test. An insoluble core component of the stoker combustor fly ash mostly consisted of Si and had a simple structure like a tube, shell, and porous shell or complicated three-dimensional structure like skeleton [11]. In contrast to the stoker combustor fly ash, the fluidized bed combustor fly ash usually had a porous shape in their insoluble cores rather than a complicated skeleton structure (see **Figure 2.3**). According to Kitamura's further research [9], not only Si-base insoluble cores but also Al- and Ca-rich cores were also found for the stoker combustor fly ash. On the other hand, as discussed in following section 3.5, the fluidized bed combustor fly ash usually had Si-base insoluble cores.

Table 2.2 Elemental composition of fly ash samples determined by XRF

Elements	**Ca**	**Cl**	**Si**	**Fe**	**Al**	**K**	**Ti**
Fly Ash [wt%]	44.79	13.73	13.08	6.19	5.89	5.25	2.35
Elements	**Zn**	**Mg**	**S**	**Cu**	**Pb**	**Ba**	**Mn**
Fly Ash [wt%]	1.82	1.79	1.24	1.01	0.47	0.45	0.28
Elements	**Sn**	**Br**	**Sr**	**Sb**	**Cr**	**Zr**	**Ni**
Fly Ash [wt%]	0.13	0.12	0.11	0.08	0.07	0.06	0.05

Fluidized bed combustor fly ash has alkaline minerals, including calcite, silicates, and alkaline oxides (shown in **Figure 2.4**). The surface of fly ash consisted of quartz (SiO_2), sylvite (KCl), halite (NaCl), calcite ($CaCO_3$), gehlenite ($Ca_2Al_2SiO_7$), aluminum (Al), perovskite ($CaTiO_3$), and ferropericlase ($FeMg_8O$). Halite and sylvite peaks were not detected on semi-soluble components of fly ash owing to NaCl/KCl dissolution. Semi-soluble components consisted mainly of quartz, calcite, gehlenite, ettringite ($3CaO{\cdot}Al_2O_3{\cdot}3CaSO_4{\cdot}32H_2O$), and titanite ($CaTiO(SO_4)$). In the insoluble core of

fly ash samples, it consisted of quartz, albite ($NaAlSi_3O_8$), rutile (TiO_2), and hematite (Fe_2O_3). These results show good agreement with previous mineralogical results [13–15].

Table 2.2 shows the elemental composition of fly ash from a fluidized bed incinerator. The constituent elements in the fly ash sample are Ca, Cl, Si (>10 wt%), Fe, Al, K, Ti, Zn, Mg, S, Cu (>1 wt%), and other heavy metals (less than 1 wt%). Although the XRF result shows a titanium concentration of less than 10 wt%, the titanium crystalline phase was detected in all components fly ash particle. Perovskite, titanite, and rutile were detected in the surface, semi-soluble, and core components of fly ash particles, respectively. Titanium randomly binds to ash particles regardless of their composition. Therefore, titanium is incorporated or combined with the aluminosilicate matrix to form ash [16]. The surface of the fly ash particle contained diverse crystal. Sylvite and halite were disappeared owing to leaching out after leaching tests.

2.3.2 Intra-particle heterogeneity of surface component of fly ash particle

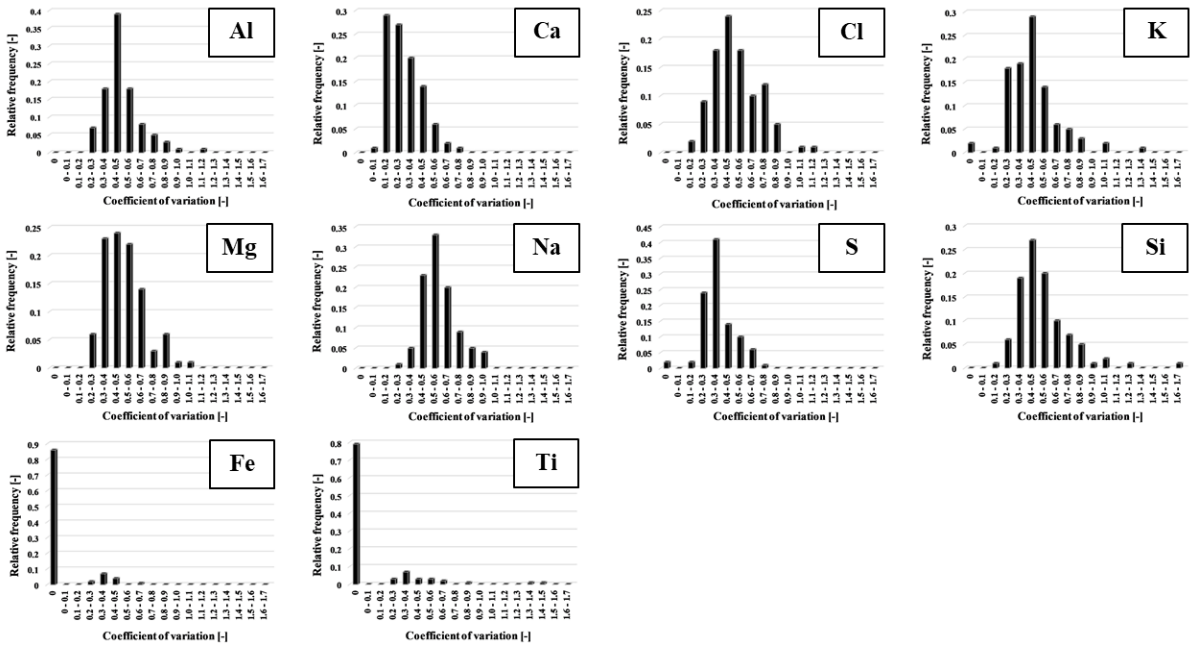

Figure 2.5 Relative frequency of coefficient variation of major elements in fly ash particles

On the other hand, intra-particle heterogeneities of Na, Cl, and K are more than 57 % higher than Ca intra-particle heterogeneity. Kitamura et al. reported that soluble NaCl/KCl-based aggregates generate hotspot on the surface of MSWI fly ash particles produced in a stoker type combustor, and it caused more than 23% higher intra-particle heterogeneities of Cl, K, and Na than other major elements [9]. It has a good agreement with the fluidized combustor fly ash. Hotspots of NaCl/KCl-based aggregates were also observed in this analysis (see **Figure 2.6**). NaCl and KCl were derived from sodium and potassium that released from MSW as gaseous metallic. When gaseous NaCl and KCl leave the furnace and enter the post-combustion, temperature decrease in this chamber. As the gases cool through the post-combustion system, the NaCl and KCl species condense, either through the formation of an aerosol of discrete particles or adsorption onto ash particles [25,26]. **Figure 2.6** shows NaCl and KCl in the small crystal in the surface of fly ash particles. It suggests NaCl and KCl condense in the post-combustor, and then physical adsorption happened to form small crystals attach onto fly ash particles.

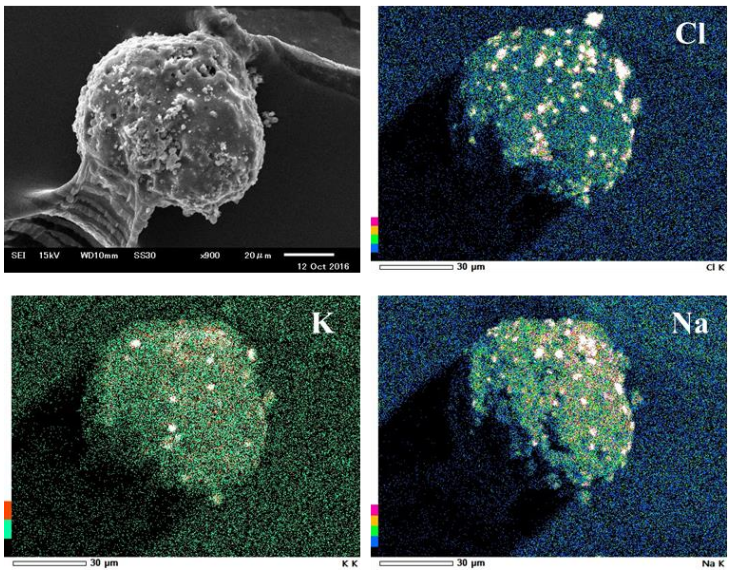

Figure 2.6 Elemental distribution of Cl, K, Na on MSWI fly ash particle surface

Although the CV value of Si ranges more widely than other major elements, the fractions of low CV values (less than 0.3) is limited (see **Figure 2.5**). In general, silica sand is used as bed materials in fluidized bed combustors [17]. Because fine silica sands, which have Si homogeneity, would fly up to exhaust gas during combustion and be trapped by fabric filter, large fractions of low CV values were

expected for Si. However, CV analysis results, shown in **Figure 2.7**, are in contrast to the expectation. It suggests that a fly-up of fine silica sand that has almost the same diameter with fly ash particles (1-20 μm) is limited. However, finer "flyable" silica sand particles might transfer to the gas phase and serve as Si-rich cores in fly ash particles during formation processes. It will be discussed again in the following section 3.5.

Al and Si have comparable intra-particle heterogeneities with each other, and they were higher than Ca intra-particle heterogeneity. It is also the same in upper/lower semi-soluble components. For MSWI fly ash of a stoker combustor, Kitamura et al. suggested that aluminosilicate domains (Al and Si-rich regions) were included in the Ca-based matrix in the semi-soluble component [9]. It should result in lower intra-particle heterogeneity of Ca and higher heterogeneities of Al and Si. Intra-particle heterogeneities of Al, Ca, and Si measured in this analysis are consistent with the previous research. It will be discussed again in the following sections. Therefore on the surface of fly ash particles, Ca has the lowest intra-particle heterogeneity due to excess $Ca(OH)_2$ injection in the neutralization process. Besides, NaCl/KCl aggregates were identified in the disperse hotspot.

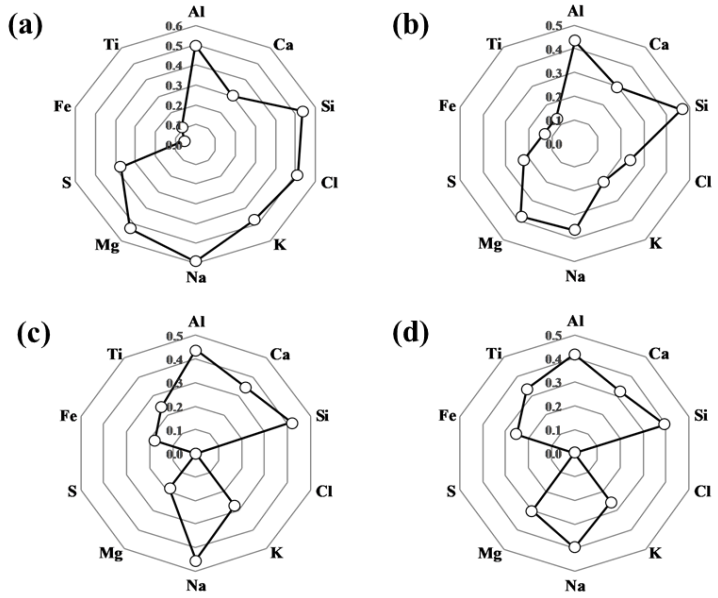

Figure 2.7 Weighted average of coefficient variation of major elements in a) surface, b) upper semi-soluble, c) lower semi-soluble, and d) insoluble core components of fly ash particles

2.3.3 Intra-particle heterogeneity of semi-soluble/insoluble core components of fly ash particles

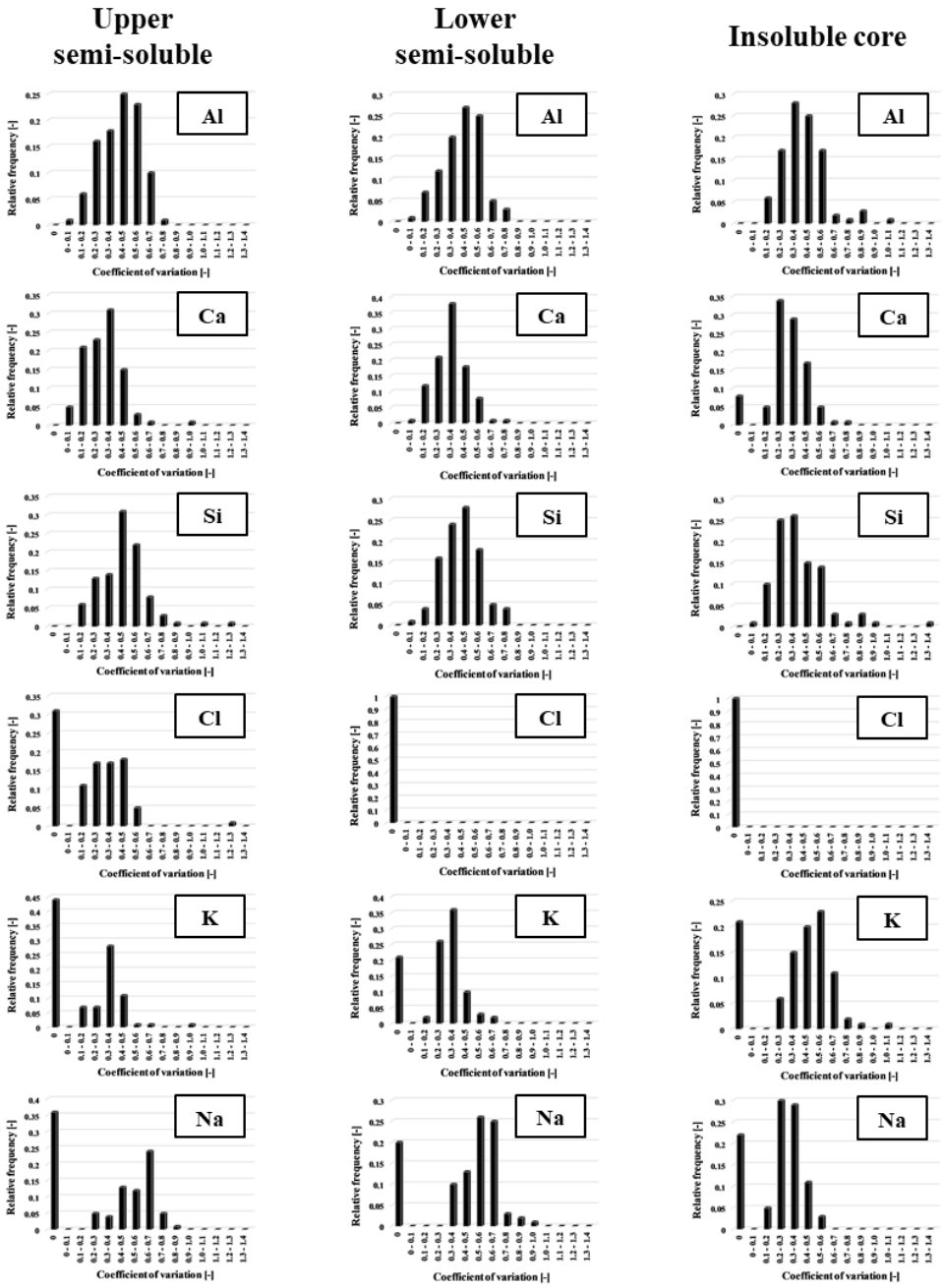

Figure 2.8 Relative frequency of coefficient variation of major elements in component matrices of fly ash particle

Figure 2.8 shows the histograms of CV values of major elements for semi-soluble and insoluble core components. The ranges of CV values in semi-soluble and insoluble core components are narrower than those of the surface components. They are around 0 to 1.4. In particular, Si in semi-soluble and insoluble core components have the broadest range of CV values than other elements. Intra-particle

heterogeneities of Al and Si in semi-soluble and insoluble core components are 17% and 22% lower than those in the surface components (see **Figure 2.7**).

On the other hand, Ca intra-particle heterogeneities of lower semi-soluble and insoluble core components are 17-70% larger than those of the surface components. In contrast, Ca intra-particle heterogeneity of upper semi-soluble components were smaller than those of the surface, lower semi-soluble, and insoluble core components. Moreover, Ca has smaller intra-particle heterogeneity than Al and Si in all components. Kitamura et al. suggested that semi-soluble components are mainly Ca-based components such as $CaCO_3$ and unreacted $Ca(OH)_2$ in which aluminosilicate domains were included [9]. It is also suggested for the fluidized bed combustor fly ash. Lower intra-particle heterogeneity of Ca and higher heterogeneities of Al and Si in both upper and lower semi-soluble components agree with this proposal. It is also supported partially by XRD analysis. Calcite ($CaCO_3$) and gehlenite ($Ca_2Al_2SiO_7$) were detected as Ca-based mineral and aluminosilicate mineral in both semi-soluble components, respectively. The line profile analysis, shown in **Figure 2.9**, also supports it. Al and Si concentrations vary similarly along with the distance despite less similarity with Ca concentration variation (see **Figure 2.9a**). Besides, it is also supported by inter-particle heterogeneity analysis presented in the following section 3.5.

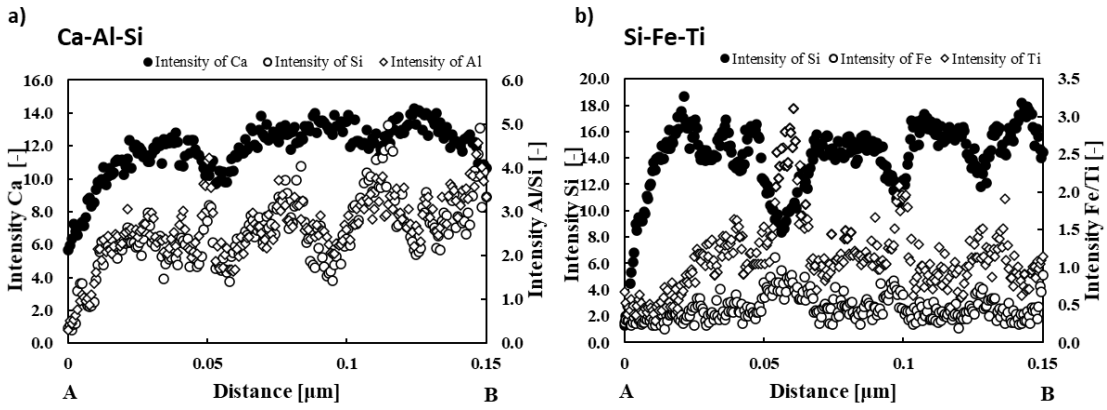

Figure 2.9 Intensity changes of a) Cal-Al-Si on semi-soluble components and b) Si-Fe-Ti on insoluble core components along with A to B

Excluding Fe and Ti, intra-particle heterogeneities of all elements in the upper semi-soluble component are lower than those on the surface. It means that the surface component of fly ash particles

is more heterogeneous than the upper semi-soluble component. On the other hand, the apparent difference of intra-particle heterogeneities was not found between upper and lower semi-soluble components. To sum up, the surface component is more heterogeneous compared to semi-soluble and core components in the fly as a particle body. Semi-soluble components are Ca-based components with aluminosilicate domains were included.

2.3.4 Inter-particle heterogeneity of surface components of fly ash particles

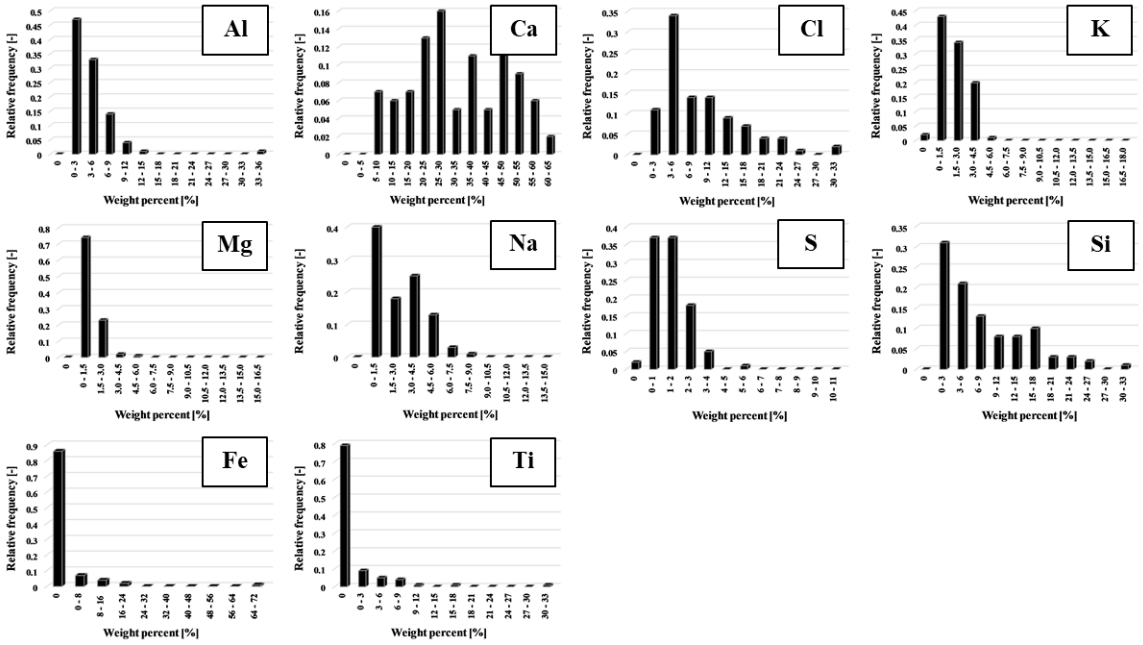

Figure 2.10 Relative frequency of major elements average concentration of chelate-treated MSWI fly ash particles (unit: weight percent)

The average concentrations of major elements in the surface components of fly ash particles have broad distributions, as shown in **Figure 2.10**. Inter-particle heterogeneity of the surface component was evaluated quantitatively based on the CV value of the average concentration data. They are summarized in **Table 2.3**. On the surface of fly ash, the concentration of Ca had the broadest range from 0 to 65 wt% than other elements. On the other hand, Ca has the lowest inter-particle heterogeneity than other elements. Although the peak of Ca appears in the middle increment, the other elements excluding Fe and Ti have the most significant peak in the second or the third smallest increment like

Poisson distribution with the low average number of occurrences in the interval. In the previous section 3.2, hotspots of NaCl/KCl-based aggregates were reported (see **Figure 2.6**). These hotspots seem to be mainly generated by adsorption of NaCl/KCl-based aggregates onto the surface. If the adsorption is random phenomena, it produces the following expectations.

Table 2.3 CV value of weight percent all components of fly ash particles

	Surface		Upper semi-soluble		Lower semi-soluble		Insoluble core	
	μ	CV	μ	CV	μ	CV	μ	CV
Al	4.07	1.06	9.80	0.67	8.90	0.73	5.82	1.25
Ca	33.22	0.45	39.49	0.60	12.59	0.59	5.51	1.35
Si	8.02	0.90	19.34	0.70	17.66	0.41	26.31	0.46
Cl	9.19	0.72	1.32	0.99	0.00	-	0.00	-
K	3.74	0.67	3.24	1.15	2.98	0.83	2.46	0.83
Na	2.53	0.75	2.53	0.99	2.21	0.72	1.77	0.79
Mg	1.14	0.68	1.53	0.96	0.89	2.55	1.12	1.57
S	1.45	0.62	1.97	0.96	0.00	-	0.00	-
Fe	1.86	4.29	4.02	2.03	6.18	2.00	7.25	1.91
Ti	1.29	3.04	1.64	1.91	1.76	1.30	3.57	1.56

Both intra-particle and inter-particle heterogeneities of Cl, K, and Na would be similar to each other. As is expected, intra-particle and inter-particle heterogeneities of these elements are within 25 % and 12% differences, respectively. One more expectation is that concentration distributions of these elements would follow Poisson or Poisson-like distribution because the adsorption of NaCl/KCl-based aggregates is random events and adsorption events linearly increase element concentrations. The χ^2 test of goodness-of-fit suggests that concentration distributions of K, Na, and Mg follow Poisson distribution but not followed for Cl, Al, and Si with a 1% significance level (see **Table 2.4**). It might propose that a significant source of K, Na, and Mg on the surface is adsorption of NaCl, KCl, and $MgCl_2$.

On the other hand, Cl might be derived from not only adsorption of these chlorides but also other chlorides like $CaCl_2$. It will be supported by ternary diagram analysis in following section 3.6.

Table 2.4 Statistical results of Poisson Test

Elements	λ	P-value
Al	11.87	< 0.01
Si	11.02	< 0.01
Cl	12.26	< 0.01
K	1.62	0.99
Na	2.22	1.00
Mg	1.06	0.94

Inter-particle heterogeneities of Al and Si are higher than those of other elements excluding Fe and Ti. Owing to a proposal of the statistical test that Al and Si concentrations do not follow a Poisson distribution, the primary source of Al and Si on the surface seems not to be random adsorption of aluminosilicates onto the surface. Kitamura et al. suggested that major forms of surface Ca was exposed surface of semi-soluble Al/Ca/Si-based component and unreacted $Ca(OH)_2$ for stoker combustor fly ash [9]. If it is the same with fluidized bed combustor fly ash, it might cause higher inter-particle heterogeneities of Al and Si than Ca. The analysis results agree with this expectation (see **Table 2.3**). It will also be verified by ternary diagram analysis in following section 3.6. In summary, random adsorption of aluminosilicates on the surface of fly ash particles causes higher heterogeneity of Al and Si than other elements among fly ash particles.

2.3.5 Inter-particle heterogeneity of semi-soluble/insoluble core components of fly ash particles

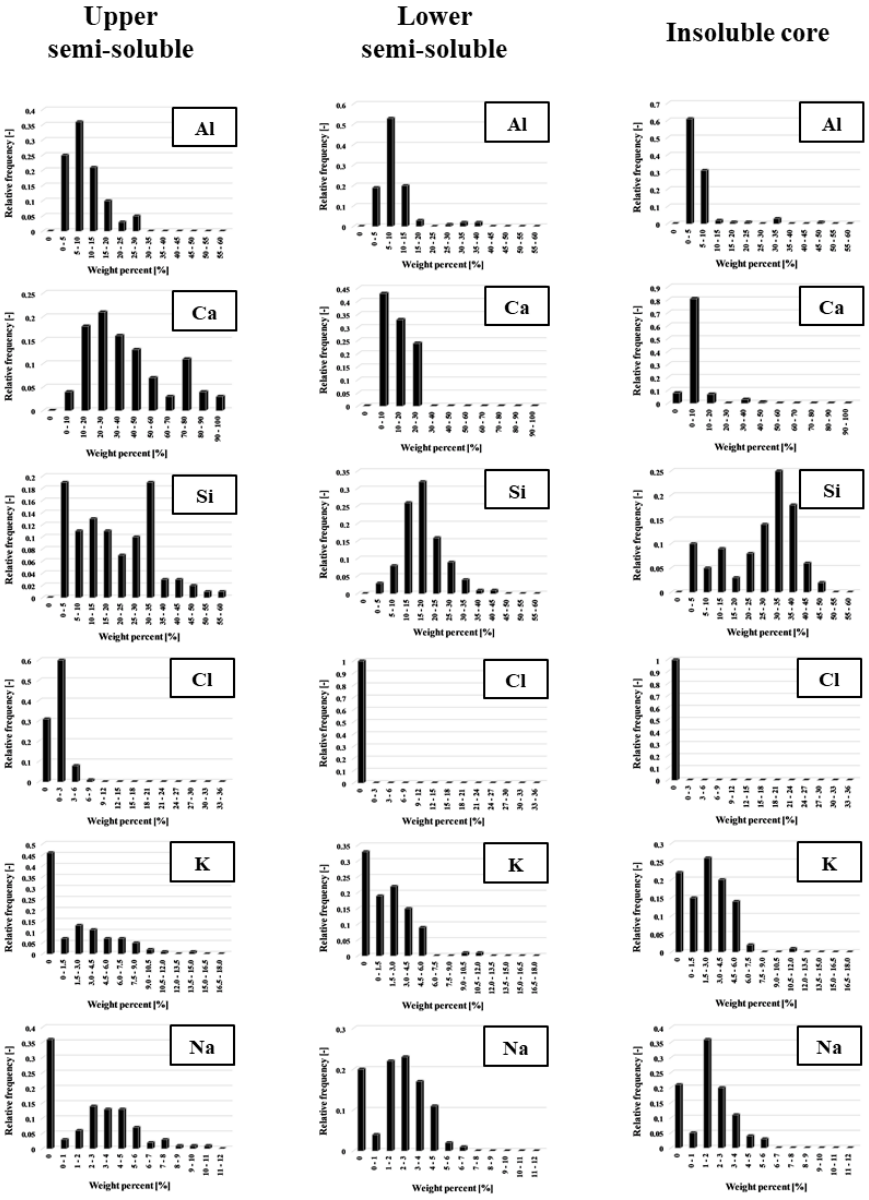

Figure 2.11 Relative frequency of major elements average concentration of elements in component matrices of fly ash particle (unit: weight percent)

The distributions of elemental concentrations in the semi-soluble and insoluble core components for fly ash is shown in **Figure 2.11**. Inter-particle heterogeneities of Cl, K, and Na in semi-soluble components are 38%, 72%, and 32% larger than those of the surface component, respectively. Moreover, inter-particle heterogeneities of Na and K in the insoluble core component are 6% and 24% larger than the surface component. Ca inter-particle heterogeneities in semi-soluble and insoluble core

components are also more than 30% larger than that of the surface component. On the other hand, Al and Si inter-particle heterogeneities of the semi-soluble component are 3-54% smaller than those of the surface component. Although Si inter-particle heterogeneity of the insoluble core components is also lower than that of the surface component, Al inter-particle heterogeneity is more significant. In the previous section 3.2, the authors suggest that finer "flyable" silica sand particles might transfer to the gas phase in the combustor. Smaller Si inter-particle heterogeneity partially supports this expectation.

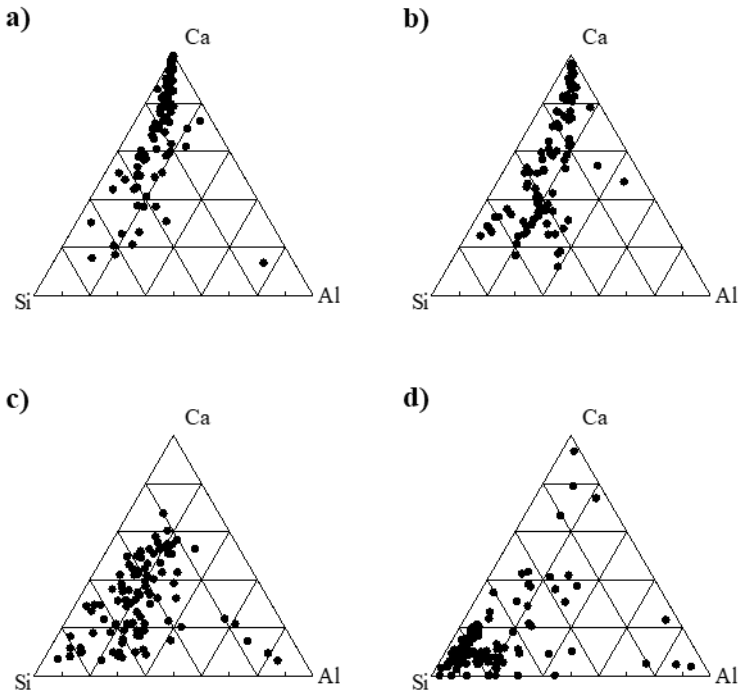

Figure 2.12 Ternary diagram of a) surface, b) upper semi-soluble, c) lower semi-soluble, and d) insoluble core components of MSWI fly ash particles

To clearly show inter-particle heterogeneity of each component of fly ash particles, the ternary diagrams of Al, Ca, and Si is shown in **Figure 2.12**. As explained in the previous section 3.1, the fly ash has more Si-rich cores. In fly ash formation processes, core components would be formed at the first stage. The ternary diagram suggests that flyable fine particles of silica sand and/or gaseous silicate evaporated from combusted wastes would predominantly establish the core component of fly ash particles. In contrast, the core component of the stoker combustor fly ash would be formed Al-, Ca- and Si-rich materials, which are considered as Al_2O_3, $CaTiO_3$, and SiO_2 [9]. After the formation of the Si-

based core component, semi-soluble Al/Ca/Si-based components would be formed around the insoluble core component. **Figure 2.12c** clearly shows that semi-soluble Al/Ca/Si-based components of the fly ash are closer to the Si-rich region. It suggests that flyable fine particles of silica sand still contributes to a major part of the formation of the lower semi-soluble component. According to **Figure 2.12b**, upper semi-soluble components of the fluidized bed combustor fly ash are shifting to the Ca-rich region. It suggests that Ca-based materials and/or unreacted $Ca(OH)_2$ are mainly contributing to the formation of the upper semi-soluble components in the fluidized bed combustor. As described in this section above, the surface component has a larger inter-particle heterogeneity of Al and Si than the semi-soluble component. **Figure 2.12** visualizes them by more full dispersive dots in the diagrams. Heterogeneity could explain the fly ash formation process. The formation of the insoluble core component of fly ash depends on the type of combustor. Stoker combustor fly ash consisted of Al/Ca/Si-based insoluble core component. However, fluidized combustor fly ash formed a Si-based core component. Nevertheless, fly ash from both combustors contained Al/Ca/Si-based semi-soluble components.

2.3.6 Element association priorities estimated based on elemental heterogeneity

The molar-based ternary diagrams for each fly ash particle component are shown in **Figure 2.13**. Dots concentrated in the center of the Cl-Na-K molar-based ternary diagram, shown in **Figure 2.13a**, suggests that chlorine is associated equally with Na and K. Chlorine is also associated with Ca and Mg equally or relatively more with Ca (see **Figure 2.13b**). In the previous section 3.4, not only NaCl/KCl but also other chlorides like $CaCl_2$ are suggested as a significant source of surface Cl. The ternary diagram agrees with this suggestion. Also, comparable associations are observed between S and alkaline elements (K and Na) (see **Figure 2.13c**). S is associated with Ca with a slightly higher priority than Mg (see **Figure 2.13d**). These results are consistent with higher HCl and SO_2 removal efficiencies of Ca than Mg [18, 19]. Al-Ca-Si diagram, shown in **Figure 2.13e,** shows concentrated dots in the center and Ca-rich region. In the previous section 3.4, significant forms of surface Ca was suggested as the exposed surface of the semi-soluble component (Ca-based matrices with aluminosilicate domains) and/or unreacted $Ca(OH)_2$. The ternary diagram supports this suggestion. According to XRD analysis,

shown in **Figure 2.4**, concentrated dots in the Ca-rich region of the diagram might be derived from calcite ($CaCO_3$), not unreacted $Ca(OH)_2$.

In both upper and lower semi-soluble components, XRD analysis, shown in **Figure 2.4**, identified gehlenite ($Ca_2Al_2SiO_7$). On the other hand, **Figure 2.14a** shows dispersed dots around the gehlenite point. It suggests that gehlenite is limited parts of the upper semi-soluble component, and major parts are amorphous Ca-based matrices with aluminosilicate domains and calcite ($CaCO_3$).

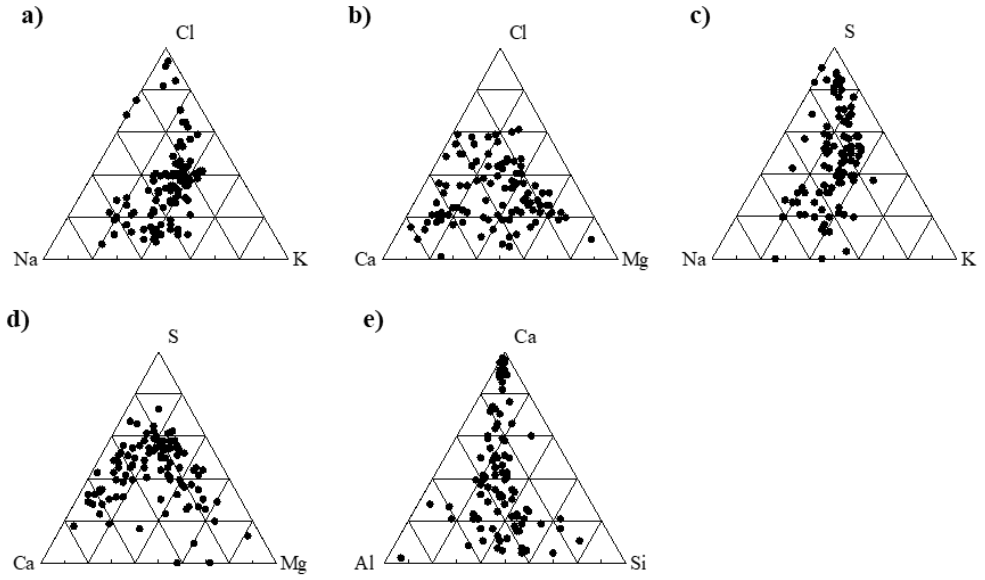

Figure 2.13 Molar-based ternary diagram of the surface of MSWI fly ash particles

In the insoluble core component, albite ($NaAlSi_3O_8$), quartz (SiO_2), rutile (TiO_2), and hematite (Fe_2O_3) were identified (see **Figure 2.4**). The Al-Na-Si molar-based ternary diagram, shown in **Figure 2.14b,** agrees with this result. The Ca-Fe-Ti diagram shows that dots are concentrated along the Fe-Ti line (see **Figure 2.14c**). On the other hand, dots are dispersed in the Si-Fe-Ti diagram (see **Figure 2.14d**). These suggest that rutile (TiO_2) and hematite (Fe_2O_3) are adsorbed onto flyable fine silica sand particles at the early stage of the fly ash formation process. It might happen before the gas neutralization process by lime injection. Besides, rutile (TiO_2) and hematite (Fe_2O_3) might be aggregated together in the gas phase before the adsorption. The line profile analysis, shown in **Figure 2.9b**, clearly displays the similar variations of these element concentrations along with the distance. On the other hand, the Al-Fe-Ti diagram also shows similar dispersion as well as the Si-Fe-Ti diagram (see **Figure 2.14e**).

Two possible pathways are proposed in terms of metal encapsulation into the insoluble core component. The first is that gaseous aluminosilicate firstly associates with evaporated metals in the gas phase and then dropped onto fine silica sand particles. The other is that metals are adsorbed onto silica sand particles first and then associated with Al. In both cases, these metals are finally encapsulated in aluminosilicate matrices. These metals, detected after the JLT19 test, were not leached out even under pH1.0 acid condition. Therefore, metal encapsulation into aluminosilicate matrices gives secure immobilization. Overall, it showed good agreement between the ternary diagram and XRD results. The ternary diagram can present of element association in fly ash particles. It is useful for a better understanding of the fly ash formation process. In this chapter, there are two possible pathways of metal encapsulation in the core components of fly ash particles.

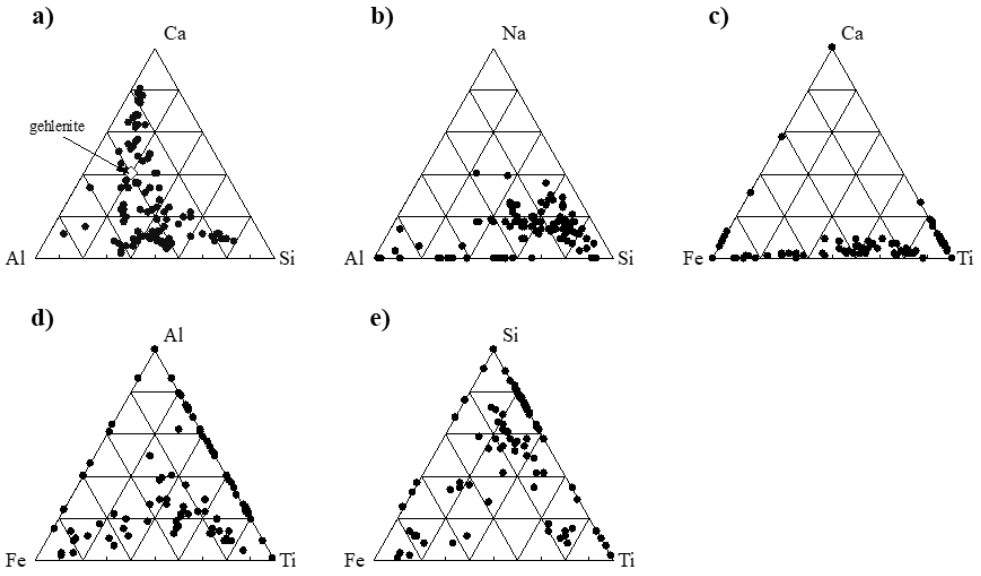

Figure 2.14 Molar-based ternary diagram of **a)** upper semi-soluble components, **b)**, **c)**, **d)** and **e)** insoluble core components of MSWI fly ash particles

2.3.7 The possible impact of elemental heterogeneity on metal leachability

In the fluidized bed combustor, a fly-up of silica sand particles with comparable diameter to fly ash particles from the bed is limited. However, flyable finer silica sand particles would contribute to the formation of insoluble core components as well as evaporated silicate. It makes the insoluble core component less heterogeneous (smaller inter-particle heterogeneity). Si-base materials still would play

an essential role in the formation of semi-soluble components in the fluidized bed combustor. Si-base materials still contribute to the semi-soluble component formation in the fly ash particle. It would cause enormous Si inter-particle heterogeneity in the upper semi-soluble and the surface components. Significant heterogeneity of semi-soluble components might give non-negligible impacts on toxic metal leaching behaviors. In general, it is assumed that toxic metal leachabilities are mainly controlled by pH and solubility of metal species [15, 20, 21].

On the other hand, some toxic metals are incorporated in Al-, Ca-, and Si-based materials like the Al-rich phase, calcite phase, and glass phase [22, 23]. Inconsistency between geochemical simulation and experimental data of incinerator residue had been clarified in other research. They found the significant gaps in the geochemical model and measured value correlate with pH value in the alkaline range. Overestimation by models dominated the behaviors of most metal in the alkaline pH range [24]. If external matrices around toxic metals also control metal leaching behaviors, their heterogeneities might be necessarily considered. It might explain gaps between experimental leaching concentrations of metals and geochemical model predictions. The impact of intra- and inter-particle heterogeneities on metal leachabilities should be evaluated as a next step.

2.4 Conclusion

In this chapter, two types of heterogeneities, intra-particle heterogeneity, and inter-particle heterogeneity, of fly ash particles produced in a fluidized bed combustor were evaluated quantitatively. Heterogeneities were measured in three components of fly ash particle bodies; surface, semi-soluble, and insoluble core components. Intra-particle heterogeneity is the heterogeneity inside each fly ash particle. Inter-particle heterogeneity is the heterogeneity among fly ash particles. The surface component of fly ash particles has 14-21 % larger intra-particle heterogeneities of Al and Si but 6-15 % smaller Ca intra-particle heterogeneity than the semi-soluble and the insoluble core components. In terms of inter-particle heterogeneity, the semi-soluble and insoluble core components have 30-72 % larger heterogeneity of Ca, Cl, K, and Na than the surface component. On the other hand, the surface component has 3-54 % larger Al and Si inter-particle heterogeneities then the semi-soluble component.

Although uncertainty owing to limited observations taken into account, this chapter concludes that fly ash is heterogeneous within its body and among individual particles.

Heterogeneity analysis presents some insight into the fly ash formation process. In the fluidized bed combustor, flyable fine particles of silicate from silica sand and/or evaporated silicate mainly contribute to the formation of the insoluble core component. At the same time, Fe and Ti oxides were encapsulated inside the core. Flyable silicate particles are still crucial in following the formation of lower semi-soluble components, but Ca adsorption becomes dominant in the formation of upper semi-soluble components. It is different from the stoker combustor.

On the other hand, Ca-based matrices with aluminosilicate domains mainly consist of upper semi-soluble components of fly ash particles for both the fluidized bed combustor and the stoker combustor. NaCl and KCl adsorptions occur in the late stage of fly ash formation. Cl and S are associated with Ca with slightly higher priority than Mg. If external matrices around toxic metals influence metal leaching behaviors, heterogeneities of fly ash particle components might explain gaps between geochemical simulation and experimental results.

2.5 References

1. Ohbuchi A, Koike Y, Nakamura T (2019) Quantitative phase analysis of fly ash of municipal solid waste by X-ray powder diffractometry/Rietveld refinement. J Mater Cycles Waste Manag 21:829–837. doi: 10.1007/s10163-019-00838-0
2. Weibel G, Eggenberger U, Kulik DA, et al. (2018) Extraction of heavy metals from MSWI fly ash using hydrochloric acid and sodium chloride solution. Waste Manag. 76:457–471
3. Phua Z, Giannis A, Dong ZL, et al. (2019) Characteristics of incineration ash for sustainable treatment and reutilization. Environ Sci Pollut Res 26:16974–16997. doi: 10.1007/s11356-019-05217-8
4. Luo H, Cheng Y, He D, Yang EH (2019) Review of leaching behavior of municipal solid waste incineration (MSWI) ash. Sci. Total Environ. 668:90–103
5. Ha J, Chae S, Chou KW, et al. (2016) Characterization of Class F Fly Ash Using STXM: Identifying Intraparticle Heterogeneity at Nanometer Scale. J Nanomater 2016. doi: 10.1155/2016/8072518
6. Fermo P, Cariati F, Pozzi A, et al. (2000) Analytical characterization of municipal solid waste incinerator fly ash. Part II. Fresenius J Anal Chem 366:267–72
7. Rémond S, Pimienta P, Bentz D. (2002) Effects of the incorporation of Municipal Solid Waste Incineration fly ash in cement pastes and mortars. Cem Concr Res 32:303–311. doi: 10.1016/S0008-8846(01)00674-3
8. Mahieux PY, Aubert JE, Cyr M, et al. (2010) Quantitative mineralogical composition of complex mineral wastes - Contribution of the Rietveld method. Waste Manag 30:378–388. doi: 10.1016/j.wasman.2009.10.023
9. Kitamura H, Dahlan AV, Tian Y, et al. (2019) Intra- and inter-particle heterogeneity of municipal solid waste incineration fly ash particles. J Mater Cycles Waste Manag 0:0. doi: 10.1007/s10163-019-00853-1
10. Camerani MC, Golosio B, Somogyi A, et al. (2004) X-ray Fluorescence Tomography of Individual Municipal Solid Waste and Biomass Fly Ash Particles. Anal Chem 76:1586–1595. doi: 10.1021/ac030282w

11. Kitamura H, Sawada T, Shimaoka T, Takahashi F (2016) Geochemically structural characteristics of municipal solid waste incineration fly ash particles and mineralogical surface conversions by chelate treatment. Environ Sci Pollut Res 23:734–743. doi: 10.1007/s11356-015-5229-5

12. Kitamura H, Dahlan AV, Tian Y, et al. (2018) Impact of secondary generated minerals on toxic element immobilization for air pollution control fly ash of a municipal solid waste incinerator. Environ Sci Pollut Res 1–13. doi: 10.1007/s11356-018-1959-5

13. Atanes E, Cuesta-García B, Nieto-Márquez A, Fernández-Martínez F (2019) A mixed separation-immobilization method for soluble salts removal and stabilization of heavy metals in municipal solid waste incineration fly ash. J Environ Manage 240:359–367. doi: 10.1016/j.jenvman.2019.03.122

14. Hu HY, Liu H, Shen WQ, et al. (2013) Comparison of CaO's effect on the fate of heavy metals during thermal treatment of two typical types of MSWI fly ashes in China. Chemosphere 93:590–596. doi: 10.1016/j.chemosphere.2013.05.077

15. Wang L, Chen Q, Jamro IA, et al. (2016) Geochemical modeling and assessment of leaching from carbonated municipal solid waste incinerator (MSWI) fly ash. Environ Sci Pollut Res 23:12107–12119. doi: 10.1007/s11356-016-6320-2

16. Kitamura H, Dahlan AV, Tian Y, et al. (2017) Geochemical form analysis of titanium in chelate-treated municipal solid waste incineration fly ash particles employing correlation analysis of elemental distribution line profiles. J Japan Soc Civ Eng 73: III_287-III_295. doi: 10.2208/jscejer.73.III_287

17. Chang FY, Wey MY (2006) Comparison of the characteristics of bottom and fly ashes generated from various incineration processes. J Hazard Mater 138:594–603. doi: 10.1016/j.jhazmat.2006.05.099

18. Cao J, Zhong W, Jin B, et al. (2014) Treatment of hydrochloric acid in flue gas from municipal solid waste incineration with Ca-Mg-Al mixed oxides at medium-high temperatures. Energy and Fuels 28:4112–4117. doi: 10.1021/ef5008193

19. Nimmo W, Patsias AA, Hall WJ, Williams PT (2005) Characterization of a process for the in-

furnace reduction of NO x, SO2, and HCl by carboxylic salts of calcium. Ind Eng Chem Res 44:4484–4494. doi: 10.1021/ie0501780

20. Zhang Y, Cetin B, Likos WJ, Edil TB (2016) Impacts of pH on leaching potential of elements from MSW incineration fly ash. Fuel 184:815–825. doi: 10.1016/j.fuel.2016.07.089

21. Astrup T, Dijkstra JJ, Comans RNJ, et al. (2006) Geochemical Modeling of Leaching from MSWI Air-Pollution-Control Residues. Environ Sci Technol 40:3551–3557. doi: 10.1021/es052250r

22. Wang L, Jin Y, Nie Y (2010) Investigation of accelerated and natural carbonation of MSWI fly ash with a high content of Ca. J Hazard Mater 174:334–343. doi: 10.1016/j.jhazmat.2009.09.055

23. Saffarzadeh A, Shimaoka T, Wei Y, et al. (2011) Impacts of natural weathering on the transformation/neoformation processes in landfilled MSWI bottom ash: A geoenvironmental perspective. Waste Manag 31:2440–2454. doi: 10.1016/j.wasman.2011.07.017

24. Yin K, Chan WP, Dou X, et al. (2018) Co-complexation effects during incineration bottom ash leaching via comparison of measurements and geochemical modeling. J Clean Prod 189:155–168. doi: 10.1016/j.jclepro.2018.03.320

25. Evan J, Williams P (2000) Heavy metal adsorption onto fly ash in waste incineration flue gases. Process Saf Environ 78:40-46. doi: 10.1205/095758200530439

26. Zhao J, Wei X, Li T, et al. (2018) Behavior of Alkali Metals in Fly Ash during Waste Heat Recovery for Municipal Solid Waste Incineration. Energy and Fuels 32:4417-4423. doi: 10.1021/acs.energyfuels.7b03001

2.6 Supplementary materials

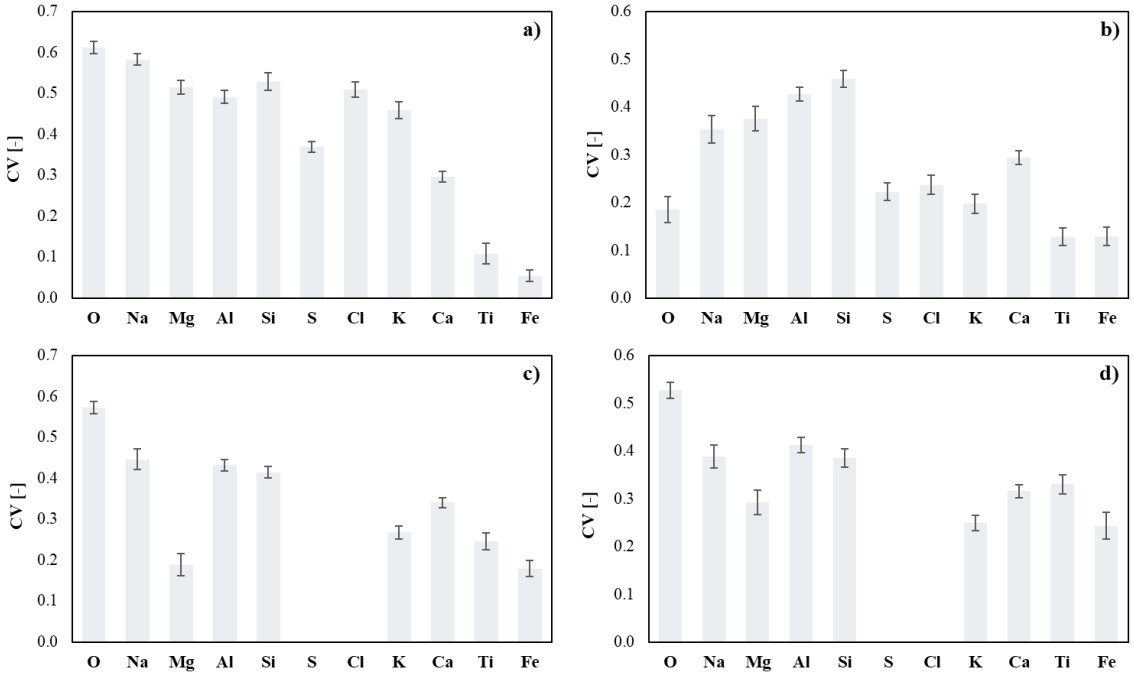

Figure S. 2-1 Average CV value of fly ash from the fluidized bed

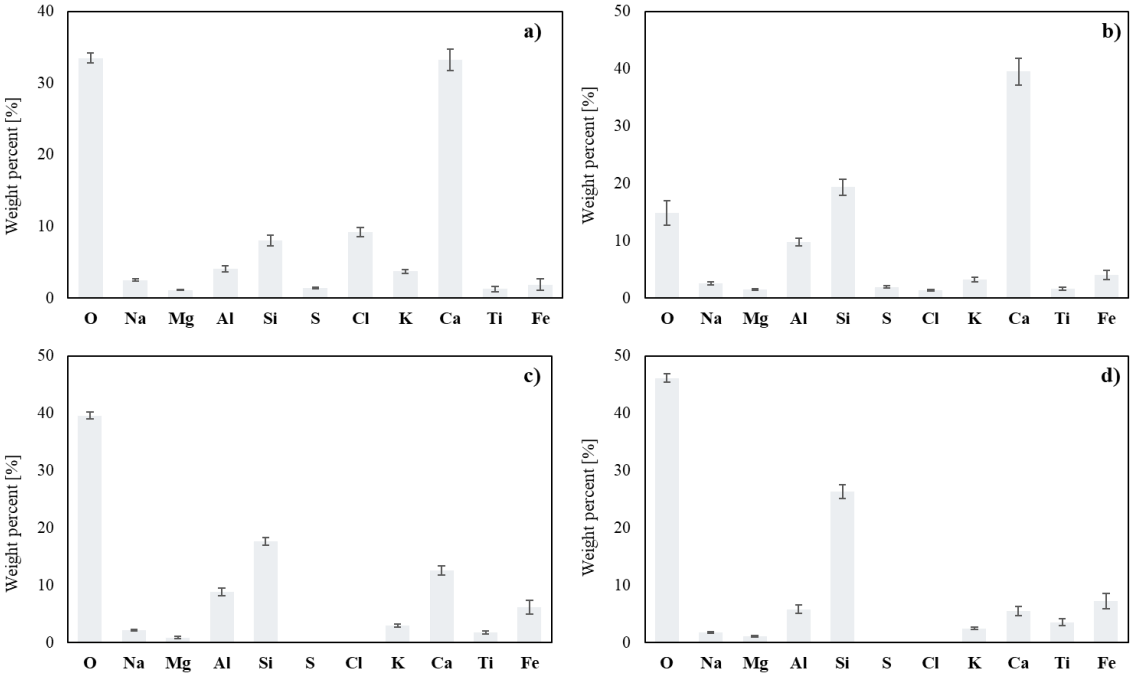

Figure S. 2-2 Average concentration of fly ash from the fluidized bed

Chapter 3

Comparison heterogeneities of fly ash particles generated from a fluidized bed combustor and a stoker combustor of municipal solid waste incineration

Abstract: Type of combustors may influence ash characterization. This study quantitatively investigated two categories of heterogeneity of fly ash produced from a stoker and a fluidized bed combustor. When two combustor fly ash is compared, the surface, semi-soluble, and insoluble core components of the fluidized bed combustor fly ash have larger intra- and inter-particle heterogeneities than the stoker combustor fly ash. This study found that this was caused partially/greatly by different Si behaviors in the fly ash formation process between the stoker and the fluidized bed combustors. Heterogeneity analysis suggests that Si plays more critical roles in the fly ash formation process of the fluidized bed combustor than that of the stocker combustor.

3.1 Introduction

Geochemical characteristics of leaching behaviors of heavy metals of fly ash have already been investigated by numerous researches [1–6]. The incineration bottom ash was a heterogeneous matrix because of the different nature of MSW burnt in the incineration system. On the other hand, MSWI fly ash is composed of fine particles. Ha, et al. reported that fly ash had been identified as compositional heterogeneity from the spherical glass phase and crystalline phase. They reported heterogeneous spatial distribution of elements in the fly ash particles [7].

Moreover, fly ash particles have homogeneous physical areas and various chemical areas in a large sample [8]. Based on mineralogical composition, Rémond et al. reported that MSWI fly ash is quite heterogeneous but regarded as homogeneous in individual particle levels [9]. Another result of micro-fluorescence tomography showed that major elements were distributed heterogeneously inside the fly ash particles [10].

Our research group investigated geochemical structures of a stoker incinerator fly ash [11]. Fly ash particles had different geochemical components that consist of soluble KCl/NaCl-based aggregates on the surface, Al/Ca/Si-based semi-soluble matrices, and Si-based insoluble core matrices. Moreover, fly ash had an active mineralogical surface on which secondary minerals could be generated under wet conditions. Although secondary mineral formation can immobilize leachable elements, its effect is limited [12]. In our previous research [13], heterogeneity in fly ash particles generated from a stoker combustor had been investigated.

On the other hand, heterogeneity of fly ash generated in another type of incinerator (fluidized bed) is still uncertain. According to previous researches, comparative analysis of fly ash particles from stoker and fluidized bed combustors showed different characteristics of their fly ash. [14–17]. Therefore, we investigated the heterogeneity of fly ash from a fluidized bed combustor and compared its heterogeneity with fly ash from a stoker combustor.

3.2 Materials and methods

3.2.1 Fly ash samples

Fly ash samples were obtained from two types of MSW incineration plants in Japan, namely stoker incinerator and fluidized bed incinerator. The capacities of the incinerator plants were 432 Mg/day and 250 Mg/day, respectively. In both incinerators, $Ca(OH)_2$ slurry and pulverized activated carbon were injected into flue gas for acidic gas neutralization and dioxin control. Fly ash was trapped by fabric filter, then transferred to a storage tank by an air pressure feeder or a mechanical feeder. After that, MSWI fly ash was conveyed from the storage tank to the chelate treatment apparatus. Fly ash samples of both incinerators were collected from the chelate treatment apparatus. All samples were dried under room conditions for one week or longer. After drying, fly ash samples were observed and analyzed. Elemental compositions of fly ash samples were analyzed by energy dispersive X-ray fluorescence spectrometer (XRF: S2 RANGER/LE, BRUKER AXS). Residual materials of both MSWI fly ash collected after JLT46, TCLP, and JLT 19 that used for elemental heterogeneity of other components of fly ash; semi-soluble and insoluble core component.

3.2.2 Microscopic observation of fly ash particles

The morphological surface of MSWI fly ash particles was observed using a scanning electron microscope (SEM; JSM-6610LA, JEOL Ltd., Japan). The fly ash samples were fixed on the carbon tape on the observation stage. Because it might cause overestimation of carbon content, carbon content would not be presented in this research. The samples were observed after Pt-Pd sputtering for 30 seconds using a sputter coating device (MSP-1S, Vacuum device Ltd., Japan). The elemental composition of fly ash particles was analyzed using energy-dispersive x-ray spectroscopy (EDX) attached to SEM (SEM-EDX JSM-6610 LA, JEOL, Ltd., Japan). Elemental mapping of fly ash particle surfaces was carried out to analyze elemental distribution. In this study, one hundred particles of original fly ash and leaching test residues were analyzed by SEM-EDX. In total, 800 particles were observed in this study. The mineral composition of fly ash particles is analyzed using x-ray diffraction (XRD; MultiFlex, Rigaku Co., Japan). The measured fly ash samples were conducted using CuKα radiation (λ

= 1.5418 Å, U=40keV, I=25mA) to identify the crystal phase on the samples. XRD analysis was conducted from 5° to 75° of 2θ at a rate of 1° min^{-1}.

3.2.3 Elemental heterogeneity analysis based on the surface elemental concentration

Surface elemental concentrations of each fly ash particle, measured by SEM-EDX as described above, were used to analyze elemental heterogeneity of fly ash particles. In this study, we investigated two types of heterogeneity. The first is intra-particle heterogeneity, and the other is inter-particle heterogeneity. Intra-particle heterogeneity means heterogeneity of individual fly ash particles. After the elemental distribution of 100 particles of the original fly ash (the stoker combustor and the fluidized bed combustor fly ash) and leaching, test residues were measured (elemental mapping), each single-particle were divided into five sections equally (see **Figure 3.1a**).

It should be noted that the area size of each section in all measured particles was different depending on particle size. Inline profile analysis, all intensity data, which directly correlated to element concentrations, were extracted from 5 sections of each particle and then integrated. Owing to the different size of section areas, the quantity of intensity data was correspondingly different for each particle. The coefficient of variation (CV value = standard deviation/average) was calculated for each element, and each particle using intensity data. The CV values were plotted in the histogram to visualize the distribution of CV values for each element. The quantity of intensity data weighted the average CV values. In this study, the weighted average of CV values was used as a quantitative indicator of the intra-particle heterogeneity.

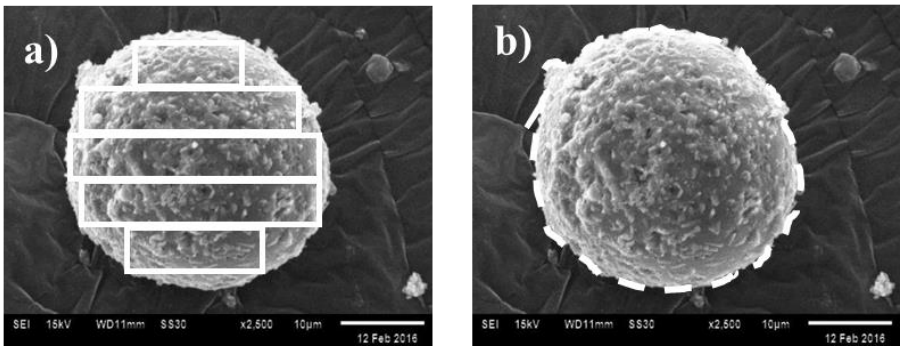

Figure 3.1 Elemental heterogeneity analysis: a) line profile analysis and b) area analysis

On the other hand, inter-particle heterogeneity means heterogeneity among fly ash particles. According to elemental mapping data, average elemental concentrations of each particle were calculated as weight percent [wt%] (see **Figure 3.1b**). They were plotted in the histogram to visualize the distribution of average elemental concentrations. CV values of average elemental concentrations were calculated and used as a quantitative indicator of inter-particle heterogeneity. It is noted again that the weighted average of CV values of 100 particles was used to evaluate intra-particle heterogeneity.

On the other hand, the CV values of 100 average elemental concentrations (100 particles) were used to evaluate inter-particle heterogeneity. It should be noted that 100 particle analysis might still be insufficient. Therefore, this analysis offers limited specific results and conclusions. Uncertainty owing to limited observations should be taken into account (see **Figure S.3-1 and S.3-2**). In this study, both heterogeneities were investigated, focusing on the surface components, semi-soluble components, and insoluble core components of fly ash particles.

3.3 Results and discussion

3.3.1 Similarity assessment of combusted wastes based on elemental contents

Fly ash samples were taken from a stoker type incinerator and a fluidized bed incinerator in different sites and at different times. Therefore, the characteristics of wastes combusted in these incinerators should be different, and it might cause vast differences in fly ash characteristics correspondingly. At first, this study assesses the similarity or differences in waste characteristics focusing on elemental content. The elemental contents of both combustor fly ash are listed in **Table 3.1**. Elemental contents of bottom ash taken from the stoker combustor are also listed in **Table 3.1**. Ca content of both combustor fly ash is almost equal. It is reasonable because Ca in fly ash is mainly derived from lime for exhaust gas neutralization. In both stoker/fluidized bed incineration plants, lime was injected with around 3-4 times a more significant rate than stoichiometry neutralization requirement.

Table 3.1 Elemental composition of MSWI bottom ash and fly ash samples determined by XRF

Elements	Stoker			Fluidized bed	Differences
	Bottom ash	Fly ash	Mixture	Fly ash	
Al	3.9706	4.645	4.105	5.891	-30%
Ca	22.379	45.51	27.00	44.79	-40%
Cl	1.5700	21.71	5.598	13.73	-59%
K	0.4298	7.297	1.803	5.253	-66%
Mg	1.5480	1.190	1.476	1.790	-18%
S	0.3500	2.546	0.789	1.240	-36%
Si	17.383	5.996	15.11	13.08	15%
Ba	0.0835	0.225	0.112	0.446	-75%
Br	0	0.419	0.084	0.123	-32%
Cd	0.0001	0.037	0.007	0	-
Cr	0.0441	0.097	0.055	0.074	-26%
Cu	0.1710	0.200	0.177	1.006	-82%
Fe	1.8060	1.928	1.830	6.188	-70%
Mn	0.0710	0.125	0.082	0.277	-70%
Ni	0.0133	0	0.011	0.047	-77%
Pb	0.1079	0.779	0.242	0.470	-48%
Sb	0.0004	0.299	0.060	0.081	-26%
Sn	0.0064	0.225	0.050	0.130	-61%
Sr	0.0362	0.070	0.043	0.110	-61%
Ti	0.9780	2.406	1.264	2.351	-46%
Zn	0.3295	3.813	1.026	1.824	-44%
Zr	0.0005	0.031	0.007	0.061	-89%

According to elemental contents of bottom ash and fly ash from the stoker combustor, elemental contents of their mixture were calculated and then compared with those of the fluidized combustor fly ash excluding Ca. It is shown in **Figure 3.2**. There is good agreement between the fluidized bed combustor fly ash and stoker combustor mixture (bottom ash with fly ash). As a reference, the same comparison using bottom/fly ash samples of 19 stoker combustors and seven fluidized bed combustors is also plotted in **Figure 3.2** [16]. Although the excellent agreement shown in **Figure 3.2** is still insufficient to verify the similarity of waste characteristics for both stoker and fluidized bed combustors,

elemental contents of major elements like Al, Mg, and Si are within ±30 % differences and those of metals like Cr, Pb, and Zn are within ±50 % differences. It might partially support the similarity of waste characteristics. However, it should be noted that some elements show significant differences between the stoker and the fluidized bed combustors. For example, 59 % difference for Cl, 36 % difference for S, 70 % difference for Fe, and 82% difference for Cu were found. In the following sections, this study assumes similar characteristics of combusted wastes in both stoker/fluidized bed incinerators and insignificant impacts of primary waste differences on fly ash heterogeneity. However, potentially non-negligible impacts of waste differences should be taken into consideration, in particular, Cl.

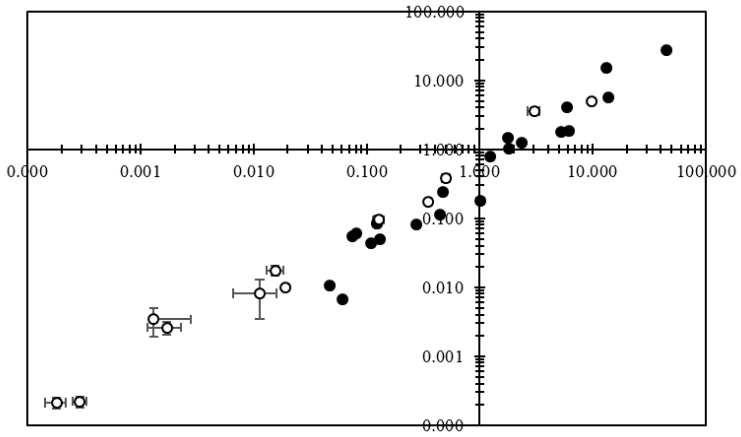

Figure 3.2 Elemental contents of mixture ash from stoker combustor and fly ash from fluidized bed combustor (black: experiments, white: literature)

3.3.2 Micro-characteristics of fly ash

The fluidized bed combustor fly ash could be categorized into two types: sphere particles and aggregates of small particles. Compared with the authors' previous results [11], the fluidized bed combustor fly ash had similar shapes with the stoker combustor fly ash, as shown in **Figure 3.3**. The chelate reagent had treated the fluidized bed combustor fly ash. However, secondary mineral crystals like cubic and spicular shapes were not found, although they were observed in the stoker combustor fly ash [11]. The fly ash from both combustors consists of quartz, calcite, sylvite, and halite, as shown in **Figure 3.4**. These crystalline phases in fly ash from fluidized bed have more variation than stoker fly

ash. The heavy metal, Fe and Ti, in the crystalline phase were detected in the surface of the fly ash particle. It might be due to non-volatile and semi-volatile elements almost wholly enriched in the fly ash of fluidized bed incinerator [16]. Fly ash from stoker has a higher peak of NaCl and KCl than fly ash from the fluidized bed.

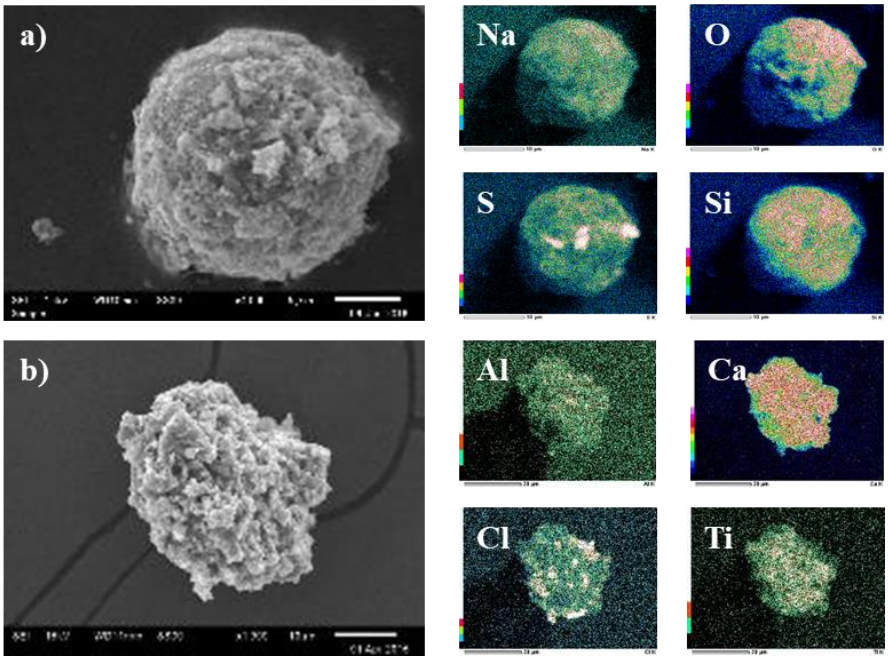

Figure 3.3 Shape and elemental mapping of fly ash particles from a) stoker-type and b) fluidized bed combustor

After leaching tests, leaching residues of both two types of fly ash have similar shapes, as shown in **Figure 3.5**. The upper semi-soluble component of fly ash particles, shown by the JLT 46 leaching test, has spicular shapes regardless of the combustor type. According to Kitamura et al., spicular shape minerals are considered as ettringite or gypsum [11]. Ettringite and gypsum were observed in both combustors. The shape of lower semi-soluble components of the fluidized bed combustor fly ash, shown by the TCLP leaching test, had more aggregates on the surface compared with the stoker combustor fly ash that had relatively smoother surface. This difference could be derived from Na and K remaining on the surface of the lower semi-soluble component of the fluidized bed combustor fly ash. It might also due to ettringite not formed in the fly ash from the fluidized bed. After the TCLP test, fly ash from a fluidized bed tends to form quartz, and Ti also detected in the upper semi-soluble components (see

Figure 3.4). In contrast, fly ash from stoker has a more ettringite crystalline phase. It might explain the different shapes of fly ash from fluidized bed and stoker combustor in the lower semi-soluble components.

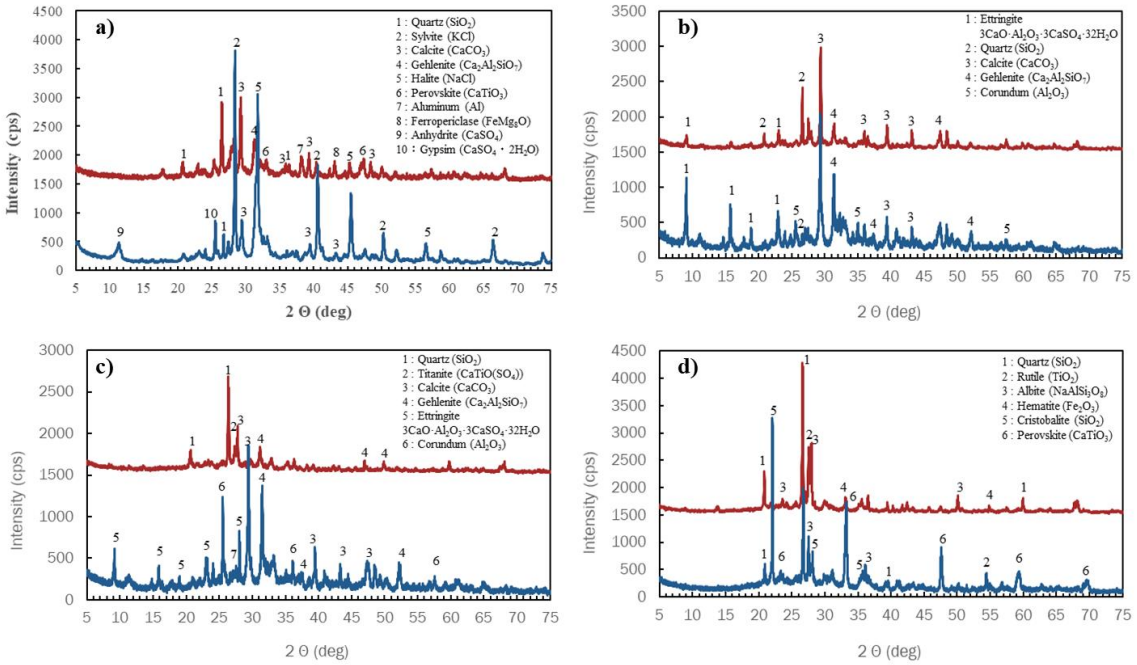

Figure 3.4 XRD patterns of **a)** surface, **b)** upper semi-soluble, **c)** lower semi-soluble, and **d)** insoluble core components of fly ash particles (blue: stoker, red: fluidized bed)

Soluble and semi-soluble components were removed entirely throughout the JLT 19 test. The insoluble core component of the stoker combustor fly ash mostly consisted of Si and had a simple structure like the tube, shell, and porous shell or complicated three-dimensional structure like skeleton [11]. In contrast to the stoker combustor fly ash, the fluidized bed combustor fly ash usually had a porous shape in their insoluble cores rather than a complicated skeleton structure (see **Figure 3.4**). According to Kitamura's further research, not only Si-base insoluble cores but also Al- and Ca-rich cores were also found for the stoker combustor fly ash [13]. On the other hand, as discussed in following section 3.6, the fluidized bed combustor fly ash usually had Si-base insoluble cores. In the core of fly ash, Fe and Ti were detected in the crystalline phase as hematite and rutile. In summary, heavy metals were detected throughout all components in the fly ash from a fluidized bed. The fluidized bed incinerator all of the ash is captured as fly ash, while stoker incinerator, the ash is separated into bottom

ash and fly ash. Therefore, the non-volatile and semi-volatile elements mainly in the bottom ash of stoker, while in the fluidized bed incinerator, tends to discharge non- and semi-volatile elements almost wholly in the fly ash.

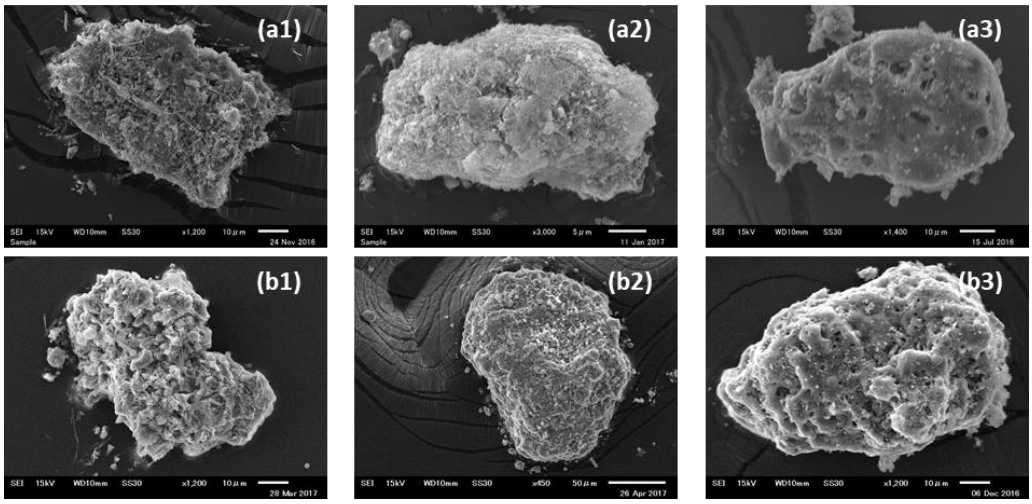

Figure 3.5 Morphological characteristics of 1) upper semi-soluble, 2) lower semi-soluble, and 3) insoluble core matrices of fly ash particles from a) stoker-type and b) fluidized bed combustor

3.3.3 Intra-particle heterogeneity of surface component of fly ash particle

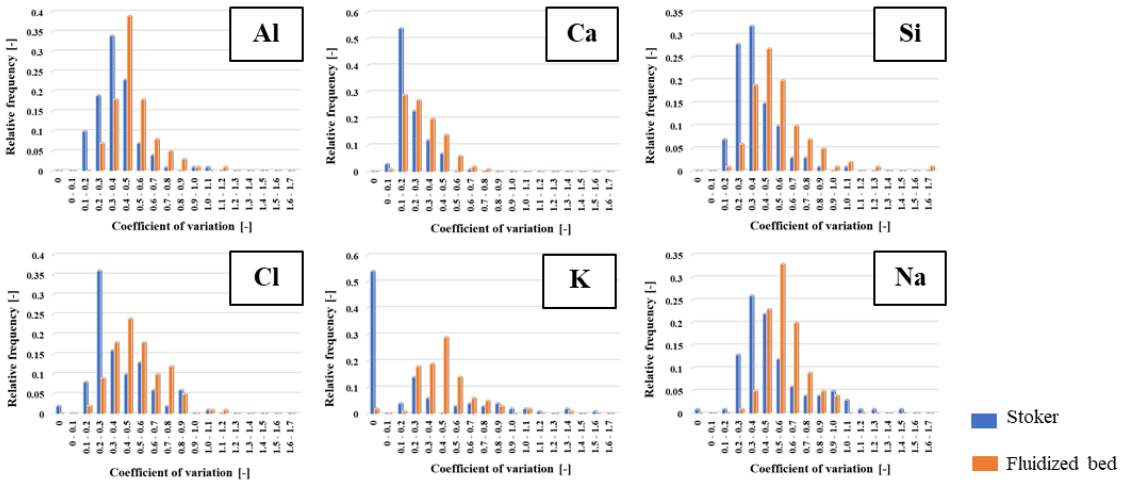

Figure 3.6 Relative frequency of coefficient variation of major elements in stoker and fluidized bed MSWI fly ash particles

The CV values of major elements in the surface component of the stoker and the fluidized bed combustor fly ash are shown in **Figure 3.6**. Their weighted averages are used for quantitative analysis

of intra-particle heterogeneity of the surface component. The ranges of CV values of Al, Ca, and Si is almost from 0 to 1.7 for both fly ash particles. Compared with other elements, Ca has the lowest intra-particle heterogeneity than other elements for both combustor fly ash, as shown in **Figure 3.7**. The lowest heterogeneity of Ca is reasonable because excess $Ca(OH)_2$ was injected in the neutralization process. In both waste incineration plants, $Ca(OH)_2$ was usually injected with a 3-4 times larger rate than stoichiometry neutralization requirement. On the other hand, a non-negligible difference of Ca heterogeneity was also found between the stoker and the fluidized bed combustor fly ash. The fluidized bed combustor fly ash has 42% larger Ca heterogeneity than the stoker combustor fly ash.

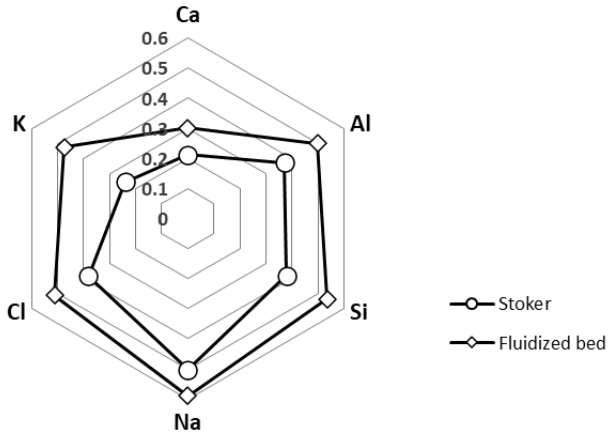

Figure 3.7 Weighted average of coefficient variation of fly ash particles

In contrast, the CV value of Si for the fluidized bed combustor fly ash ranges more widely than other major elements. The maximum CV value of Si reaches to 1.7. In general, silica sand is used as bed materials in fluidized bed combustors [14]. Because fine silica sands, which have Si homogeneity, would fly up to exhaust gas during combustion and be trapped by fabric filter, large fractions of low Si CV values were expected. However, CV analysis results shown in **Figure 3.7** are a contrast to the expectation. It suggests that a fly-up of fine silica sand that has almost the same diameter with fly ash particles (1-20 μm) is limited. However, finer "flyable" silica sand particles might transfer to the gas phase and serve as Si-rich cores in fly ash particles during formation processes. It will be discussed again in the following section 3.6. Si intra-particle heterogeneity of the fluidized bed combustor fly ash

is also 41% larger than the stoker combustor fly ash. The other major element (Al) also has larger heterogeneity for the fluidized bed combustor fly ash than the stoker combustor fly ash (see **Figure 3.7**).

The ranges of CV values of other elements (Al, Ca, Cl, and K) are not significantly different from Ca for both combustor fly ash. They are almost from 0 to 1.6. In this case, the stoker combustor fly ash has a slightly more extensive range of Na and K CV values than the fluidized bed combustor fly ash. On the other hand, intra-particle heterogeneities of Cl, K, and Na for the stoker combustor fly ash are around 25%, 49%, 15% smaller than those of the fluidized bed combustor fly ash, respectively. As clearly shown in **Figure 3.8**, the fluidized bed combustor fly ash has dispersed hotspots of Cl, K, and Na on its surface. On the other hand, those elements are more homogeneously distributed on the surface for the stoker combustor fly ash.

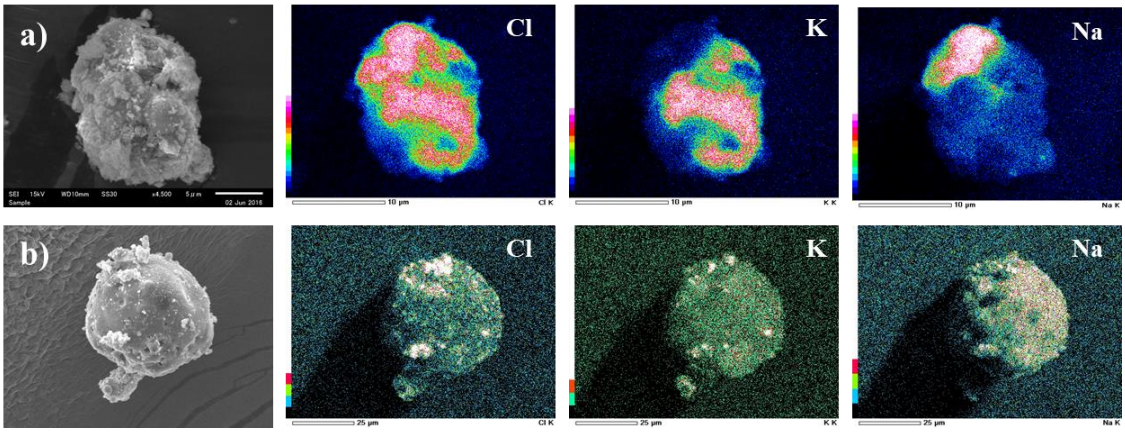

Figure 3.8 Elemental distribution of MSWI fly ash particle surface generated from a) stoker and b) fluidized bed

As a summary, weighted average CV values of major six elements (Al, Ca, Cl, K, Na, and Si) for the fluidized bed combustor fly ash are 5-1420% higher than those of the stoker combustor fly ash. It means that the surface component of the fluidized bed combustor fly ash is more heterogeneous (larger intra-particle heterogeneity) than that of fly ash particles from stoker combustor. This study assumes similar characteristics of combusted wastes in both combustors (see **Figure 3.2**) and $Ca(OH)_2$ injection rates are also comparable. Therefore, it is suggested that the fluidized bed combustor generated a more heterogeneous surface on fly ash particles than the stoker combustor.

3.3.4 Intra-particle heterogeneity of semi-soluble/insoluble core components of fly ash particles

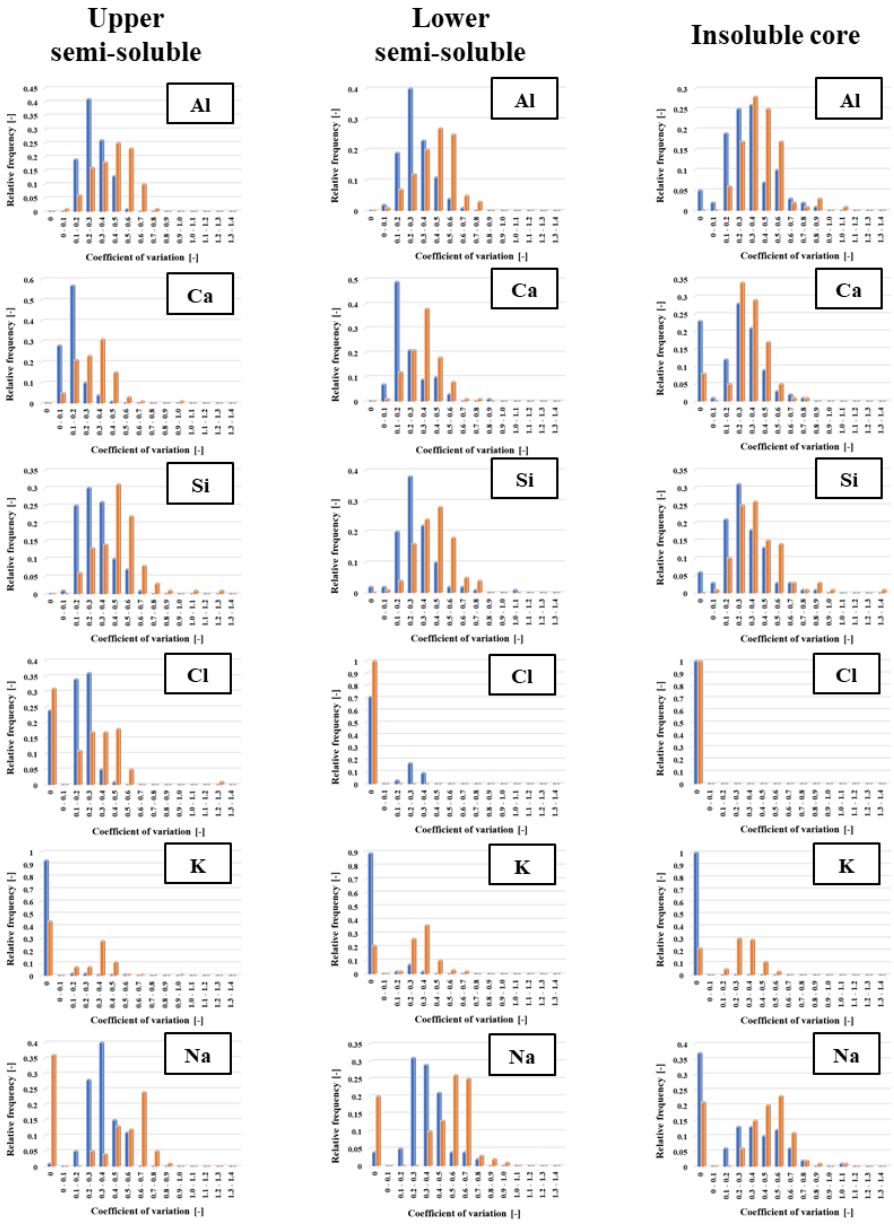

Figure 3.9 Relative frequency of coefficient variation of major elements in component matrices of fly ash particle (blue: stoker, orange: fluidized bed)

Figure 3.9 is histograms of CV values of major elements for semi-soluble and insoluble core components of fly ash from two combustors. The ranges of CV values in semi-soluble and insoluble core components are narrower than those of the surface components for both combustor fly ash. They are around 0 to 1.4. In particular, Si in semi-soluble and insoluble core components have the broadest

range of CV values than other elements. Weighted average CV values of Al and Si in semi-soluble and insoluble core components are 14% and 21% lower than those in the surface components for the fluidized bed combustor fly ash (see **Figure 3.10**). Smaller Al and Si intra-particle heterogeneities of semi-soluble and insoluble components were also observed for the stoker combustor fly ash. On the other hand, Ca intra-particle heterogeneities of lower semi-soluble and insoluble core components are 6-15% larger than those of the surface components for both combustor fly ash. In contrast, Ca intra-particle heterogeneity of upper semi-soluble components were smaller than those of the surface, lower semi-soluble, and insoluble core components for both combustor fly ash.

All components in the semi-soluble component of fly ash have 4-109% larger intra-particle heterogeneity than stokers. Moreover, Ca has smaller intra-particle heterogeneity than Al and Si in all components of both combustor fly ash. According to smaller Ca intra-particle heterogeneity than Al and Si in semi-soluble components of the stoker combustor fly ash, Kitamura et al. suggested that semi-soluble components are mainly Ca-based matrices such as $CaCl_2$, $CaCO_3$, and unreacted $Ca(OH)_2$ in which aluminosilicate domains were included [13]. It is also suggested for the fluidized bed combustor fly ash. When two combustor fly ash is compared, intra-particle heterogeneities of Al, Ca, and Si of semi-soluble and insoluble core components for the fluidized bed combustor fly ash is always 30-98 % larger than those of the stoker combustor fly ash. In comparison for all major elements, intra-particle heterogeneity of fluidized bed fly ash is 10-299% larger than the stoker combustor in the insoluble core component. It is concluded that fly ash particles from the fluidized bed combustor have more heterogeneous bodies from the surface to insoluble core components than the stoker combustor fly ash.

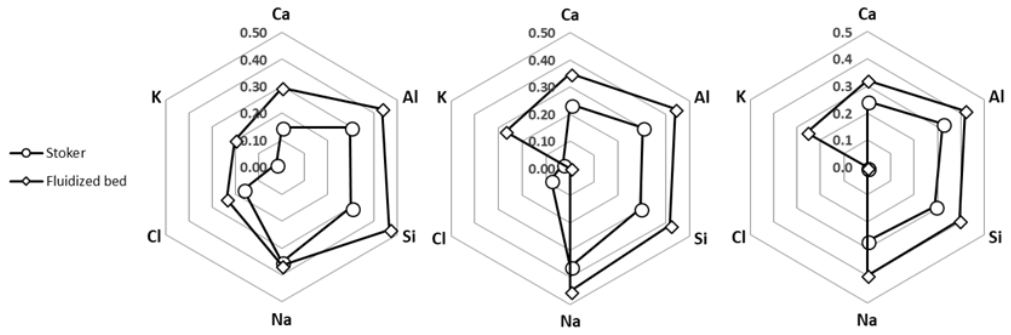

Figure 3.10 Weighted average of coefficient variation of major elements in component matrices of fly ash particles

3.3.5 Inter-particle heterogeneity of surface components of fly ash particles

The average concentrations of major elements in the surface components of fly ash particles generated from the stoker and the fluidized bed incinerators have broad distributions, as shown in **Figure 3.11**. Inter-particle heterogeneity of the surface component was evaluated quantitatively based on the CV value of the average concentration data. On the surface of fly ash, the concentration of Ca had the broadest range from 0 to 65 wt% than other elements. When the stoker and the fluidized bed combustor fly ash are compared, CV values of Al, Ca, and Si concentrations for the fluidized bed combustor fly ash are 68-99% higher than the stoker combustor fly ash. As similar to intra-particle heterogeneity, inter-particle heterogeneities of Al, Ca, and Si in the surface component of the fluidized bed combustor fly ash are also larger than those of the stoker combustor fly ash.

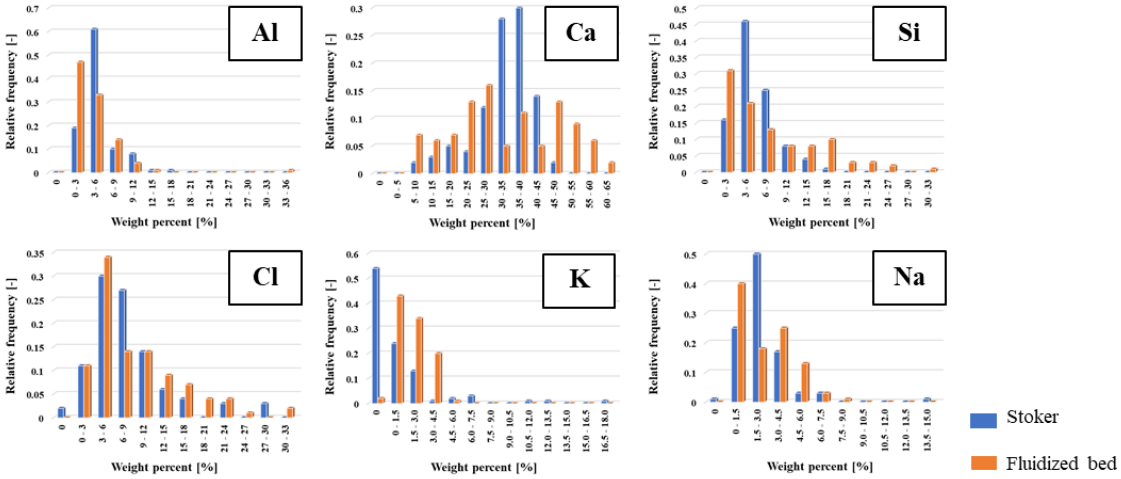

Figure 3.11 Relative frequency of major elements average concentration of chelate-treated MSWI fly ash particles (unit: weight percent)

In the case of Na, its concentration range (0 to 15 wt%) is the smallest than other elements. Inter-particle heterogeneities of Cl and Na for the fluidized bed combustor fly ash are almost comparable with those of the stoker combustor fly ash. On the other hand, K inter-particle heterogeneity of the fluidized bed combustor fly ash is 69% smaller than that of the stoker combustor fly ash. It might be derived from analysis errors of the stoker combustor fly ash. After semi-soluble components are formed around insoluble core components in fly ash formation processes, NaCl and KCl produced during gas neutralization would be adsorbed to the surface of semi-soluble components and generates

the surface component. It is considered physical sorption in which NaCl/KCl will be randomly adsorbed to the surface of fly ash particle precursors. Therefore, both intra- and inter-particle heterogeneities of Cl, K, and Na of the surface component should be similar or within a specific range. As the same with the expectation, both heterogeneities of these elements for the fluidized bed combustor fly ash are within ±14 % difference (see **Figure 3.8** and **Table 3.2**). On the other hand, the stoker combustor fly ash has significant differences among Cl, K, and Na intra-particle heterogeneities and larger K inter-particle heterogeneity than the other major elements. It might imply that other sorptions of NaCl/KCl, like chemisorption, driven and/or controlled by surface electrostatic charge, is not negligible in the fly ash formation process of the stoker combustor.

In summary, it is concluded that the fluidized bed combustor fly ash has 68-99% larger inter-particle heterogeneities of Al, Ca, and Si in the surface component than the stoker combustor fly ash. On the other hand, Na and Cl inter-particle heterogeneities are comparable between two combustor fly ash. Similar inter-particle and intra-particle heterogeneities of Cl, K, and Na were found in the surface component of the fluidized bed combustor fly ash. It supports NaCl/KCl physical sorption to the surface of fly ash particle precursors in fly ash formation processes. On the other hand, other sorption like chemisorption might be non-negligible in the stoker combustor.

3.3.6 Inter-particle heterogeneity of semi-soluble/insoluble core components of fly ash particles

The distributions of elemental concentrations in the semi-soluble and insoluble core components for both combustor fly ash are shown in **Figure 3.12**. In the case of the stoker combustor fly ash, inter-particle heterogeneities of Al, Ca, and Si in semi-soluble and insoluble core components are comparable or larger than those of the surface component. On the other hand, the fluidized bed combustor fly ash shows complicated trends. Inter-particle heterogeneities of Cl, K, and Na in semi-soluble components are 38%, 72%, and 32% larger than those of the surface component, respectively. Moreover, inter-particle heterogeneities of Na and K in the insoluble core component are 6% and 24% larger than the surface component. In semi-soluble and insoluble core components of the fluidized bed combustor fly ash, Ca inter-particle heterogeneities are larger more than 30% than the surface component. On the other hand, Al and Si inter-particle heterogeneities in the semi-soluble component

are 3-54% smaller than those of the surface component. Although Si inter-particle heterogeneity in the insoluble core components is also lower than that of the surface component, Al inter-particle heterogeneity is larger.

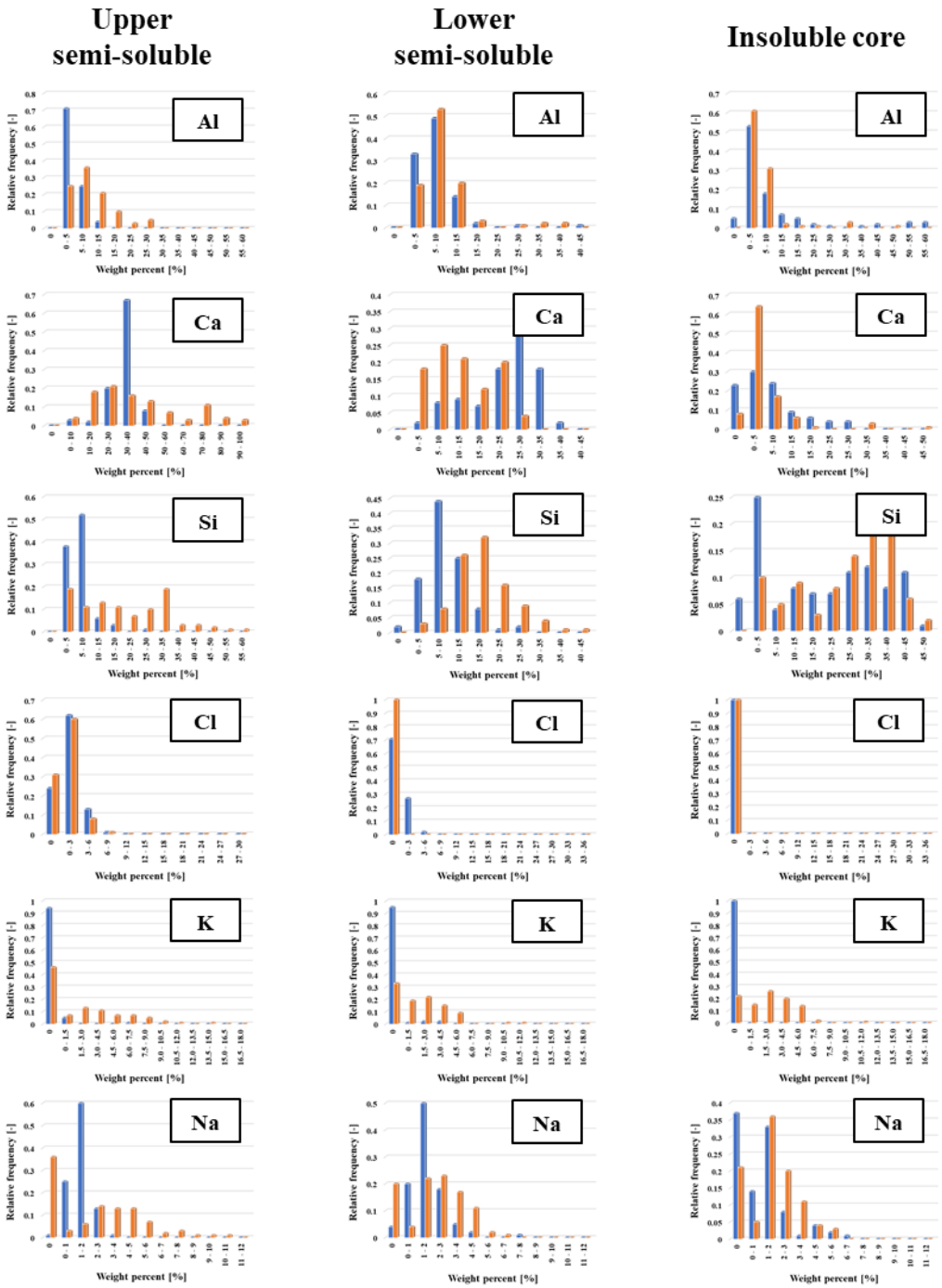

Figure 3.12 Relative frequency of major elements average concentration of elements in component matrices of fly ash particle (unit: weight percent) (blue: stoker, orange: fluidized bed)

When both combustor fly ash is compared, Ca inter-particle heterogeneities in the semi-soluble and insoluble core components of the fluidized bed combustor fly ash are 18-177 % larger than those of the stoker combustor fly ash. Larger Al and Si inter-particle heterogeneity of the fluidized bed combustor fly ash were also found in the upper semi-soluble component. On the other hand, inter-particle heterogeneity of these elements in the insoluble core component of the fluidized bed combustor fly ash is 16% smaller for Al and 41% smaller for Si, respectively. In the insoluble core component, there are less than 20 % differences between Al and Ca inter-particle heterogeneities between two combustor fly ash. On the other hand, Si inter-particle heterogeneity of the fluidized bed combustor fly ash is 41% smaller, as described above. In the previous section 3.3, the authors suggest that finer "flyable" silica sand particles might transfer to the gas phase in the combustor. Smaller Si inter-particle heterogeneity partially supports this expectation.

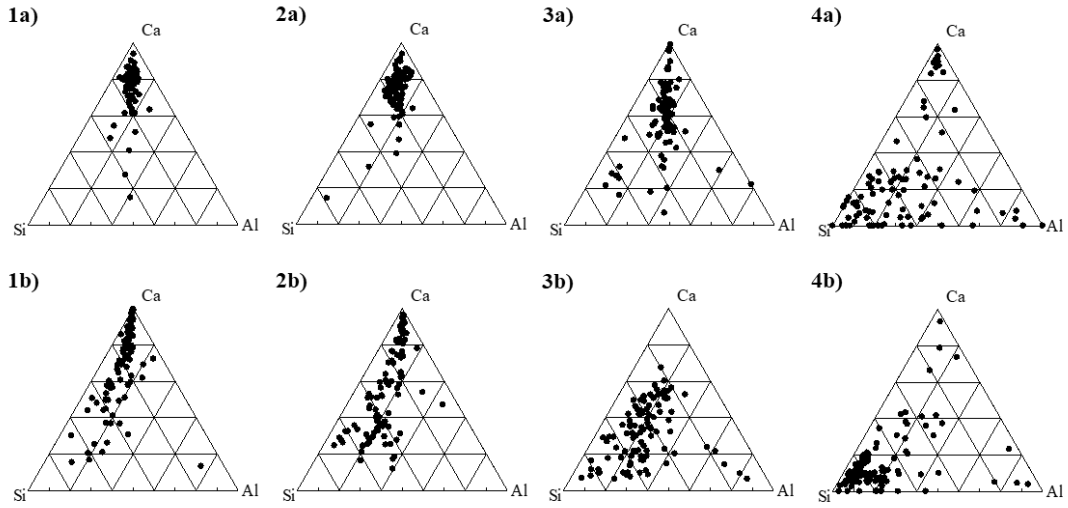

Figure 3.13 Ternary diagram of 1) surface, 2) upper semi-soluble matrices, 3) lower semi-soluble matrices, and 4) insoluble core of MSWI fly ash particles generated from a) stoker and b) fluidized bed combustor

To clearly show inter-particle heterogeneity of each component of fly ash particles, the ternary diagrams of Al, Ca, and Si is shown in **Figure 3.13**. As explained in the previous section 3.2, the stoker combustor fly ash has Al-, Ca-, and Si-based insoluble core components. On the other hand, the fluidized bed combustor fly ash has more Si-rich cores. It visualizes that the insoluble core component

of the fluidized bed combustor fly ash is less heterogeneous than that of the stoker combustor fly ash. In fly ash formation processes, core components would be formed at the first stage. The ternary diagram suggests that flyable fine particles of silica sand and/or gaseous silicate evaporated from combusted wastes would predominantly establish the core component of fly ash particles in the fluidized bed combustors. The bed in the fluidized bed is generally quartz sand. Quartz has a very high melting point (1600°C) and is often reported to be inert. Quartz can be transported through the combustion process without any changes [23,24]. In contrast, the core component of the stoker combustor fly ash would be formed Al-, Ca- and Si-rich materials, which are considered as Al_2O_3, $CaTiO_3$, and SiO_2 [13]. Also, it is supported by XRF results, which Si in the fluidized bed 118% higher than fly ash from stoker (see **Table 3.1**).

After the core component formation, semi-soluble Al/Ca/Si-based components would be formed around the insoluble core component. **Figure 3.13-3a and 3b** clearly show that semi-soluble Al/Ca/Si-based components of the fluidized bed combustor fly ash are closer to the Si-rich region than the stoker combustor fly ash. It suggests that flyable fine particles of silica sand still contribute to the significant part of the formation of the lower semi-soluble component. According to **Figure 3.13-2a and 2b**, upper semi-soluble components of the stoker fly ash are concentrated in the Ca-rich region, but those of the fluidized bed combustor fly ash are still dispersed to Si-rich region. It suggests that Ca-based materials, including aluminosilicate, would be adsorbed onto the insoluble cores and form semi-soluble components in the stoker combustor.

On the other hand, Si-based materials are still contributing to the formation of the upper semi-soluble components in the fluidized bed combustor. As described in section 3.5 and this section above, the surface and the semi-soluble components of the fluidized bed combustor fly ash have larger inter-particle heterogeneities of Al, Ca, and Si than those of the stoker combustor fly ash. **Figure 3.13** visualizes them by dispersive dots in the diagrams.

In summary, it is concluded that intra- and inter-particle heterogeneities in the surface, semi-soluble, and insoluble core components of the fluidized bed combustor fly ash are larger than the stoker combustor fly ash. The significant difference between stoker and the fluidized bed is mainly from the ash collection methods in the incinerators. The fluidized bed incinerator all of the ash is captured as fly

ash, while stoker incinerator, the ash is separated into bottom ash and fly ash. Therefore, the different ash discharge location in the incinerator affect the distribution of elements. The non-volatile and semi-volatile elements mainly in the bottom ash of stoker, while in the fluidized bed incinerator, tends to discharge non- and semi-volatile elements almost wholly in the fly ash. With non-volatile and semi-volatile elements enrich in the fly ash from the fluidized bed; therefore, the element speciation might become more diverse than stoker.

Moreover, this study found that this was caused partially/greatly by different Si behaviors in the fly ash formation process between the stoker and the fluidized bed combustors. In the fluidized bed combustor, a fly-up of silica sand particles with comparable diameter to fly ash particles from the bed is limited. However, flyable finer silica sand particles would contribute to the formation of insoluble core components as well as evaporated silicate. It makes the insoluble core component less heterogeneous (smaller inter-particle heterogeneity) than that of the stoker combustor fly ash. Si-base materials still would play an essential role in the formation of semi-soluble components in the fluidized bed combustor. In the stoker combustor, Ca-base materials like unreacted $Ca(OH)_2$ and $CaCl_2$ after neutralization reactions mainly contribute to the formation of a semi-soluble component, and it makes Ca inter-particle heterogeneity smaller than the fluidized bed combustor.

On the other hand, Si-base materials still contribute to the semi-soluble component formation in the fluidized bed combustor. It would cause larger Si inter-particle heterogeneity in the upper semi-soluble and the surface components than the stoker combustor. Significant heterogeneity of semi-soluble components might give non-negligible impacts on toxic metal leaching behaviors. In general, it is assumed that toxic metal leachabilities are mainly controlled by pH and solubility of metal species [18–20]. On the other hand, some toxic metals are incorporated in Al-, Ca-, and Si-based materials like the Al-rich phase, calcite phase, and glass phase [21, 22]. If external matrices around toxic metals also control metal leaching behaviors, their heterogeneities might be necessarily considered. It might explain gaps between experimental leaching concentrations of metals and geochemical model predictions. The impact of intra- and inter-particle heterogeneities on metal leachabilities should be evaluated as a next step.

3.4 Conclusion

Two types of heterogeneities were compared between the fluidized bed combustor fly ash and the stoker combustor fly ash. They were intra-particle heterogeneity and inter-particle heterogeneity. They were quantitatively evaluated, focusing on three components of fly ash particle bodies; surface, semi-soluble, and insoluble core components. Intra-particle heterogeneity is the heterogeneity inside each fly ash particle. Inter-particle heterogeneity is the heterogeneity among fly ash particles. In the fluidized bed fly ash particles, the surface component has 14-21 % larger intra-particle heterogeneities of Al and Si but 6-15 % smaller Ca intra-particle heterogeneity than the semi-soluble and the insoluble core components. When two combustor fly ash is compared, the fluidized bed combustor fly ash has more heterogeneous bodies than the stoker combustor fly ash. All components of the fluidized bed combustor fly ash have 4-1420 % larger intra-particle heterogeneities of major six elements (Al, Ca, Cl, K, Na, and Si) than the stoker combustor fly ash. In terms of inter-particle heterogeneity, the semi-soluble and insoluble core components of the fluidized bed combustor fly ash have 14-74 % larger heterogeneity than stoker fly ash.

On the other hand, the surface component has 3-54 % larger Al and Si inter-particle heterogeneities then the semi-soluble component. When the surface and the semi-soluble components of two combustor fly ash are compared, the fluidized bed combustor fly ash has 14-177 % larger inter-particle heterogeneities of Al, Ca, and Si than the stoker combustor fly ash. Na and Cl heterogeneities of the surface component are comparable between them. In the insoluble core component of fly ash from fluidized bed, inter-particle heterogeneity of Ca is 19 % larger than the other fly ash. On the other hand, Al and Si heterogeneities are 16% smaller for the fluidized bed combustor fly ash. Heterogeneity analysis presents some insight into the fly ash formation process. In the fluidized bed combustor, flyable fine particles of silicate from silica sand and/or combusted wastes mainly contribute to the formation of the insoluble core component. It is still essential in following semi-soluble component formation. It is different from the stoker combustor. If external matrices around toxic metals influence metal leaching behaviors, heterogeneities of fly ash particle components might explain gaps between geochemical simulation and experimental results.

3.5 References

1. Hyks J, Astrup T, Christensen TH (2009) Long-term leaching from MSWI air-pollution-control residues: Leaching characterization and modeling. J Hazard Mater 162:80–91. doi: 10.1016/j.jhazmat.2008.05.011
2. Wan X, Wang W, Ye T, et al. (2006) A study on the chemical and mineralogical characterization of MSWI fly ash using a sequential extraction procedure. J Hazard Mater 134:197–201. doi: 10.1016/j.jhazmat.2005.10.048
3. Fisher GL, Chang DPY, Brummer M (1976) Fly ash collected from electrostatic precipitators: Microcrystalline structures and the mystery of the spheres. Science (80-) 192:553–555 . doi: 10.1126/science.192.4239.553
4. Hulett LD, Weinberger AJ (1980) Some Etching Studies of the Microstructure and Composition of Large Aluminosilicate Particles in Fly Ash from Coal-Burning Power Plants. Environ Sci Technol 14:965–970. doi: 10.1021/es60168a013
5. Kirby CS, Rimstidt JD (1995) Mineralogy and surface properties of municipal solid waste ash. Environ Sci Technol 29:288. doi: 10.1021/es00001a601
6. Thipse SS, Schoenitz M, Dreizin EL (2002) Morphology and composition of the fly ash particles produced in incineration of municipal solid waste. Fuel Process Technol 75:173–184. doi: 10.1016/S0378-3820(02)00007-3
7. Ha J, Chae S, Chou KW, et al. (2016) Characterization of Class F Fly Ash Using STXM: Identifying Intraparticle Heterogeneity at Nanometer Scale. J Nanomater 2016. doi: 10.1155/2016/8072518
8. Fermo P, Cariati F, Pozzi A, et al. (2000) Analytical characterization of municipal solid waste incinerator fly ash. Part II. Fresenius J Anal Chem 366:267–72
9. Rémond S, Pimienta P, Bentz D. (2002) Effects of the incorporation of Municipal Solid Waste Incineration fly ash in cement pastes and mortars. Cem Concr Res 32:303–311. doi: 10.1016/S0008-8846(01)00674-3
10. Camerani MC, Golosio B, Somogyi A, et al. (2004) X-ray Fluorescence Tomography of Individual Municipal Solid Waste and Biomass Fly Ash Particles. Anal Chem 76:1586–1595.

doi: 10.1021/ac030282w

11. Kitamura H, Sawada T, Shimaoka T, Takahashi F (2016) Geochemically structural characteristics of municipal solid waste incineration fly ash particles and mineralogical surface conversions by chelate treatment. Environ Sci Pollut Res 23:734–743. doi: 10.1007/s11356-015-5229-5
12. Kitamura H, Dahlan AV, Tian Y, et al. (2018) Impact of secondary generated minerals on toxic element immobilization for air pollution control fly ash of a municipal solid waste incinerator. Environ Sci Pollut Res 1–13. doi: 10.1007/s11356-018-1959-5
13. Kitamura H, Dahlan AV, Tian Y, et al. (2019) Intra- and inter-particle heterogeneity of municipal solid waste incineration fly ash particles. J Mater Cycles Waste Manag 0:0. doi: 10.1007/s10163-019-00853-1
14. Chang FY, Wey MY (2006) Comparison of the characteristics of bottom and fly ashes generated from various incineration processes. J Hazard Mater 138:594–603. doi: 10.1016/j.jhazmat.2006.05.099
15. Hu HY, Liu H, Shen WQ, et al. (2013) Comparison of CaO's effect on the fate of heavy metals during thermal treatment of two typical types of MSWI fly ashes in China. Chemosphere 93:590–596. doi: 10.1016/j.chemosphere.2013.05.077
16. Jung CH, Matsuto T, Tanaka N, Okada T (2004) Metal distribution in incineration residues of municipal solid waste (MSW) in Japan. Waste Manag 24:381–391. doi: 10.1016/S0956-053X(03)00137-5
17. Li M, Xiang J, Hu S, et al. (2004) Characterization of solid residues from municipal solid waste incinerator. Fuel 83:1397–1405. doi: 10.1016/j.fuel.2004.01.005
18. Wang L, Chen Q, Jamro IA, et al. (2016) Geochemical modeling and assessment of leaching from carbonated municipal solid waste incinerator (MSWI) fly ash. Environ Sci Pollut Res 23:12107–12119. doi: 10.1007/s11356-016-6320-2
19. Zhang Y, Cetin B, Likos WJ, Edil TB (2016) Impacts of pH on leaching potential of elements from MSW incineration fly ash. Fuel 184:815–825. doi: 10.1016/j.fuel.2016.07.089
20. Astrup T, Dijkstra JJ, Comans RNJ, et al. (2006) Geochemical Modeling of Leaching from

MSWI Air-Pollution-Control Residues. Environ Sci Technol 40:3551–3557. doi: 10.1021/es052250r

21. Wang L, Jin Y, Nie Y (2010) Investigation of accelerated and natural carbonation of MSWI fly ash with a high content of Ca. J Hazard Mater 174:334–343. doi: 10.1016/j.jhazmat.2009.09.055
22. Saffarzadeh A, Shimaoka T, Wei Y, et al. (2011) Impacts of natural weathering on the transformation/neoformation processes in landfilled MSWI bottom ash: A geoenvironmental perspective. Waste Manag 31:2440–2454. doi: 10.1016/j.wasman.2011.07.017
23. Zevenhoven M, Yrjas P, Skrifvars B, et al. (2012) Characterization of ash-forming matter in various solid fuels by selective leaching and its implications for fluidized-bed combustion. Energy and Fuels 26:6366-6386. doi: 10.1021/ef300621j
24. Kleinhans U, Wieland C, Frandsen F, et al. (2018) Ash formation and deposition in coal and biomass-fired combustion systems: Progress and challenges in the field of ash particle sticking and rebound behavior. Prog 68:65-168. doi: 10.1016/j.pecs.2018.02.001

3.6 Supplementary materials

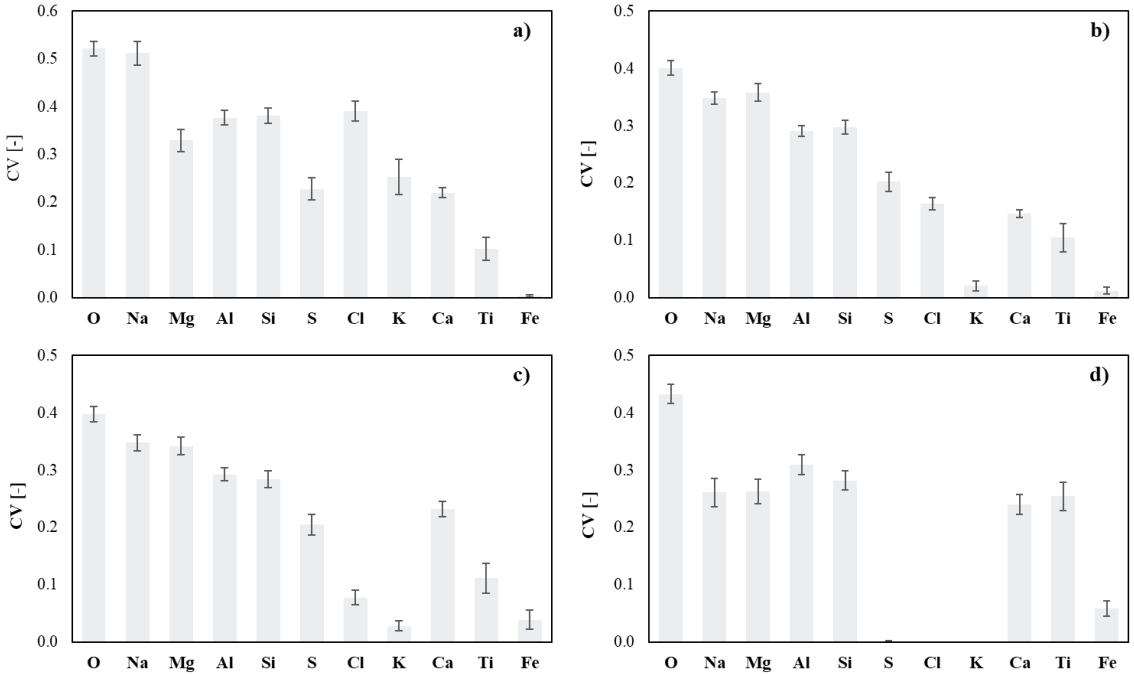

Figure S. 3-1 Average CV value of fly ash from the stoker combustor

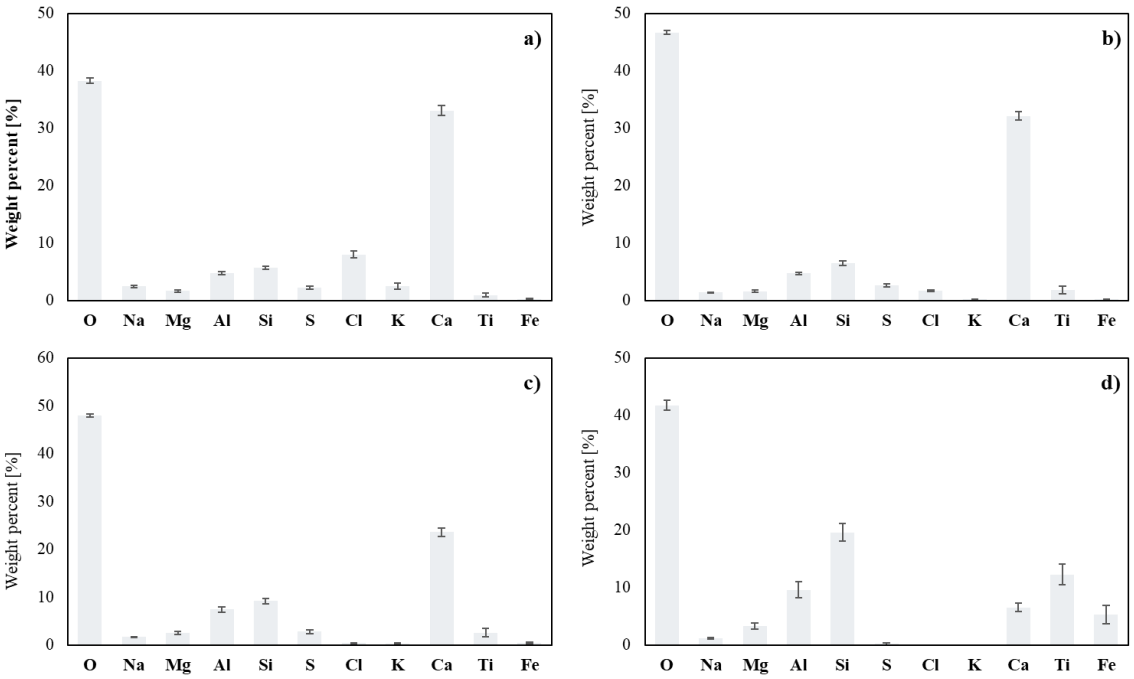

Figure S. 3-2 Average concentration of fly ash from the stoker combustor

Chapter 4

Micro-scale correlation of heavy metals speciation within single fly ash particles of municipal solid waste incineration

Abstract: Heavy metal associations can determine the leachability of metals during leaching processes and have been observed heavy metals in fly ash particles and also their leachability by using several methods. This study aims to propose new possible metal speciation in all components of the fly ash particle by using micro-scale correlation analysis. Micro-scale correlation analysis can estimate possible metal speciation at individual particle levels. Heavy metals, such as Cr and Cu, might be trapped into spinel structure and formed onto $MgCr_2O_4$, $CuAl_2O_4$, and $CuFe_2O_4$ in the insoluble core of fly ash. Other heavy metals, Fe and Zn, can host other heavy metals and presented into mineral complexation in semi-soluble component and/or insoluble core of fly ash. Correlation analysis at the micro-scale suggested that heavy metal speciation is different in the individual fly ash particle. Heavy metal leachability might be controlled by the leachability of metal speciation and Al/Ca/Si-based matrix around metal speciation.

4.1 Introduction

Metals are either carried along with the flue gas and are enriched in mineral aggregates (quartz, feldspar, wollastonite, glass) or vaporized and condensed as chlorides or sulfates. These metal associations determine the mobilization of metals during subsequent leaching processes [1]. Alam et al. investigating the association of toxic elements association in bottom ash by combining microanalysis and indirect experimental methods. The highest content of calcite, melilite, and iron oxides was present in bottom ash [2]. Many studies have been identified heavy metals in fly ash particles and also their leachability by using several methods such as X-ray diffraction (XRD) to identify metal-bearing in the crystalline phase, and X-ray absorption spectroscopy (XAS) to identify metal speciation at low concentration level [3–6]. Another study using a scanning electron microscope coupled with energy-disperse X-ray spectroscopy (SEM-EDX) to estimate metal speciation in the fly ash particle [7–9]. SEM–EDX provides detailed about the morphology and surface texture of individual fly ash particles, as well as the elemental composition of samples [10]. Besides, the SEM-EDX method can provide semi-quantitative compositional in formation and element associations of fly ash [11].

In the previous work, the author's group proposed a new method to estimate possible metal speciation and the matrix of fly ash from municipal solid waste incineration (MSWI). The method can estimate metal speciation at the individual particle level by using the SEM-EDX [12]. SEM-EDX analysis can estimate possible metal speciation at individual particle levels even at low concentration and regardless of the crystalline or amorphous phase. Correlation analysis can be useful for the comprehensive characterization of heavy metal speciation with other analyses such as XRD analysis. However, metal speciation of unmeasured particles in a previous study might have the possibility to be other forms such as carbonate, sulfate, sulfide, and so on. Therefore, this chapter aims to analyze possible metal speciation in the fly ash particle from the fluidized bed and to propose a new possible metal correlation in all components of the fly ash particle.

4.2 Materials and methods

4.2.1 Fly ash samples

The fly ash sample was used in this study, from a fluidized bed type municipal solid waste incinerator plant in Japan. Lime and activated carbon were added during the incineration process for acidic gas neutralization and dioxin control. The fly ash was entrapped in the fabric filter and collected to the storage tank before transported to the chelate treatment plant. The fly ash sample was used in this study, were collected from the chelate treatment plant. The fly ash samples were homogenized and dried at room temperature for one week or longer, before further experiments and analyses.

According to the previous study, MSWI fly ash particle consisted of Si-based insoluble core component, Al/Ca/Si-based semi-soluble component, and KCl/NaCl-based soluble aggregates on the surface. Leaching experiments were used to remove surface and semi-soluble Al/Ca/Si-based components of fly ash particles. Three kinds of leaching methods were used: Japan leaching test 46 (JLT 46), toxicity characteristic leaching procedure (TCLP), and Japan leaching test 19 (JLT 19). The details of these leaching tests were described in [13].

4.2.2 Microscopic observation

The elemental composition of fly ash particles was analyzed using a scanning electron microscope coupled with energy-dispersive x-ray spectroscopy (SEM-EDX JSM-6610 LA, JEOL, Ltd., Japan). The fly ash samples were fixed on the carbon tape on the observation stage. Because it might cause overestimation of carbon content, carbon content would not be presented in this research. The samples were observed after Pt-Pd sputtering for 30 seconds using a sputter coating device (MSP-1S, Vacuum device Ltd., Japan). Therefore, these elemental concentrations were excluded during the measurement in this analysis. Elemental mapping of fly ash particle surfaces was carried out to analyze elemental distribution.

4.2.3 Mineralogical and elemental composition analysis

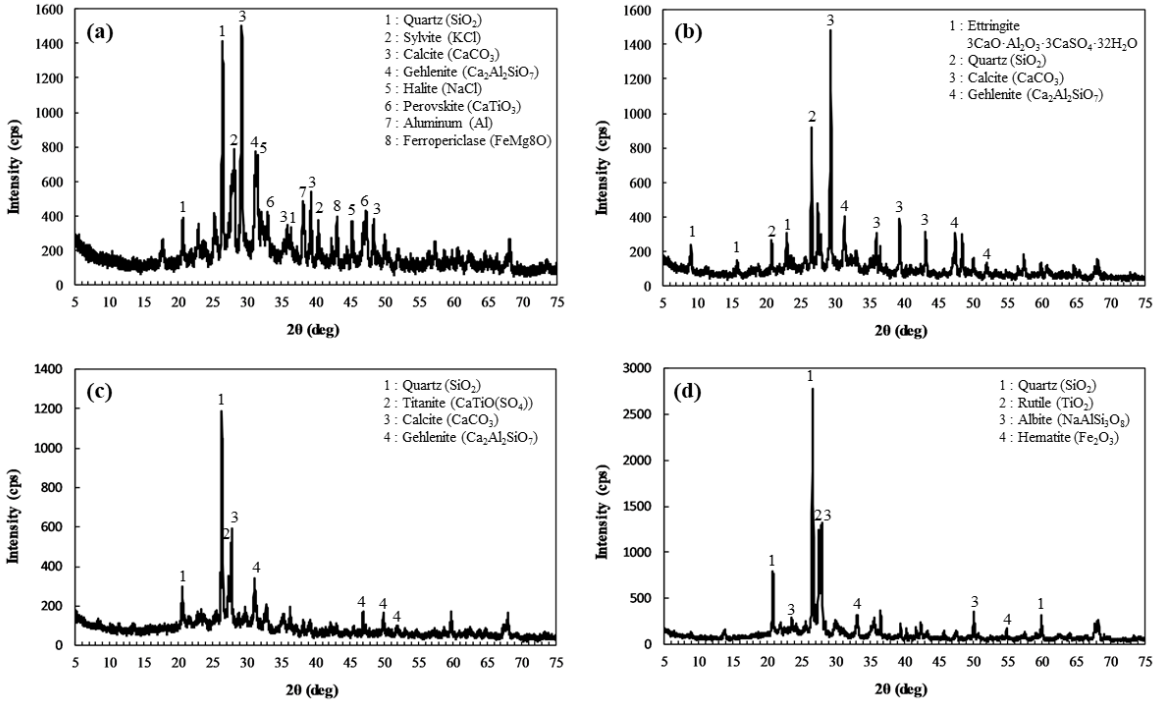

Figure 4.1 XRD patterns of a) surface, b) upper semi-soluble, c) lower semi-soluble, and d) insoluble core components of fly ash particles

The mineral composition of fly ash particles was analyzed using x-ray diffraction (XRD; MultiFlex, Rigaku Co., Japan). The measured fly ash samples were conducted using CuKα radiation (λ = 1.5418 Å, U=40keV, I=25mA) to identify the crystal phase on the samples. XRD analysis was conducted from 5° to 75° of 2θ at a rate of 1° min^{-1}. XRD of fly ash samples is shown in **Figure 4.1** [14]. Heavy metal speciation that can be detected by XRD is perovskite ($CaTiO_3$), ferropericlase ($FeMg_8O$), titanite ($CaTiO(SO_4)$), rutile (TiO_2), and hematite (Fe_2O_3). Heavy metal was detected in all components of the fly ash particle. It suggested that heavy metal in the fly ash formed in the crystalline phase and also in the amorphous phase and/or at a low concentration level. Elemental compositions of fly ash samples were analyzed by energy dispersive X-ray fluorescence spectrometer (XRF: S2 RANGER/LE, BRUKER AXS), as shown in **Table 4.1**. The constituent elements in MSWI fly ash samples are Ca, Cl, Si (>10 wt%), Fe, Al, K, Ti, Zn, Mg, S, Cu (> 1 wt%), and other metals (less than 1 wt%) [14].

Table 4.1 Elemental composition of fly ash samples determined by XRF

Elements	Ca	Cl	Si	Fe	Al	K	Ti	Zn	Mg	S	Cu
Fly Ash [wt%]	44.79	13.73	13.08	6.19	5.89	5.25	2.35	1.82	1.79	1.24	1.01

Elements	Pb	Ba	Mn	Sn	Br	Sr	Sb	Cr	Zr	Ni	Cd
Fly Ash [wt%]	0.47	0.45	0.28	0.13	0.12	0.11	0.08	0.07	0.06	0.05	0.00

4.2.4 Micro-scale correlation analysis

After the elemental mapping of the original fly ash and leaching residues were measured, each single-particle was divided into five sections equally (see **Figure 4.2**). Line profile analysis for each horizontal section was conducted based on elemental mapping data of measure elements. It should be noted that the area size of each section in all measured particles was different depending on particle size. The author's group proposed a new method to estimate possible metal speciation. Correlation coefficients (r) between major elements and metal were calculated based on the intensity data in each horizontal section. The correlation coefficient is a numerical measure of the strength of the statistical relationship between two variables. The value of the correlation coefficient varies between − 1 and + 1, whereby ± 1 indicates the strongest positive or negative correlation, and 0 indicates no correlation.

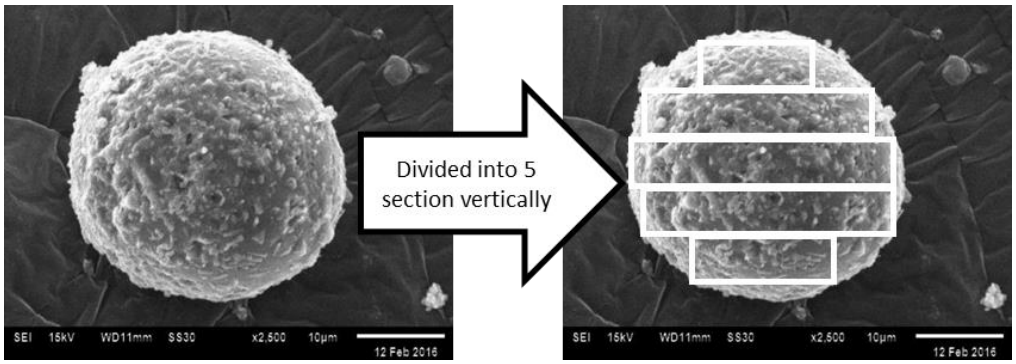

Figure 4.2 Dividing method of a metal species particle for micro-scale correlation analysis

It should be noted that intensity data obtained from each section cannot be integrated to estimate possible metal speciation. When intensity data of all horizontal sections were integrated into one data set, such a pseudo-negative correlation coefficient could be determined [12]. Therefore, this study

focused on a section of an individual fly ash particle. Correlation analysis of the elemental focused on a specific section from points A to B, as shown in **Figure 4.3**. Elemental mapping data is the elemental dispersion on the fly ash particle, which derived from the SEM image. All of the elements have their dispersion of elemental mapping data, which shows elements concentrated by color contrast, high concentration shows brighter color than low concentration on the surface. The correlation graph is showing the elemental dispersion along with the distance A and B that was conducted based on the elemental mapping data. The relation between the elemental mapping data and the correlation graph is showing in **Figure 4.3**. The elemental mapping data shows the overall elemental distribution in the fly ash and the correlation graph showing the elemental distribution in a specific horizontal section (from A to B) based on elemental mapping data.

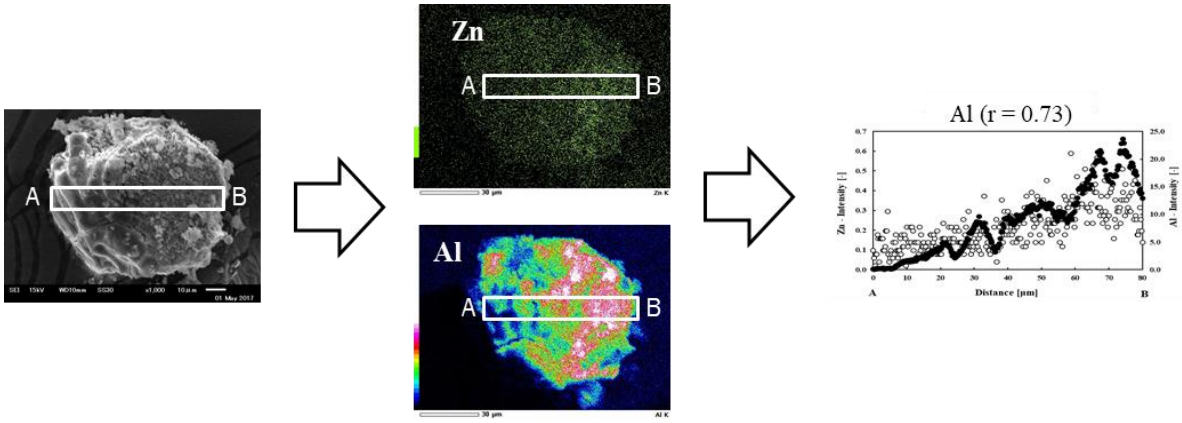

Figure 4.3 Correlation analysis graph

In this analysis, a ternary diagram was used to visualize the element association of fly ash particles. Therefore, element concentrations [wt%] of each fly ash particle were transformed to molar concentrations and then standardized by molar-based elemental contents of whole fly ash samples measured by XRF (listed in **Table 4.1**). Plotted molar-based ternary diagrams visualize prior associations of tested elements. In this analysis, the molar-based ternary diagram can clarify the crystalline phase based on XRD analysis and further description of element interrelation on the amorphous phase.

4.3 Results and discussion

4.3.1 Heavy metal element association in fly ash

Table 4.2 Metal speciation previously identified in MSWI fly ash

Heavy metal	Metal speciation	Literatures
Cr	Cr_2O_3, $CaCrO_4$.	[16] [9]
Cu	CuO and $CuSO_4 \cdot 5H_2O$, $CuCl_2(Cu(OH)_2)_3$, $Cu_{1.02}ZnNi_{3.27}O_{5.29}$, $K_2Cu_3O(SO_4)_3$, $Cu_{0.6}Zn_{0.4}$.	[17] [18] [1]
Fe	Fe_2O_3, Fe_3O_4, $MgFe_2O_4$, $FeTiO_3$.	[19] [20]
Mn	MnO	[21] [22]
Ti	TiO_2, $CaTiO_3$, $FeTiO_3$.	[22] [23] [20]
Zn	ZnO K_2ZnCl_4, $ZnAl_2O_4$, $Cu_{0.6}Zn_{0.4}$, ZnS, Zn_2SiO_4.	[21] [5] [18] [1] [20]

The investigation of heavy metal in fly ash mostly detected as mineralogical components. The heavy metal mineral phase in fly ash has been identified by previously studied are summarized in **Table 4.2**. Most of the heavy metal that detected by XRD analysis and metal concentration in bulk samples. The heavy metal speciation in the fly ash particles is affected by the waste input. Jung et al. observed

that several metals concentration depends on different furnace types, but the effect of furnace temperature is not significant in the range 850–950ºC [15].

Compare to another study mineralogical composition fly ash, fly ash samples contained titanium and iron-bearing phase, and it is easily detected as the crystalline phase in fly ash (as shown in **Figure 4.1**). Moreover, it is detected on the surface of fly ash particles. It is also supported by Fe and Ti content more than 1%wt based on XRF analysis. Besides those Fe and Ti, primarily heavy metals are zinc and copper. However, it is not detected as the crystalline phase in all components (surface, semi-soluble, and insoluble core) fly ash particles. Therefore, it is expected that other heavy metals might be found as a non-crystalline phase or amorphous phase in the fly ash particle.

4.3.2 Possible metal species and their external matrix estimated by correlation analysis

4.3.2.1 Chromium (Cr)

Chromium was detected as a hotspot by SEM-EDX in the semi-soluble and insoluble core components in the fly ash sample. Although Cr was barely detected due to lower concentration remained in the fly ash particles. The chromium-bearing phase was commonly detected as Cr_2O_3 and $CaCrO_4$ in the MSWI fly ash, as shown in **Table 4.2**. Those metal bearings were found in this study, as shown in **Figure S1** and **S2**, respectively. Cr_2O_3 was spotted in the core of the fly ash particle (see **Figure S1**). Besides, Cr also showed a positive correlation with Al. It proposed Cr_2O_3 might be encapsulated in the Al-based matrix in the core of fly ash in the fluidized bed. In the semi-soluble component of fly ash, Cr has a positive correlation with Ca and O, as shown in **Figure S2**. It suggested that $CaCrO_4$ is available in the semi-soluble component of fly ash. Cr(III) form more favorable than Cr(VI) formation due to its not leachable properties. However, free CaO and/or presence of Ca promote oxidation of Cr during thermal treatment. In the higher temperature, Ca binding with Al and Si to form Ca-aluminosilicate. Al/Fe/Si-compounds in ash residue competed with un-oxidized Cr-compound to react with free CaO and well suppressed Cr(VI) formation [24]. Chromium in the core of the fly ash particle is in the Cr(III) form as Cr_2O_3. Most detected Cr was found in the core components, which is consisted of Si-rich insoluble core. SiO_2 might inhibit the formation of Cr(VI) due to Ca be incorporated into $CaSiO_3$ [25].

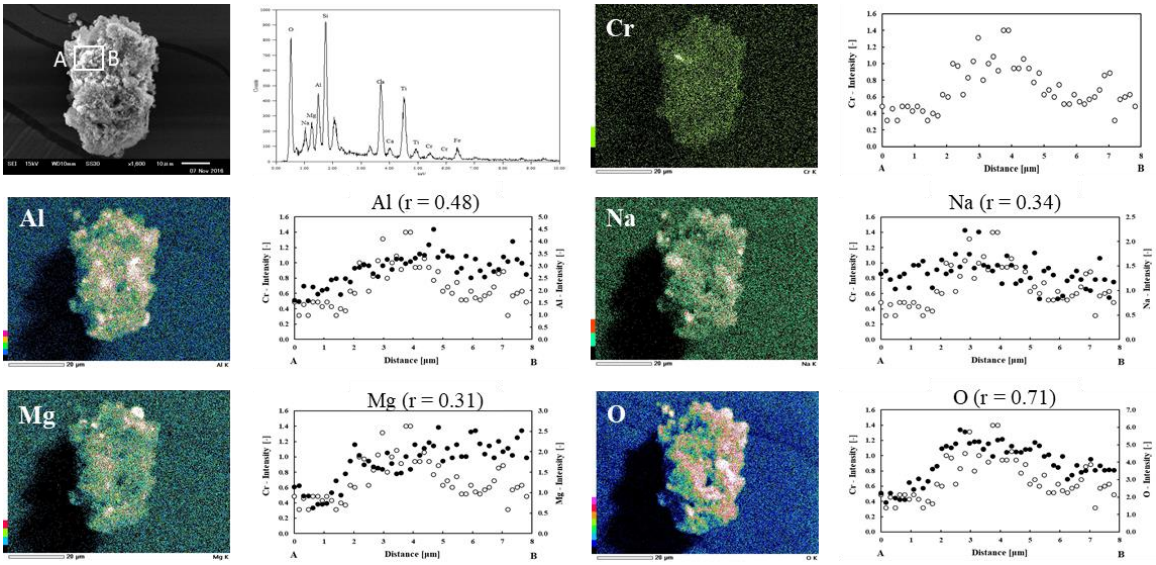

Figure 4.4 Chromium correlation in the core components of fly ash particle

By the correlation analysis, the positive correlation between Cr with other elements was obtained. It might propose a new possible metal bearing phase in the fly ash particle. Cr showed a positive correlation with Mg were shown in **Figure 4.4,** which offered new possible Cr speciation is magnesium chromium spinel ($MgCr_2O_4$). Mao, L studied the formation of $MgCr_2O_4$, which Cr(VI) thermal decomposition could result in the formation of $MgCr_2O_4$ [26]. Another study found that Mg-Cr-spinel was present during thermal treatment [27]. So, there is a possibility during the combustion process, Cr formed into magnesium chromium spinel. A positive correlation with Al also observed in this fly ash particle. It might be suggested new possible metal speciation as Al-chromite or Cr_2O_3 included in the Al-based core of fly ash. Cr in the core of fly ash, mainly as Cr(III), is due to the reduction of Cr(VI) with aluminum. Al present in the fly ash can control Cr leaching by reducing Cr(VI) released from the solid phase by dissolution into Cr(III) formed [28, 29]. Therefore, the Al-based matrix in the fly ash might inhibit Cr leaching into the environment.

4.3.2.2 Copper (Cu)

SEM-EDX rarely detected copper (Cu) due to lower concentration present in the fly as particles. Cu was commonly detected as brass and copper oxide (see **Table 4.2**). Cu shows a positive correlation

only with Zn, as shown in **Figure S3**. It explains the Cu speciation in the fly ash particle is alloy brass. Based on previous SEM-EDS results, the alloy brass made of copper and zinc in the proportions of 60% Cu and 40% Zn ($Cu_{0.6}Zn_{0.4}$) in fly ash. Brass ($Cu_{0.6}Zn_{0.4}$) is often incorporated in Ca-silicates or finely distributed within the ash matrix [1]. In this fly ash particle, brass has a negative correlation with Ca and Si that suggested that brass was finely distributed in the core of fly ash.

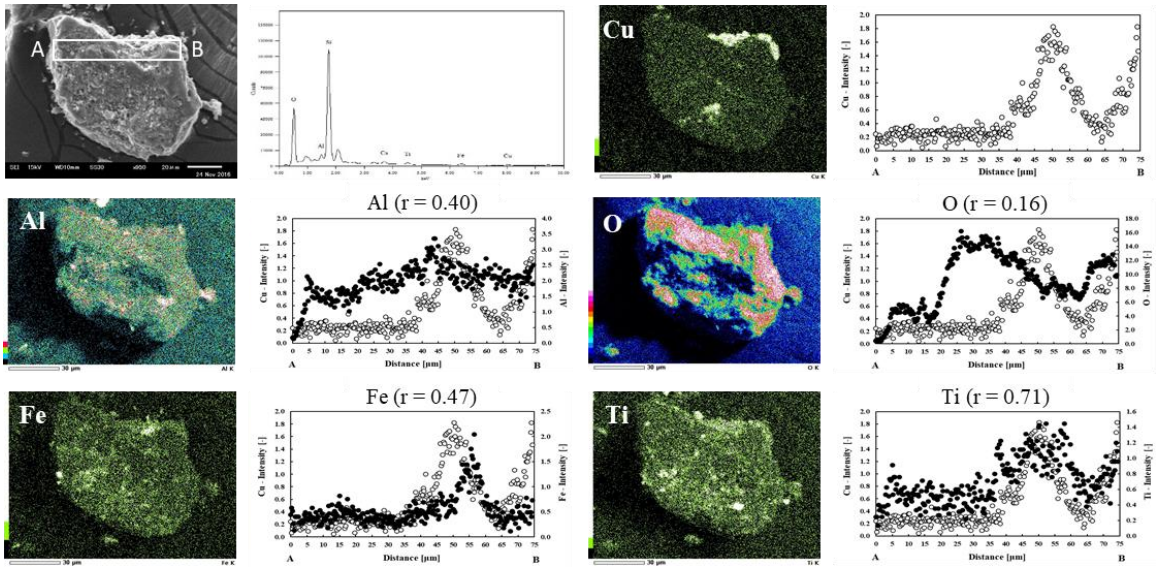

Figure 4.5 Copper correlation in the core components of fly ash particle

Cu also has positive correlation Al, Ca, Fe, and O, as in **Figure 4.5**. Therefore, the Cu speciation is estimated as CuO that incorporated with Al/Ca-based insoluble core. The previous study also cannot detect Cu by using XRD due to the poor quality of copper compound crystals that were formed during heat treatment and not detectable by standard XRD methods. Cu in fly ash is mainly CuO that was able to detect by using XANES [17]. Cu has a negative correlation with Si in observed particles. It was explained that CuO and SiO_2 have no reaction, and SiO_2 showed a minor role in the immobilization of Cu [25]. Therefore, it suggested that CuO not incorporated in the Si-based insoluble core. New possible Cu speciation was estimated from the correlation analysis. The positive correlation between Cu with Al and Fe were observed in this fly ash particle. It proposed Cu incorporated into spinel structure that formed $CuAl_2O_4$ and $CuFe_2O_4$. Studies found incorporating copper into spinel structure such as $CuAl_2O_4$ and $CuFe_2O_4$ achieved excellent performance in the copper immobilization [30, 31].

4.3.2.3 Iron (Fe)

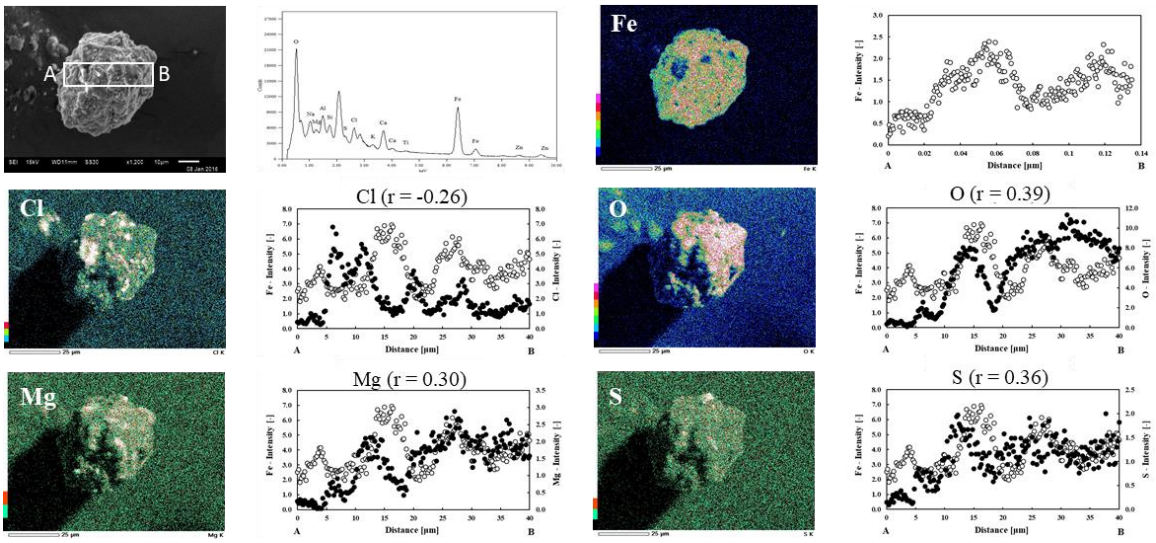

Figure 4.6 Iron correlation in the surface of fly ash particle

Fe-bearing phases are the most common metal-containing components found in fly ash. Previous research showed that after the water leaching process, iron and zinc quickly detected in the fly ash particle. Fe and Zn enrich the insoluble core of fly ash particles. These elements were observed in the sub-micron region of fly ash particles [32]. In this study, iron was observed in the surface, semi-soluble, and insoluble core components fly ash particle. Crystalline of Fe-bearing was also observed as ferropericlase ($FeMg_8O$) and hematite (Fe_2O_3) by XRD analysis. Correlation analysis showed that Fe has a positive correlation with Al, Ca, Mn, O, Si, and Ti in the insoluble core (see **Figure S4**). Possible speciation is Fe_2O_3, Fe_3O_4, $FeTiO_3$ incorporated in the Al/Ca/Si-based core fly ash. It is in good agreement with the previous study that observed hematite or magnetite incorporated in the Ca-silicates sphere [1]. A positive correlation between Fe-oxides and Ti was also supported by the previous study that hematite incorporated with Al, Ti, and Ni in the bottom ash [2]. Iron oxide also hosted other heavy metals such as Ti, Mn, that showing positive correlation Fe with Mn and Ti. Kitamura et al. suggested that iron-based mineral can absorb toxic heavy metals in the fly ash particle [33].

Crystalline of iron-bearing in the surface of fly ash was detected as ferropericlase ($FeMg_8O$). It is also found that a positive correlation between iron and magnesium were measured (see **Figure 4.6**).

Negative correlation with chlorine showed $FeCl_2$ was not present in the surface of the fly ash particle. $FeCl_2$ are generated in the combustor and changed into iron oxide in the post-combustion area [32].

4.3.2.4 Manganese (Mn)

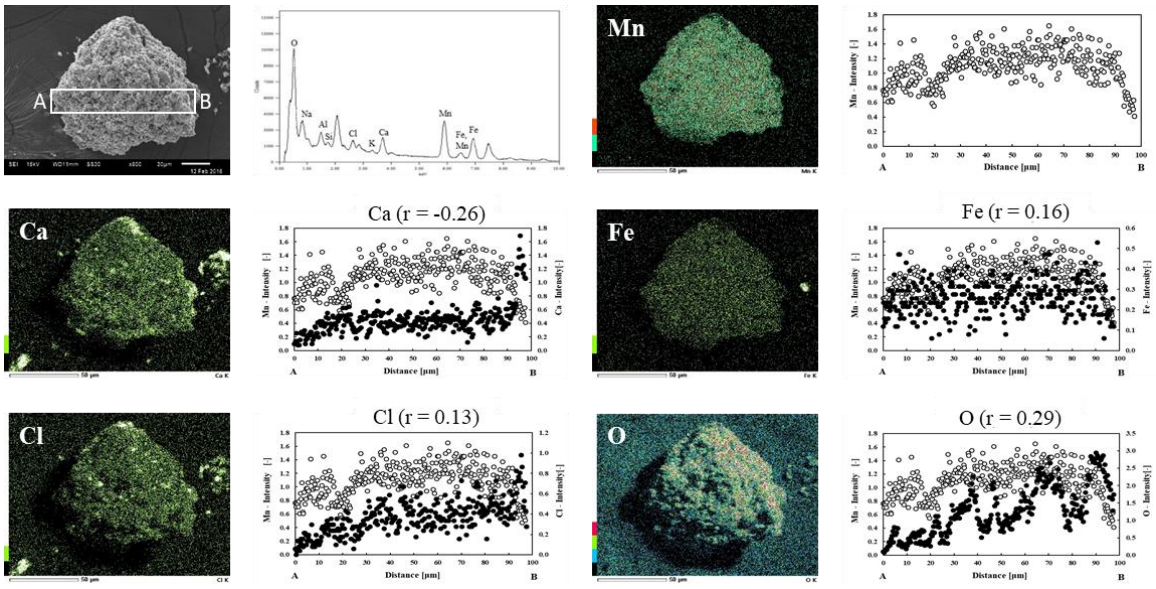

Figure 4.7 Manganese correlation in the surface of fly ash particle

Manganese (Mn) has a positive correlation with O and Si in the core of the fly ash particle shown in **Figure S5**. It suggested that Mn speciation is MnO, which encapsulated in the Si-based insoluble core of fly ash. Mn was not easily dissolved in water. It is suggesting that Mn was firmly bound to the matrix of fly ash and would not be quickly released into the environment under natural conditions [34].

MnO also was observed in the surface of the fly ash particle in **Figure 4.7**. MnO not incorporated with Ca-based aluminosilicate in the surface of fly ash. Also, Mn has a positive correlation with Cl and Fe. $MnCl_2$ might be present in the small amount on the surface of the fly ash particle. The previous study was also observed the manganese could present as chlorides and oxides in the MSWI fly ash [32].

4.3.2.5 Titanium (Ti)

Similar to Fe, titanium (Ti) also was observed in the surface, semi-soluble, and insoluble core components fly ash particle by SEM-EDX and XRD analysis. As a noticeable amount titanium was found in the fly ash, TiO_2 had to be transported with the flue gas. In the combustion bed, small fly ash particles covered with TiO_2 removal from bed combustor and adsorb into fly ash particles [35]. Ti speciation in the surface of fly ash is perovskite ($CaTiO_3$), showing by the positive correlation between Ti with Ca and O, as shown in **Figure 4.8,** which proved the XRD result. Ti shows a negative correlation with Al and Si in the surface of the fly ash particle. On the surface, titanium not incorporated with aluminosilicate; however, Ti combines with the Ca-based matrix. Fedje et al. also detected a negative correlation between Ti with Al and Si on fly ash particles from the fluidized bed. However, most Ti on fly ash particles has a positive correlation with Ca. It showed Ti on fly ash particles mostly in the perovskite crystalline form. They suggested Cr, Pb, Ti, and Zn adsorbed to fly ash particles through a random process [19].

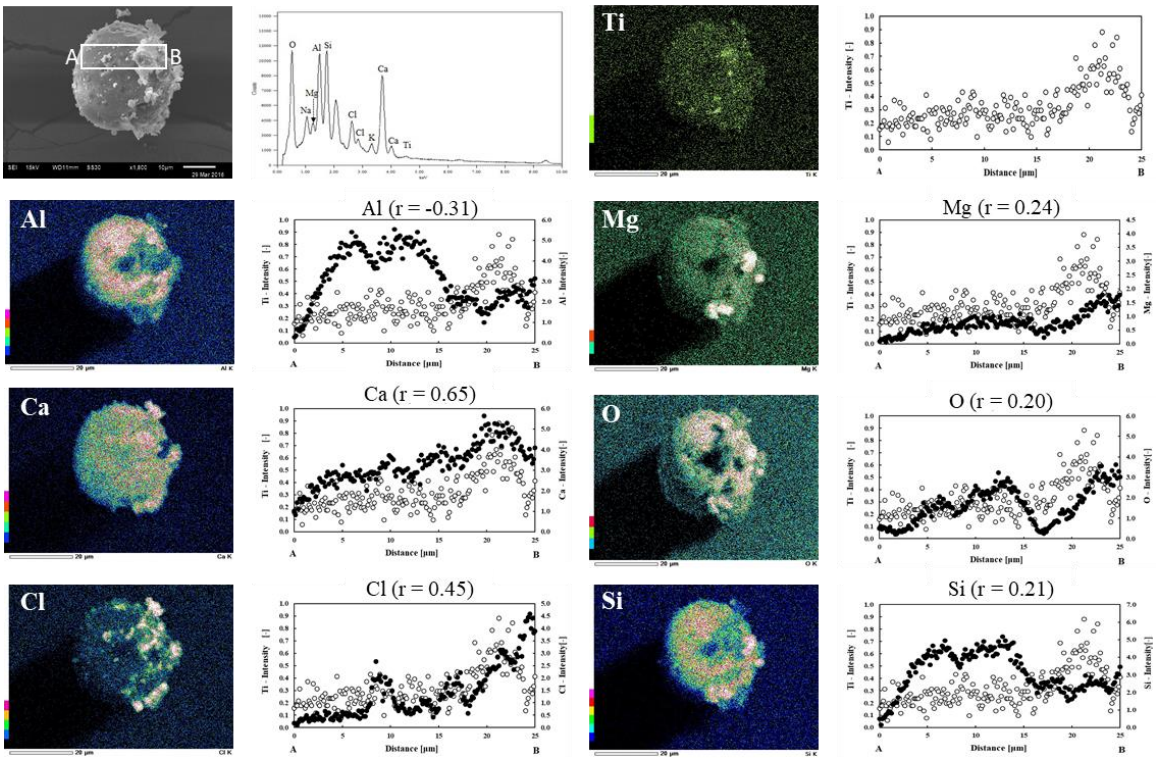

Figure 4.8 Titanium correlation in the surface of fly ash particle

In the semi soluble component, Ti has a negative correlation with other elements (see **Figure 4.8**). It might propose new speciation of Ti in the fly ash particle can be as metallic formed. In the core of fly ash particle, rutile (TiO_2) incorporated with Al/Ca/Si-based insoluble core of fly ash particle (see **Figure S6**). TiO_2 nanoparticles added in paints may undergo to physicochemical transformation during the incineration, and that Ti found in ashes may be strongly immobilized in glass matrix [36]. Titanium randomly binds to ash particles regardless of their composition. Therefore, titanium is incorporated or combined with the aluminosilicate matrix to form ash [23].

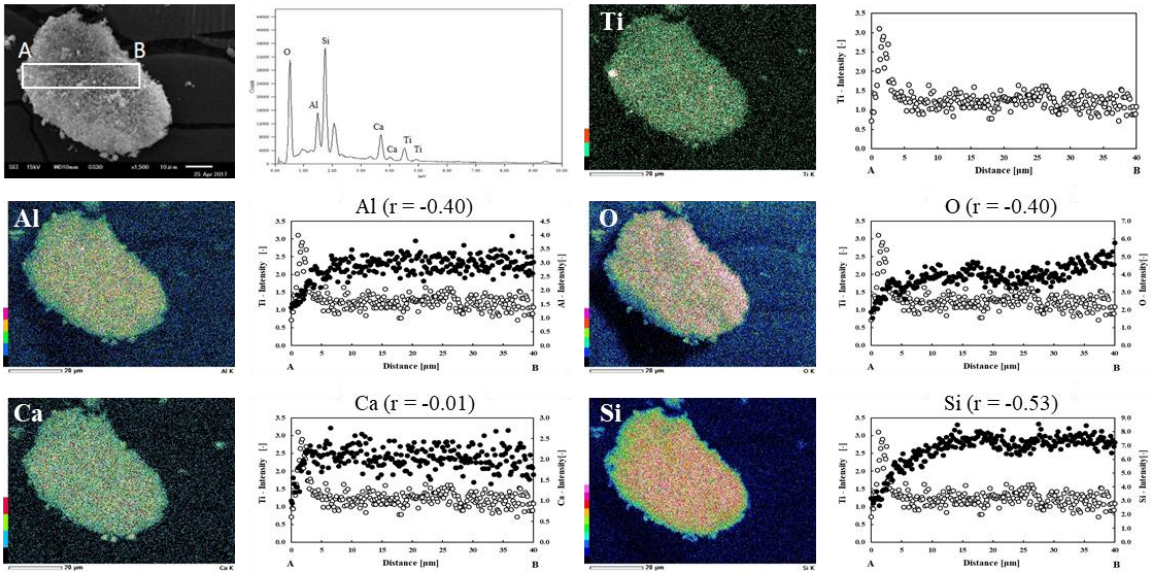

Figure 4.9 Titanium correlation in the semi-soluble component of fly ash particle

4.3.2.6 Zinc (Zn)

Zinc tended to accumulate within the entire ash matrix and was the heavy metal that quickly detected in the fly ash, as shown in **Table 4.2**. Zn speciation in the surface of fly ash is K_2ZnCl_4, ZnO, and Zn_2SiO_4 because of a positive correlation with those elements, as shown in **Figure S7**. Although, that XRD cannot detect Zn speciation due to low concentration. That speciation not incorporated with

Ca-based component that might be Zn in the surface of fly ash is readily leachable. Sylvite was found to take up Zn and can leach them readily [18].

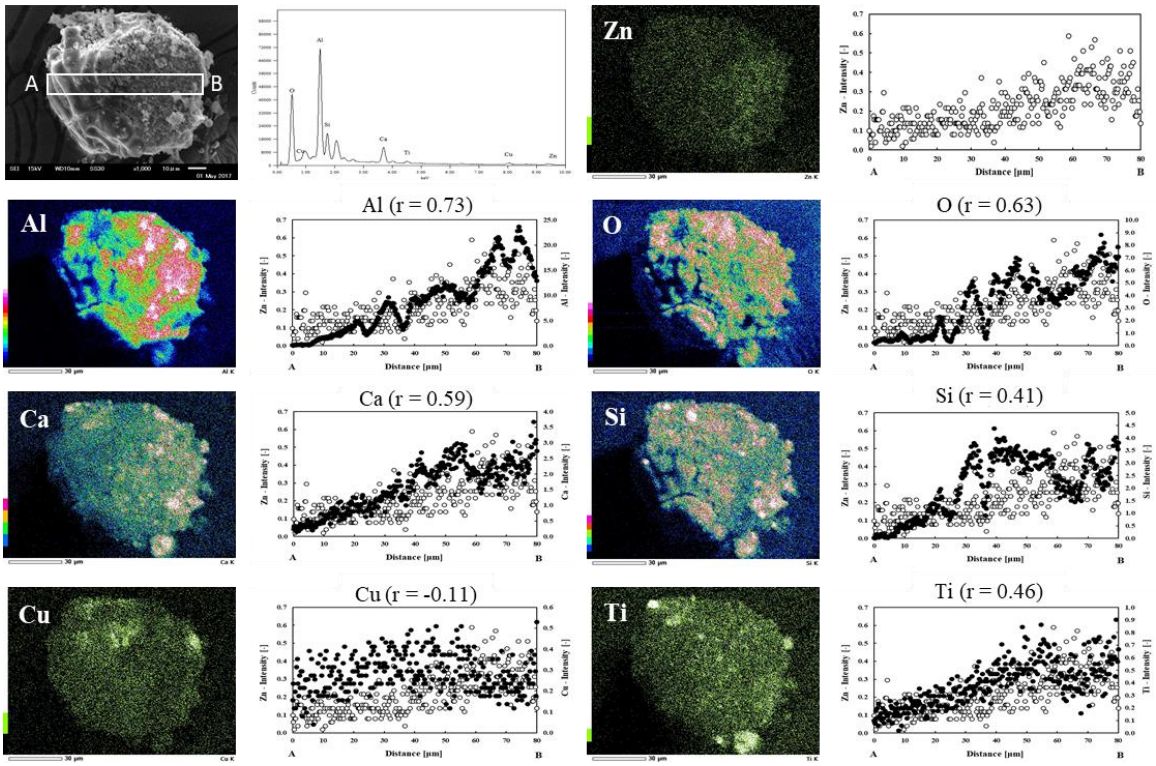

Figure 4.10 Zinc correlation in the semi-soluble of fly ash particle

In contrast to the surface, Zn shows positive with Al and Fe, as seen in **Figure S8**. Zn speciation in the insoluble core of fly ash was more in the stable form, which are $ZnAl_2O_4$, $ZnFe_2O_4$ encapsulated in the Ca-based component. Previous work showed Zn was incorporated substantially into the spinel structure (are $ZnAl_2O_4$, $ZnFe_2O_4$) that performed better in the resistance to the attack against acid [25]. Therefore, Zn was immobilized in the core of fly ash and not easily leached out of the fly ash particle. In the semi-soluble component of fly ash, zinc shows a positive correlation with Al, Ca, Si (see **Figure 4.10**) that suggested ZnO incorporated in the Al/Ca/Si-based semi-soluble components. Besides, Zn also shows a positive correlation with Ti. It might give new possible speciation of zinc in the fly ash particle. Zn and Ti might be included together into alloy or oxide.

4.3.3 Element association priorities estimated based on elemental heterogeneity

The molar-based ternary diagrams for each fly ash particle component are shown in **Figure 4.11**. In the Cr-Al-Mg molar-based ternary diagram, shown in **Figure 4.11a**, dots concentrated in the Cr-Mg area. In the previous section 3.2.1, new possible Cr speciation in one section single fly ash particle is proposed, which are $MgCr_2O_4$ and Al-Cr oxide. Ternary diagram suggested Cr associated more with Mg than Al. It proposed Cr speciation in that section of fly ash particle mostly $MgCr_2O_4$ and small presence of Al-chromite. Ternary diagram of Cr-Al-O (see **Figure 4.11b**) visualize dot dispersion into Cr and O side while the lowest side of Al. It suggested that Cr_2O_3 encapsulated in the Al-matrix insoluble core of fly ash. In the previous section 3.2.2, copper observed incorporated in the spinel structure. Both copper's spinel structures, $CuAl_2O_4$ and $CuFe_2O_4$, were detected in the same section of fly ash. Therefore, Cu-Al-Fe molar-based ternary diagram was calculated, as seen in **Figure 4.11c**. Dots more concentrated between the Cu-Al area. It is likely Cu spinel, $CuAl_2O_4$, were formed early than remained Cu form $CuFe_2O_4$ afterward. Iron hosted other heavy metals such as Ti and Mn that have been discussed in section 3.2.3.

Figure 4.11d shows Fe oxide hosted more onto Mn than Ti. Fe oxide in the fly ash is quickly bonding with heavy metal and enrichment of heavy metal in the fly ash particle relative to Fe-speciation [37]. Jiao et al. found Fe was the primary host for Cu and Zn-bearing, which Fe-bearing was encapsulated in the silicate matrix in the fly ash [38]. This study suggested that Fe-bearing can be a significant host for other metals and entrapped in Si-based insoluble core of fly ash. The new possible Cr, Cu, and Fe speciation were detected in the core of the fly ash particle. In our previous study, two possible pathways are proposed in terms of metal encapsulation into the insoluble core component [14]. The first is that gaseous aluminosilicate firstly associates with evaporated metals in the gas phase and then dropped onto fine silica sand particles. The other is that metals are adsorbed onto silica sand particles first and then associated with Al. Cr and Fe have a positive correlation with Al, Ca, and Si (see **Figure 4.4** and **Figure S4**). It suggested that those metal might be encapsulated into the core of fly ash by those two pathways. In contrast, Cu has a positive correlation only with Ca and Al (see **Figure 4.5**). It is likely Cu in the gas phase formed into spinel structure and encapsulated with Al/Ca-matrix and then dropped into fine silica core of fly ash.

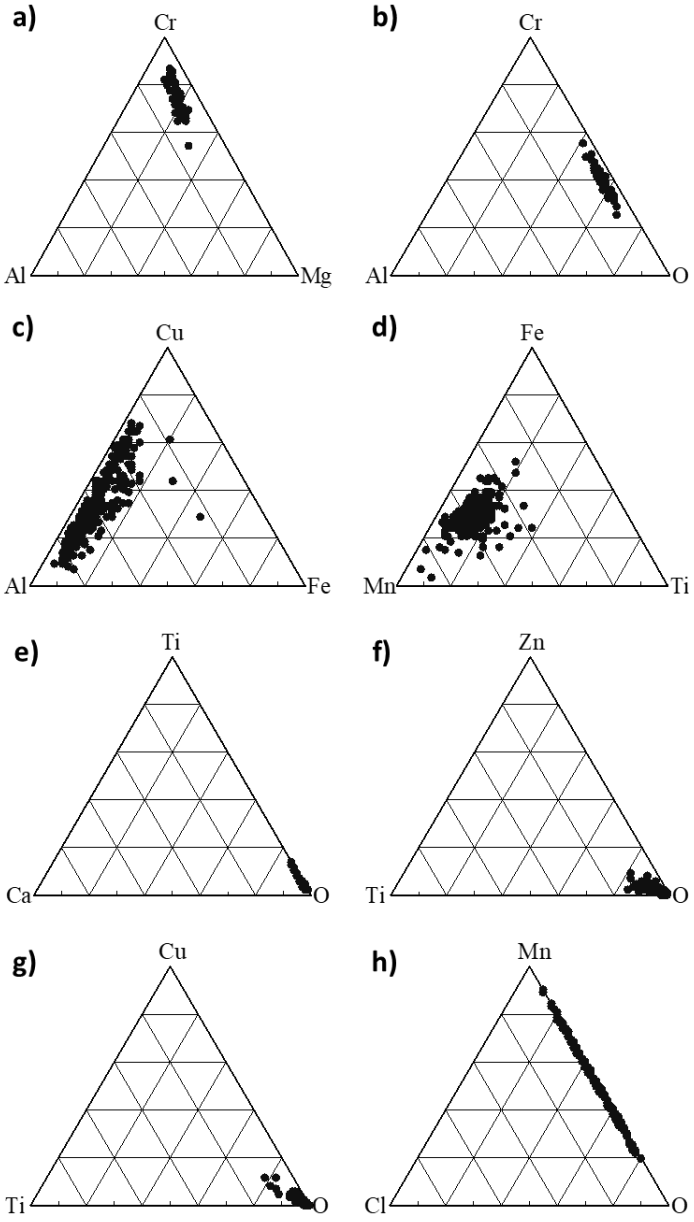

Figure 4.11 Molar-based ternary diagram of new possible heavy metal speciation

Titanium was detected as the metallic form in the semi-soluble component fly ash, as discussed in the previous section 3.2.4. Although Ti has a negative correlation with O (see **Figure 4.8**), the dot concentrated in the O area along to the Ti line in the ternary diagram (see **Figure 4.11e**). So, there is a possibility Ti oxide also included in a small amount. It might suggest that heavy metal have random physical adsorption to semi-soluble components of fly ash particle. The suggestion of Zn speciation is Zn-Ti in the semi-soluble component of fly ash, as explained in section 3.2.5. **Figure 4.11f** of the Zn-

Ti-O molar-based ternary diagram, the dot concentrated in the O area, which suggested Zn and Ti exist as Zn oxide and Ti oxide. A positive correlation between Zn and Ti might suggest Zn-oxide and Ti-oxide were incorporated together in the semi-soluble component of fly ash. Besides, a positive correlation is observed between Ti and Cu (see **Figure 4.5**), and the ternary diagram of Cu-Ti-O shows Cu oxide and Ti oxide existed in the fly ash particles (see **Figure 4.11g**). The dominant crystalline phase, such as SiO_2, Fe_2O_3, $CaTiO_3$, and $CaAl_2SiO_8 \cdot 4H_2O$, in fly ash able to act as host to the heavy metal. By model calculation, titanate able to host Cd, which potentially inhibited their mobility [38]. This study proposed that Ti oxide might also host other heavy metals such as Ti and Zn in semi-soluble and the insoluble core of fly ash particles.

Manganese in the surface likely exist as more into MnO than $MnCl_2$, and it is visualized by dot dispersion along Mn and O area (see **Figure 4.11h**). Although there is a positive correlation between Mn and Cl, it might present in limited concentration. MnO and $MnCl_2$ in the surface of fly ash not bond to Ca-aluminosilicate. It suggested that heavy metal oxides and chlorides enrich by randomly adsorption into the surface of fly ash particles. This speciation likely easily leached out from the fly ash particle. Metal oxides and chlorides are natural to evaporate at high temperatures (700–1000 °C). When volatile heavy metals in the flue gas flowed into the post-combustion area (300–500 °C), it could promptly cool down and form metal species on the surface of fly ash [38].

4.3.4 Summary possible metal speciation

Heavy metal speciation observes in this study is summarized in **Table 4.3**. Heavy metal speciation and their bonding states are different in the individual fly ash particle body and all components of fly ash particles. Cr and Cu-bearing were observed as oxide and also formed in the spinel structure. Besides that, Cr(III) and Cr(VI) were observed in the fly ash particle. Fly ash particles may contain two types of Cr in one sample. Cr(VI) remained in the semi-soluble and not easily leached out by water or weak acid. However, in the insoluble core of fly ash Cr in the stabilize form and entrapped in the Si-insoluble core of fly ash from the fluidized bed.

Table 4.3 Summary metal speciation in the MSWI fly ash

Heavy metal	Metal speciation	
	Common Possible	**New possible**
Cr	Cr_2O_3, $CaCrO_4$.	$MgCr_2O_4$, Al-Cr oxide.
Cu	CuO, $Cu_{0.6}Zn_{0.4}$.	$CuAl_2O_4$, $CuFe_2O_4$.
Fe	Fe_2O_3, Fe_3O_4, $FeTiO_3$.	$FeMg_8O$ Fe oxide-Mn-Ti
Mn	MnO	$MnCl_2$
Ti	TiO_2, $CaTiO_3$.	Ti Ti oxide-Zn-Cu
Zn	ZnO K_2ZnCl_4, $Cu_{0.6}Zn_{0.4}$, Zn_2SiO_4. $ZnAl_2O_4$, $ZnFe_2O_4$	Zn oxide – Ti oxide

Heavy metals speciation that has been discovered in this study, encapsulated in the Al/Ca/Si-based semi-soluble component and the insoluble core of fly ash. The contents of the glass phase or Ca, Si, and Al can influence heavy metals leaching behavior and fly ash can be stabilized by increasing Ca, Si, and Al content [39]. The carbonate and glass-derived secondary products also contributed to the immobilization of heavy metals. The glass-derived products could perceive the heavy metal in a long period in the residue of MSWI [40]. It suggested heavy metal speciation in this sample was stabilized inside the fly ash particle and not quickly to leached out to the environment. Micro-scale correlation analysis in all components fly ash particle suggests leaching behaviors of insoluble metal oxides

incorporated in the Al/Ca/Si-based component. Because metal oxides are incorporated in the Al/Ca/Si-based matrix, metal leachability might be controlled by not only the leachability of metal oxide but also Al/Ca/ Si-based components around metal oxides.

4.4 Conclusion

Correlation analysis at the micro-level suggests the possibility of heterogeneity of metal speciation in a fly ash particle. Heavy metal speciation mostly observed as a crystalline phase. This method can give insight metal speciation in the amorphous or non-crystalline phase in the fly ash. In this study, we observed new possible metal speciation that might be formed in the fly ash particle. The Cr-bearing phase was present as Cr(III) and Cr(VI) oxide and in the spinel structure($MgCr_2O_4$). Brass ($Cu_{0.6}Zn_{0.4}$) and Cu oxide are observed, and Cu in the Al-Fe spinel structure ($CuAl_2O_4$, $CuFe_2O_4$) is discovered. Iron oxide (Fe_2O_3, Fe_3O_4, $FeTiO_3$) as the primary speciation of Fe-bearing were detected in all components of fly ash particle. The surface of fly ash detected $FeMg_8O$, and it is good agreement with XRD analysis. For manganese, present in oxide and chloride form, and it can be observed on the surface of fly ash. Similar to XRD results, rutile (TiO_2) and perovskite ($CaTiO_3$) were observed by correlation analysis. Ti in metallic form was observed in the semi-soluble component. Iron and titanium that mostly detected in this fly ash samples can act as host to heavy metals and form complex metal speciation. Although Zn not detected in the crystalline phase, common Zn speciation also discovered in this study, such as ZnO, K_2ZnCl_4, $Cu_{0.6}Zn_{0.4}$, Zn_2SiO_4, $ZnAl_2O_4$, and $ZnFe_2O_4$. It might be due to low concentration or Zn-bearing in the amorphous phase. Further metal speciation analysis such as XRD and XAS was needed to improve comprehensive analysis of the possible metal speciation. Metal leachability might be controlled by metal speciation leachability and leachability of Al/Ca/Si-based matrix around metal speciation.

4.5 References

1. Weibel G, Eggenberger U, Schlumberger S, Mäder UK (2017) Chemical associations and mobilization of heavy metals in fly ash from municipal solid waste incineration. Waste Manag 62:147–159. doi: 10.1016/j.wasman.2016.12.004
2. Alam Q, Schollbach K, van Hoek C, et al. (2019) In-depth mineralogical quantification of MSWI bottom ash phases and their association with potentially toxic elements. Waste Manag 87:1–12. doi: 10.1016/j.wasman.2019.01.031
3. Sarbak Z, Stańczyk A, Kramer-Wachowiak M (2004) Characterisation of surface properties of various fly ashes. Powder Technol 145:82–87. doi: 10.1016/j.powtec.2004.04.041
4. Wan X, Wang W, Ye T, et al. (2006) A study on the chemical and mineralogical characterization of MSWI fly ash using a sequential extraction procedure. J Hazard Mater 134:197–201. doi: 10.1016/j.jhazmat.2005.10.048
5. Bayuseno AP, Schmahl WW (2011) Characterization of MSWI fly ash through mineralogy and water extraction. Resour Conserv Recycl 55:524–534. doi: 10.1016/j.resconrec.2011.01.002
6. Struis RPWJ, Ludwig C, Lutz H, Scheidegger AM (2004) Speciation of zinc in municipal solid waste incineration fly ash after heat treatment: An X-ray absorption spectroscopy study. Environ Sci Technol 38:3760–3767. doi: 10.1021/es0346126
7. Mollah MY a, Hess TR, Cocke DL (1994) Surface and bulk studies of leached and unleached fly ash using XPS, SEM, EDS, and FTIR techniques. Cem Concr Res 24:109–118
8. Piispanen MH, Arvilommi SA, Van Den Broeck B, et al. (2009) A comparative study of fly ash characterization by LA-ICP-MS and SEM-EDS. Energy and Fuels 23:3451–3456. doi: 10.1021/ef801037a
9. Liu Y, Zheng L, Li X, Xie S (2009) SEM/EDS and XRD characterization of raw and washed MSWI fly ash sintered at different temperatures. J Hazard Mater 162:161–173. doi: 10.1016/j.jhazmat.2008.05.029
10. KUTCHKO B, KIM A (2006) Fly ash characterization by SEM-EDS. Fuel 85:2537–2544. doi: 10.1016/j.fuel.2006.05.016
11. Taylor Eighmy T, Dykstra Eusden J, Krzanowski JE, et al. (1995) Comprehensive Approach

toward Understanding Element Speciation and Leaching Behavior in Municipal Solid Waste Incineration Electrostatic Precipitator Ash. Environ Sci Technol 29:629–646. doi: 10.1021/es00003a010

12. Kitamura H, Dahlan AV, Tian Y, et al. (2020) Application of micro-scale correlation analysis to estimate metal speciation and the matrix in municipal solid waste incineration fly ash. J Mater Cycles Waste Manag. doi: 10.1007/s10163-020-01001-w
13. Kitamura H, Sawada T, Shimaoka T, Takahashi F (2016) Geochemically structural characteristics of municipal solid waste incineration fly ash particles and mineralogical surface conversions by chelate treatment. Environ Sci Pollut Res 23:734–743. doi: 10.1007/s11356-015-5229-5
14. Dahlan AV, Kitamura H, Tian Y, et al. (2020) Heterogeneities of fly ash particles generated from a fluidized bed combustor of municipal solid waste incineration. J Mater Cycles Waste Manag. doi: 10.1007/s10163-020-00973-z
15. Jung CH, Matsuto T, Tanaka N, Okada T (2004) Metal distribution in incineration residues of municipal solid waste (MSW) in Japan. Waste Manag 24:381–391. doi: 10.1016/S0956-053X(03)00137-5
16. Wang KS, Sun CJ, Liu CY (2001) Effects of the type of sintering atmosphere on the chromium leachability of thermal-treated municipal solid waste incinerator fly ash. Waste Manag 21:85–91. doi: 10.1016/S0956-053X(00)00041-6
17. Tian S, Yu M, Wang W, et al. (2009) Investigating the speciation of copper in secondary fly ash by X-ray absorption spectroscopy. Environ Sci Technol 43:9084–9088. doi: 10.1021/es902039x
18. Bogush A, Stegemann JA, Wood I, Roy A (2015) Element composition and mineralogical characterisation of air pollution control residue from UK energy-from-waste facilities. Waste Manag 36:119–129. doi: 10.1016/j.wasman.2014.11.017
19. Karlfeldt Fedje K, Rauch S, Cho P, Steenari BM (2010) Element associations in ash from waste combustion in fluidized bed. Waste Manag 30:1273–1279. doi: 10.1016/j.wasman.2009.09.012
20. Loginova E, Proskurnin M, Brouwers HJH (2019) Municipal solid waste incineration (MSWI) fly ash composition analysis: A case study of combined chelatant-based washing treatment

efficiency. J Environ Manage 235:480–488. doi: 10.1016/j.jenvman.2019.01.096

21. Quina MJ, Bordado JC, Quinta-Ferreira RM (2008) Treatment and use of air pollution control residues from MSW incineration: An overview. Waste Manag 28:2097–2121. doi: 10.1016/j.wasman.2007.08.030

22. Wang L, Jin Y, Nie Y (2010) Investigation of accelerated and natural carbonation of MSWI fly ash with a high content of Ca. J Hazard Mater 174:334–343. doi: 10.1016/j.jhazmat.2009.09.055

23. Kitamura H, Dahlan AV, Tian Y, et al. (2017) Geochemical form analysis of titanium in chelate-treated municipal solid waste incineration fly ash particles employing correlation analysis of elemental distribution line profiles. J Japan Soc Civ Eng 73: III_287-III_295. doi: 10.2208/jscejer.73.III_287

24. Hu HY, Liu H, Zhang Q, et al. (2016) Sintering characteristics of CaO-rich municipal solid waste incineration fly ash through the addition of Si/Al-rich ash residues. J Mater Cycles Waste Manag 18:340–347. doi: 10.1007/s10163-014-0341-z

25. Li M, Su P, Guo Y, et al. (2017) Effects of SiO2, Al2O3 and Fe2O3 on leachability of Zn, Cu and Cr in ceramics incorporated with electroplating sludge. J Environ Chem Eng 5:3143–3150. doi: 10.1016/j.jece.2017.06.019

26. Mao L, Cui H, Miao C, et al. (2016) Preparation of MgCr2O4 from waste tannery solution and effect of sulfate, chloride, and calcium on leachability of chromium. J Mater Cycles Waste Manag 18:573–581. doi: 10.1007/s10163-015-0354-2

27. Volzone C, Cesio AM (2003) Changes in OH-Cr-montmorillonite after heating in air and nitrogen atmospheres. Mater Chem Phys 79:98–102. doi: 10.1016/S0254-0584(02)00430-3

28. Cai Z, Chen D, Lundtorp K, Christensen TH (2003) Evidence of Al-Cr interactions affecting Cr-leaching from waste incineration ashes. Waste Manag 23:89–95. doi: 10.1016/S0956-053X(02)00113-7

29. Astrup T, Rosenblad C, Trapp S, Christensen TH (2005) Chromium release from waste incineration air-pollution-control residues. Environ Sci Technol 39:3321–3329. doi: 10.1021/es049346q

30. Tang Y, Chui SSY, Shih K, Zhang L (2011) Copper stabilization via spinel formation during

the sintering of simulated copper-laden sludge with aluminum-rich ceramic precursors. Environ Sci Technol 45:3598–3604. doi: 10.1021/es103596k

31. Yuanyuan Tang, Kaimin Shih CL, Liao, and C (2018) Cubic and tetragonal ferrite crystal structures for copper ion immobilization in an iron-rich ceramic matrix. RSC Adv 8:8805–8812
32. Gilardoni S, Fermo P, Cariati F, et al. (2004) MSWI fly ash particle analysis by scanning electron microscopy-energy dispersive X-ray spectroscopy. Environ Sci Technol 38:6669–6675. doi: 10.1021/es0494961
33. Kitamura H, Dahlan AV, Tian Y, et al. (2018) Impact of secondary generated minerals on toxic element immobilization for air pollution control fly ash of a municipal solid waste incinerator. Environ Sci Pollut Res 1–13. doi: 10.1007/s11356-018-1959-5
34. Chang CY, Wang CF, Mui DT, Chiang HL (2009) Application of methods (sequential extraction procedures and high-pressure digestion method) to fly ash particles to determine the element constituents: A case study for BCR 176. J Hazard Mater 163:578–587. doi: 10.1016/j.jhazmat.2008.07.039
35. Oischinger J, Meiller M, Daschner R, et al. (2019) Fate of nano titanium dioxide during combustion of engineered nanomaterial-containing waste in a municipal solid waste incineration plant. Waste Manag Res 37:1033–1042. doi: 10.1177/0734242X19862603
36. Massari A, Beggio M, Hreglich S, et al. (2014) Behavior of TiO2 nanoparticles during incineration of solid paint waste: A lab-scale test. Waste Manag 34:1897–1907. doi: 10.1016/j.wasman.2014.05.015
37. Zhou J, Wu S, Pan Y, et al. (2015) Enrichment of heavy metals in fine particles of municipal solid waste incinerator (MSWI) fly ash and associated health risk. Waste Manag 43:239–246. doi: 10.1016/j.wasman.2015.06.026
38. Jiao F, Zhang L, Dong Z, et al. (2016) Study on the species of heavy metals in MSW incineration fly ash and their leaching behavior. Fuel Process Technol 152:108–115. doi: 10.1016/j.fuproc.2016.06.013
39. Haiying Z, Youcai Z, Jingyu Q (2010) Characterization of heavy metals in fly ash from municipal solid waste incinerators in Shanghai. Process Saf Environ Prot 88:114–124. doi:

10.1016/j.psep.2010.01.001

40. Wei Y, Shimaoka T, Saffarzadeh A, Takahashi F (2011) Mineralogical characterization of municipal solid waste incineration bottom ash with an emphasis on heavy metal-bearing phases. J Hazard Mater 187:534–543. doi: 10.1016/j.jhazmat.2011.01.070

4.6 Supplementary materials

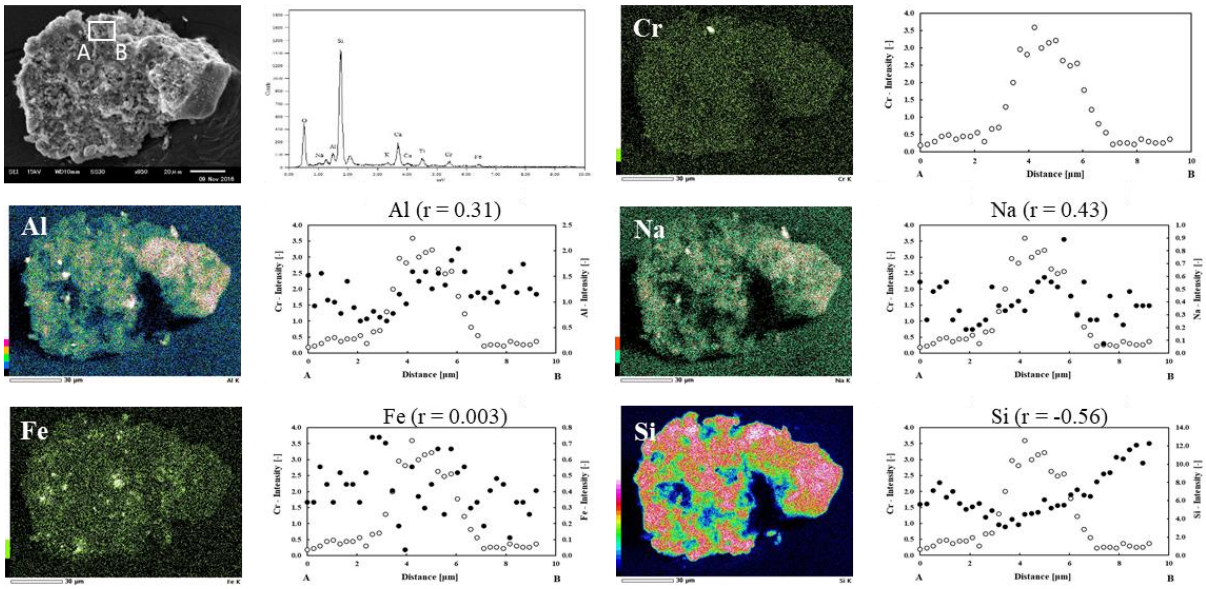

Figure S.4-1 Chromium correlation in the core components of fly ash particle

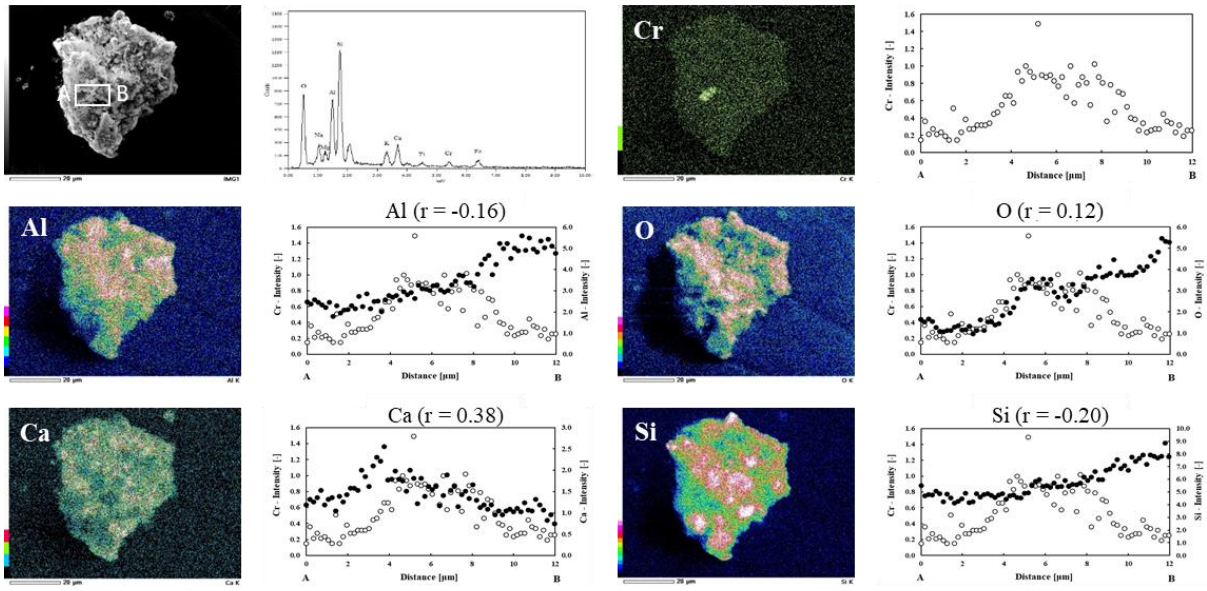

Figure S.4-2 Chromium correlation in the semi-soluble components of fly ash particle

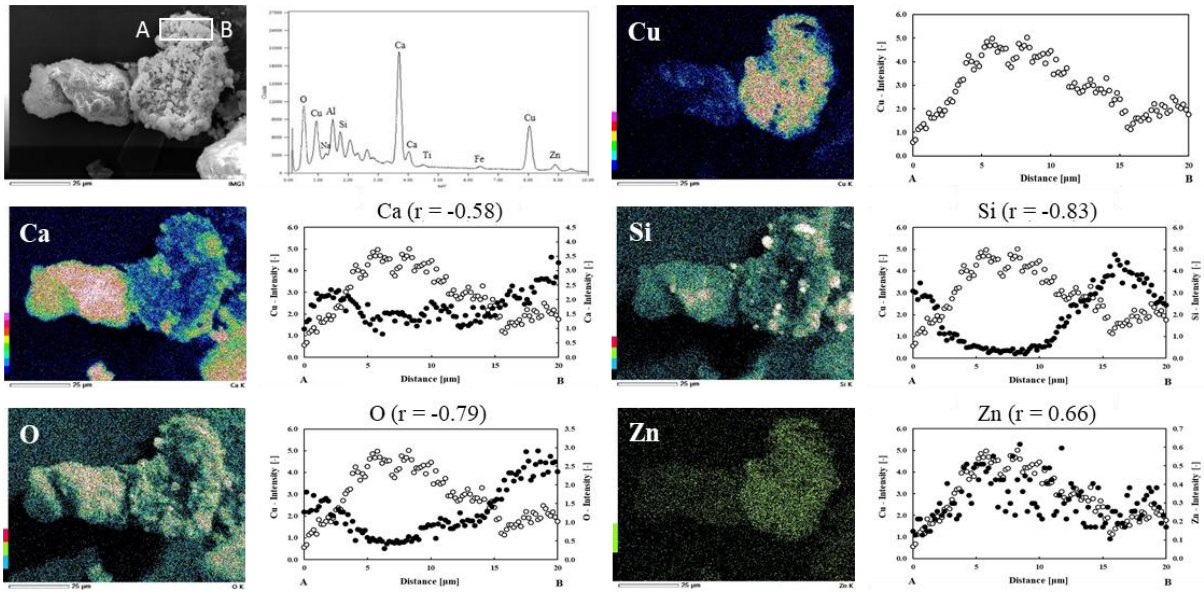

Figure S.4-3 Copper correlation in the core components of fly ash particle

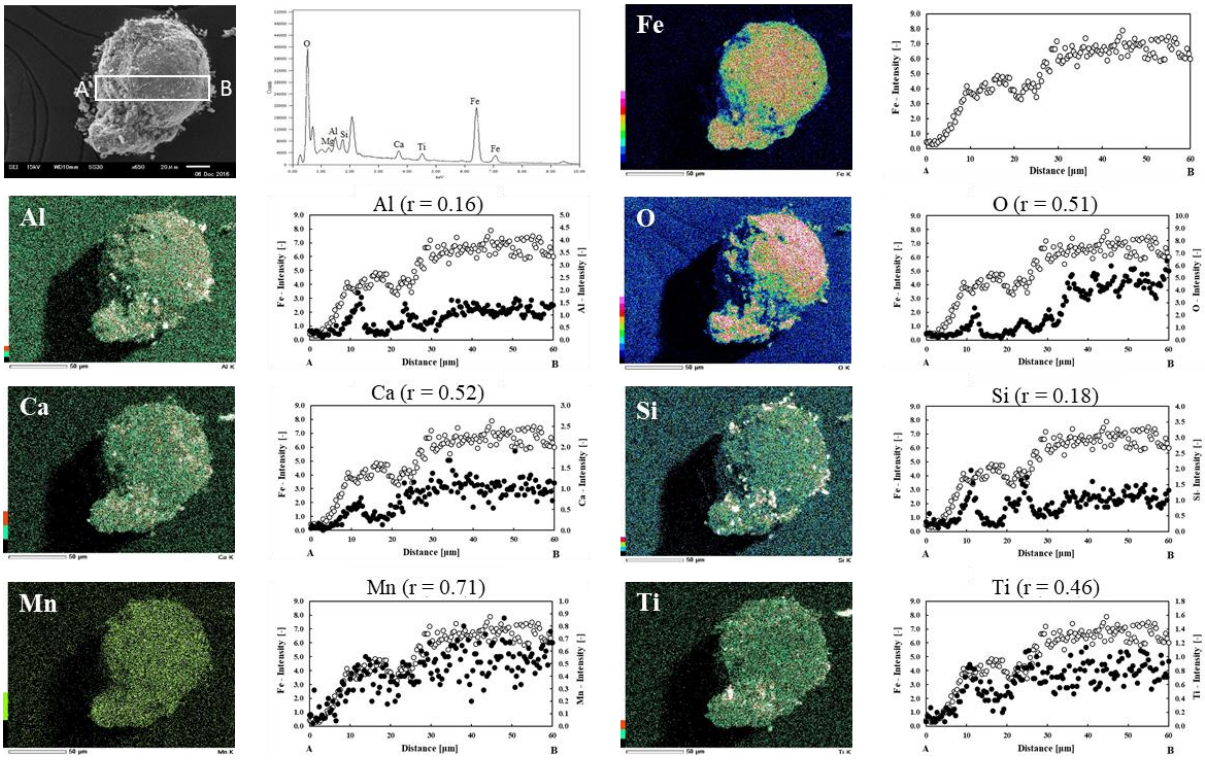

Figure S.4-4 Iron correlation in the core components of fly ash particle

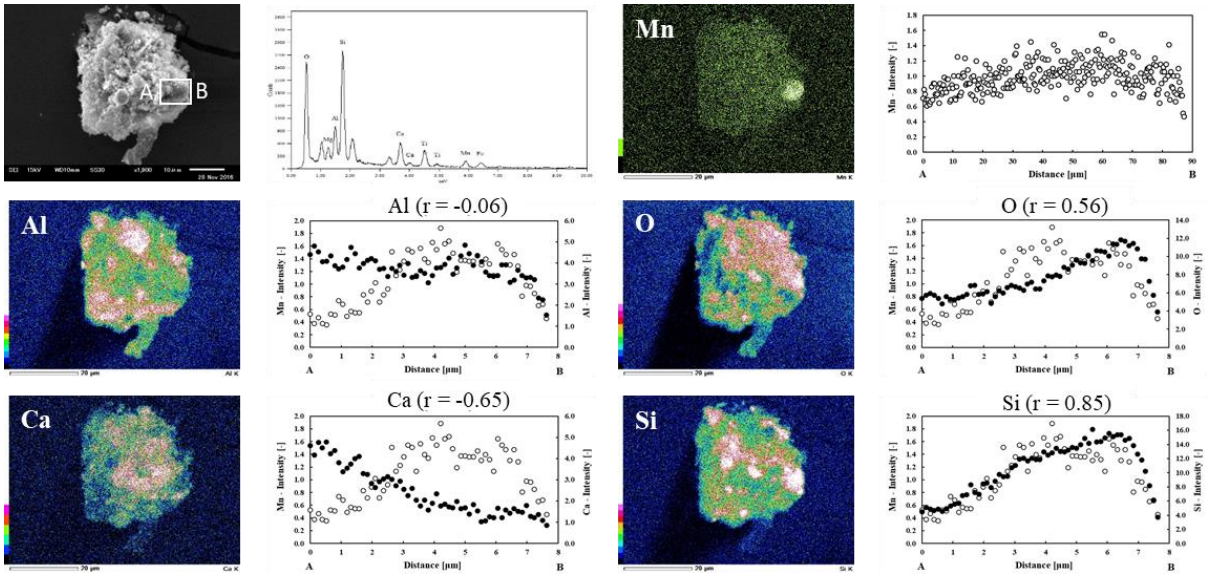

Figure S.4-5 Manganese correlation in the core components of fly ash particle

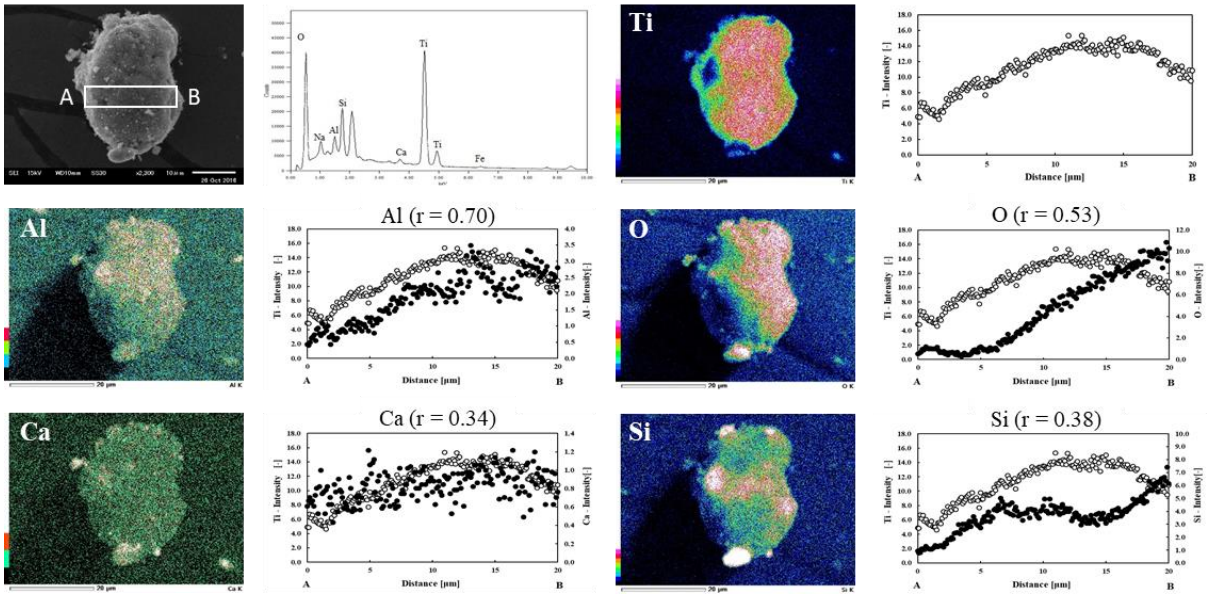

Figure S.4-6 Titanium correlation in the insoluble core component of fly ash particle

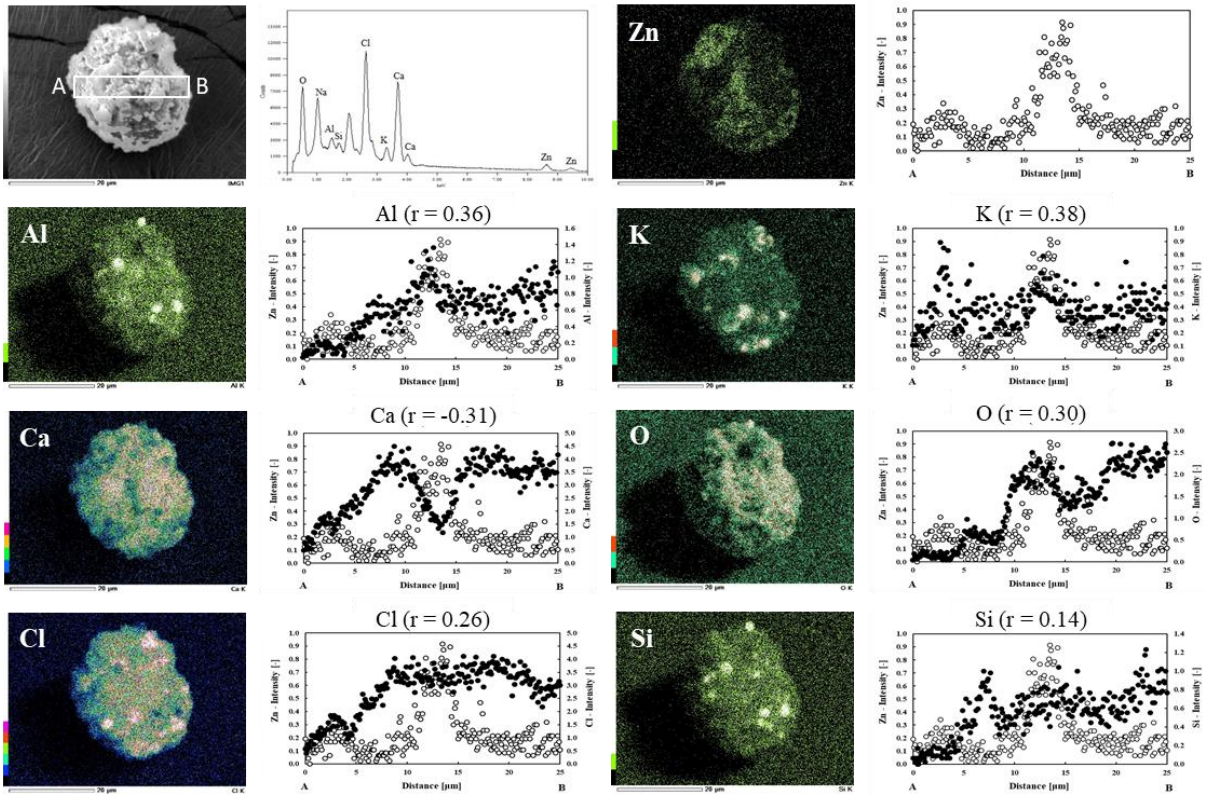

Figure S.4-7 Zinc correlation in the surface of fly ash particle

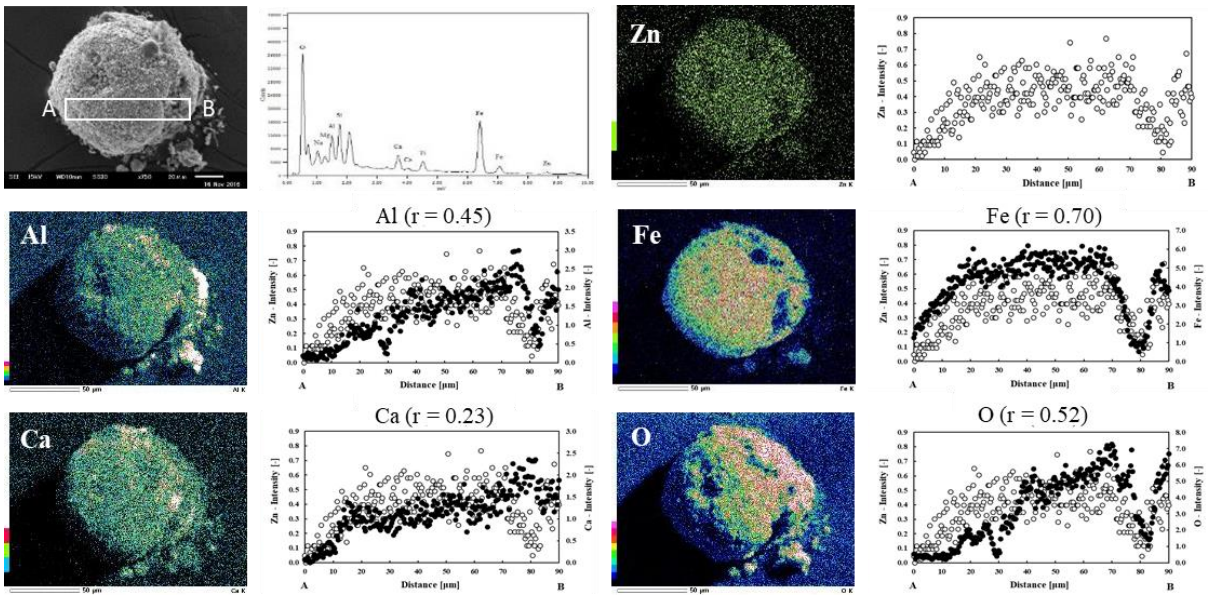

Figure S.4-8 Zinc correlation in the core of fly ash particle

Chapter 5

Impact heterogeneities characteristic on elemental leachability in fly ash generated from fluidized bed municipal solid waste incineration

Abstract: MSWI fly ash from a fluidized bed combustor have a heterogeneous characteristic. This study aims to investigate the impact of heterogeneity on elemental heterogeneity. Geochemical simulation is using to model solid-phase dissolution behavior in the total availability leaching test. pH after leaching is in the range 11- 13, in the high alkaline pH range. Heavy metals that are detected by SEM-EDS are Fe and Ti. Fe exists as solid-phase might be possible for Fe precipitated into a solid phase. The iron occurs as celadonite and saponite, which is rarely observed in the mineralogical characteristic of MSWI fly ash. Titanium exists as a rutile based on simulation and experimental data. Those metals are precipitated into the solid phase, which has dispersed concentration. It suggested elemental heterogeneity can be affected by the formation of elements in their solid phase. Elemental heterogeneity might have a negligible effect on heavy metal leachability.

5.1 Introduction

While the development of municipal solid waste (MSW) treatment technology is increasingly sophisticated, incineration still a common way to treat MSW in many countries. MSW incineration (MSWI) can decrease the waste mass by 70% and waste volume by 90%, destroy pathogenic agents and produce energy (waste-to-energy) [1–3]. Accordingly, MSWI generates secondary solid residues, which are bottom ash and fly ash. Fly ash has major elements, including Ca, Cl, Si, Al, K, Na, S, Mg, Fe, and Ti. Fly ash contains a significant amount of alkaline oxides (CaO) and a high amount of acidic oxide (SiO_2). Therefore, fly ash has alkaline pH around 10-11 but with low acid-neutralizing capacity (ANC) [4]. The primary concerns of the disposal or utilization of municipal solid waste incineration (MWSI) fly ash is that it contains considerable amounts of chlorides, especially alkali metal chlorides and high heavy metal, including lead, mercury, chromium, cadmium, copper, and zinc, leaching concentration [5–7]. A comprehensive characterization of fly ash is necessary for the long-term impact of its disposal under various environmental situations. The leaching properties of heavy metal from fly ash correlated with characteristics of the fly ash [8]. The high amount of calcium is the controlling factor for metal leaching behavior in fly ash, and the high calcium content resulted from the excess lime addition is used to ensure the emission compliance of acid gases [9]. Other factors that can influence leaching characteristics are pH, liquid to solid (L/S) ratio, and aging and weathering [10]. Various leaching methods were developed to assess the ash leaching potential, such as toxicity characteristic leaching potential (TCLP) methods, batch leaching methods, and column leaching methods [11].

Estimation of leaching potential of trace element of MSWI ash upon its disposal or utilization can use geochemical modeling. Geochemical modeling can calculate the composition of leachate in equilibrium with solubility/sorption-controlled minerals and can calculate the leaching potential of elements under different circumstances [12]. Geochemical models such as Visual MINTEQ, ORCHESTRA, and PHREEQC are widely used to predict metal release from MSWI ash and further describe its leaching behavior [13–15]. Geochemical modeling also able to predict pH-dependent leaching behavior of major and trace elements, and it has good agreement with the result of the pH-dependent test. The pH value of leachate can significantly influence the leaching behavior of MSWI fly ash [16]. The geochemical modeling predicted element concentration in the range of pH 4.5-12.5 based

on solubility control. Some cases were below concentration predicted by mineral solubility, other mechanisms such as sorption, redox processes, or incorporation into different mineral phases may be necessary for these elements at certain pH-values [17].

Geochemical simulation and experimental data of incinerator residue have gap value that had been found in other research. Overestimation of geochemical simulation occurred at alkaline pH of incineration residue, whereby mineral dissolution was limited [18]. In our previous study, fly ash particles have elemental heterogeneity characterization [19]. On the other hand, some toxic metals are incorporated in Al-, Ca-, and Si-based materials like the Al-rich phase, calcite phase, and glass phase [20, 21]. If external matrices around toxic metals also control metal leaching behaviors, their heterogeneities might be necessarily considered. It might lower gaps between experimental leaching concentrations of metals and geochemical model predictions. Therefore, in this study, heterogeneity characterization was included in the geochemical modeling of the leaching behavior of major elements and heavy metals. This study aims to evaluate the impact of elemental heterogeneities on their leachabilities.

5.2 Materials and methods

5.2.1 Fly ash samples

A fluidized bed incineration plant in Japan that has a capacity of around 250Mg/day is producing fly ash. In this study, fly ash was sampled from this incineration plant. For gas neutralization and dioxin control, lime slurry and powdered activated carbon were injected into flue gas during the post-combustion area. Fly ash was collected in the air pollution control, fabric filter then transferred to the ash storage tank by an air pressure feeder or a mechanical feeder. That fly ash was moved into the chelate treatment apparatus and sampled for the study. The fly ash sample was dried under room conditions for a week or longer. After the drying process, fly ash was observed and analyzed.

5.2.2 Microscopic observation of fly ash particles

The morphological surface and elemental composition of MSWI fly ash particles were observed using a scanning electron microscope coupled with energy-dispersive x-ray spectroscopy (SEM-EDX

JSM-6610 LA, JEOL, Ltd., Japan). The fly ash samples were fixed on the carbon tape on the observation stage. Because it might cause overestimation of carbon content, carbon content would not be presented in this research. The samples were observed after Pt-Pd sputtering for 30 seconds using a sputter coating device (MSP-1S, Vacuum device Ltd., Japan). Elemental mapping of fly ash particle surfaces was carried out to analyze elemental distribution. In this study, one hundred particles of fly ash samples were analyzed by SEM-EDX.

5.2.3 Elemental heterogeneity analysis

Focusing on a single fly ash particle by using SEM-EDX, surface elemental concentration on each of fly ash particle is measured to describe elemental heterogeneity of fly ash particle. In this study observed in total 100 single fly ash particles, afterward, each single fly ash particle divided into five horizontal sections, as shown in **Figure 5.1**. The elemental intensity of each section was different for each particle because of varied areas of section. The coefficient of variation (CV value = standard deviation/average) was calculated for each element, and each section using intensity data. A total of 500 sections were summarized and categorized.

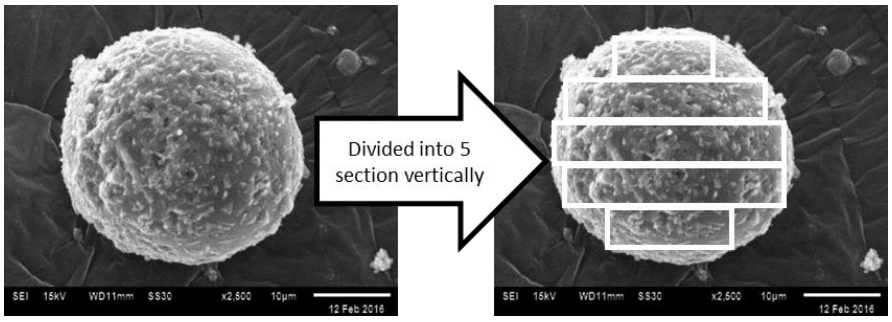

Figure 5.1 Line profile analysis of elemental heterogeneity

In Chapter 4, the Al/Ca/Si-based matrix in the fly ash might control the leaching behavior of heavy metals. Therefore, in this Chapter, the group for geochemical simulation is based on the Al, Ca, and Si to identify their influence in elemental leachability. The model's groups are five groups of CV in each of Al, Ca, and Si, which are very high (CV >10), high (CV 7.5-10), medium (CV 5-7.5), low (CV 2.5-5), and very low (CV < 2.5). Groups 1-1 until 1-5 based on the categorization of Ca's CV value.

Other elements in each group of CVs are an average of elements' CV in section along with the Ca's CV. It is also the same way to the Al group (2-1 – 2-5) and Si group (3-1 – 3-5). Groups of CV were summarized in **Table 5.1**.

Table 5.1 Model groups based on CV values

Group name	Elements	CV
1-1	Ca	>10
1-2	Ca	7.5 - 10
1-3	Ca	5 - 7.5
1-4	Ca	2.5 - 5
1-5	Ca	0 - 2.5
2-1	Al	>10
2-2	Al	7.5 - 10
2-3	Al	5 - 7.5
2-4	Al	2.5 - 5
2-5	Al	0 - 2.5
3-1	Si	>10
3-2	Si	7.5 - 10
3-3	Si	5 - 7.5
3-4	Si	2.5 - 5
3-5	Si	0 - 2.5

5.2.4 Geochemical modeling

This study investigated the leaching of elements from the MSWI fly ashes controlled by the heterogeneity of major elements in the fly ash particle via geochemical modeling. The PHREEQC (version 2) was used to calculate element speciation after the leaching test and the degree of saturation concerning the mineral phases [22]. The LLNL.dat database was used for all calculations. Thermodynamic activities and mass-action equations describe the chemical speciation, ion exchange, and surface species by using a modified Newton-Raphson method to solve the simultaneous nonlinear equations. The full equations were added in section **5.6 Supplementary materials**. A set of minerals that controls solubility of major elements was selected based on the mineralogical analysis in the fly ash particle. The model proposed the final pH after the leaching test in each group. The model was composed of elemental quantities that were estimated based on the experimental data of elemental intra-particle heterogeneity. Completely dissolved elemental after leaching tests such as Na, K, Cl, and S

also included in the model because these elements might be influence prediction of Al/Ca/Si. The geochemical simulation produces several kinds of precipitated deposition.

5.3 Results and discussion

5.3.1 pH after simulation

Figure 5.2 shows the final pH after the leaching test in each group. After the geochemical simulation, pH in each group is diverse; however, it is still in the alkaline pH range. Groups 1-1 until 1-5 are based on control of Ca CV value—the range of final pH from11.8 – 13.2. Based on Astrup et al. modeling results, Ca concentration increased in the scope of pH 11 – 12.5 [17]. Ca mineral phased in the fly ash from a fluidized bed is form mainly as calcite ($CaCO_3$). However, the model results indicated that alkaline compounds like oxides and hydroxides exist in the fly ash, such as CaO and its conversion alkaline products, which have been explained by Hu et al.'s finding [23]. Therefore, the dissolution of CaO, which mainly from unreacted lime, increased the pH value in the leaching solution.

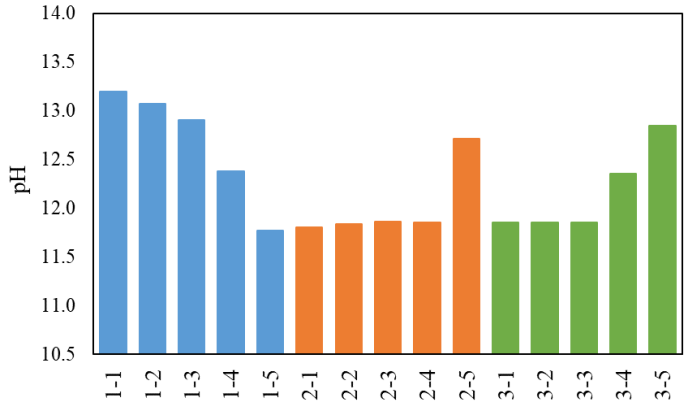

Figure 5.2 pH after leaching in all groups of CV

Moreover, the pH in the Ca's group has decreased along with the decrease of CV value. It showed Ca concentration as a factor for the pH in the fly ash particle. Alkaline pH in the fly ash significantly depends on the CaO and MgO mineral content in the fly ash and its dissolution rates in the aqueous solution [24]. In contrast, the dissolution of Al_2O_3 in fly ashes decreases the alkalinity because Al_2O_3 in the fly ash has a function as primary neutralizing basic oxide. In contrast, the pH of Al and Si after the geochemical simulation has a similar pattern. The pH of Al and Si increases while their CV

value decreases. Group of 2-1 until 2-5 that is controlled by the CV value of Al have range pH from 11.8 – 12.7, as shown in **Figure 5.2**. Although significant constituent of Al, pH after leaching test of fly ash still in the alkaline range. It might be due to the CaO in the fly ash that is significantly affecting the pH. The previous geochemical simulation was giving aluminum between pH 4 and 13 that aluminum is precipitated as diaspore (AlOOH) at pH higher than 13 [25]. Aluminum in this fly ash sample in the gehlenite mineral phase. Besides that, aluminum exists as Al_2O_3 and alumino-silicate compound in the fly ash. As mention in Chapter 2, alumino-silicate mainly included with Ca-based aggregates. It suggested aluminum in this fly ash samples not mainly formed as Al_2O_3. Therefore, the final pH after leaching in the alkaline range.

The group of silica's CV values, 3-1 until 3-5, have pH 11.9 – 12.9, which is the same range as Al (see **Figure 5.2**). Previous research also found a similar leaching pattern of Si to those of Al. Dissolution of akermanite or strätlingite caused by depletion of other Ca-containing minerals is suggested to control the Si leaching from incineration residues [14]. Si mineral phase in this fly ash sample forms as quartz and gehlenite. Eighmy et al. suggested that the dissolution of Si controlled by kinetically driven dissolution reaction and not by the dissolution of quartz [26]. In summary, elemental heterogeneity proposed local pH in the individual level of fly ash particle. Alkaline pH in most of the groups might be due to dissolution CaO as the main factor of alkalinity in the fly ash.

5.3.2 Elemental leachability

After the geochemical simulation, elemental concentration after leaching diverse each of the groups. Solid-phase was detected in several elemental components such as Al, Si, Mg, Fe, and Ti. **Figure 5.3** shows the elemental concentration in the solid-phase state after geochemical simulation. The Ca solubility mainly controlled by gypsum at pH below 9.5 and ettringite for pH above 9.5 [17]. Based on the geochemical simulation, the pH of fly ash samples above 11. It shows ettringite is the mineral controlled in the solubility of Ca. Ettringite was detected in the mineral phase of fly ash after water leaching treatment. However, after acid leaching treatment, mostly Ca is found in the calcite form. Hyks et al. modeled elemental leachability with L/S ratio, and only the solubility-controlled elements were considered. Overall, the interaction between the Ca-mineral phase was shown crucial as these

minerals influenced both pH and leaching of major elements (Ca and S), which in turn had an impact on the remaining elements. Calcite played a limited role at pH >10.5 in the portlandite–gypsum–ettringite system [14]. In the solid-phase of Ca is calculated by total Ca. Although ettringite and portlandite ($Ca(OH)_2$) are formed in the mineral phase, it possibly Ca exist in the solution form higher than in the solid phase. Therefore, by calculation, there is no solid-phase of Ca is formed in all groups. Molar balance during simulation is not perfect and might cause a non-negligible error. In the solution form, Ca mainly exists as Ca^{2+} and $CaCl^{+}$ at pH 0-12 and as $CaOH^{+}$ in the pH 12 -13 [16]. Based on pH simulation, groups 1-3, 1-4, and 1-5 are between pH 11.8 – 12.9, which possibly ettringite is formed in this group. For groups 1-1 and 1-2, Ca exist as portlandite. Figure 5.3 shows that Ca is not affecting by heterogeneity characteristics. Ca heterogeneity mostly controlled by the solubility of Ca speciation, which highly pH-dependent.

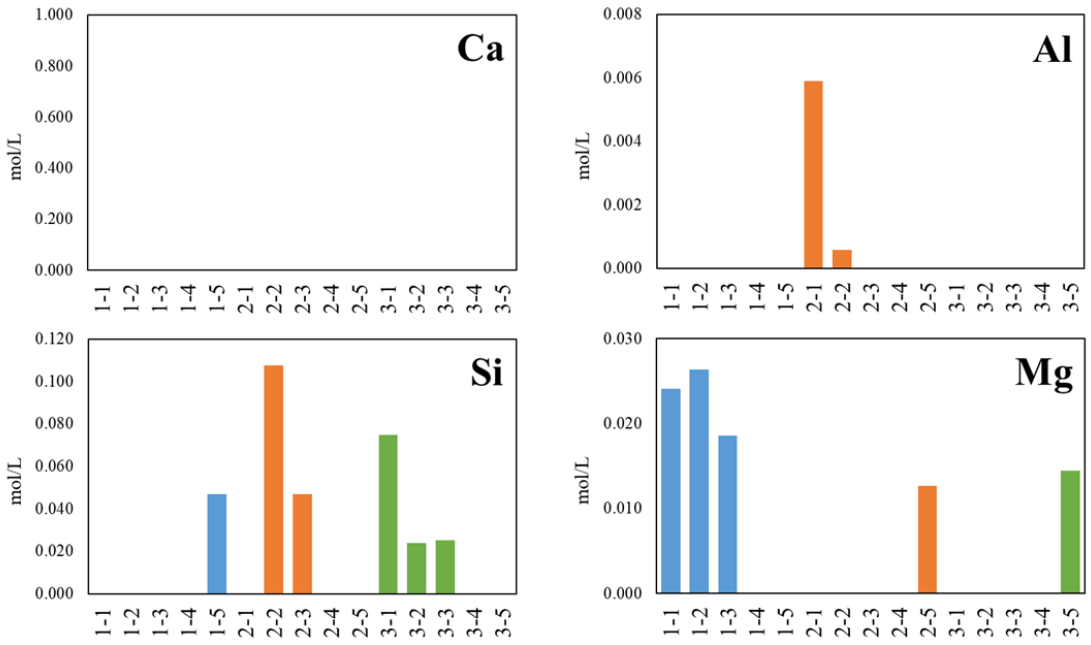

Figure 5.3 Elemental concentration in the solid phase after leaching

Based on the simulation, only group 2-1 and 2-2 are the only formed solid phase after leaching. Those groups have a high CV value of Al more than 7.5. Similar to Ca, Al also not depend on elemental heterogeneity. Based on the simulation, precipitated deposition of Al might be diaspore (AlO(OH)), gibbsite ($Al(OH)_3$), and gehlenite. Gibbsite is controlling the dissolution of Al at pH>9, which is

observed increasing Al concentration into the solution from another study [24]. These minerals do not found by XRD and XPS; it is likely in the solid phase that forms diagenetically from the dissolution of more soluble aluminum-containing minerals, which are present in the ash [26].

Figure 5.3 shows a solid-phase of Si that is formed in the medium until a very high CV of Si (3-1 – 3-3), very low CV of Ca (1-5), and medium-high CV of Al (2-2 – 2-3). Si formed into solid-phase in the low heterogeneity of Ca, however, in the higher heterogeneity of Al and Si. It suggested after leaching silica in the form of aluminosilicate included in the Ca-based materials. Proposed depositions of Si-based on simulation are gehlenite, wairakite, and wollastonite. Astrup et al. described that quartz is not controlled solubility of Si. However, leucite ($KAlSi_2O_6$) or wairakite ($CaAl_2Si_4O_{12},2H_2O$) controlled Si at pH 10-11. Possibly, wollastonite ($CaSiO_3$) managed solubility at high pH [17]. Based on the simulation, minerals in the solid phase of Mg are brucite ($Mg(OH)_2$), forsterite (Mg_2SiO_4), periclase (MgO), and spinel ($MgAl_2O_4$). These minerals emerged in the groups medium – very high Ca (1-1 – 1-3), and very low Al and Si (2-5, 3-5) that formed Mg in the solid deposition after leaching simulation (see **Figure 5.3**). Mg remained in the solid-phase in high heterogeneity of Ca and low heterogeneity of Al and Si. The heterogeneity of Ca/Al/Si in the fly ash particle can control Mg leaching behavior. Baciocchi et al. investigated mineral solubility of Mg in the fly ash incinerator. Forsterite (Mg_2SiO_4) controlled solubility in the pH range 8-11 and $Mg(OH)_2$ at higher pH [27]. In summary, elemental heterogeneities have impacted metal deposition into a solid phase of fly ash after leaching.

5.3.3 Heavy metal leachability

Heavy metals in the simulation based on elemental composition in the fly ash. Detected heavy metals in the fly ash samples are only Fe and Ti. Although some heavy metals such as Zn and Cu have more than 1 wt% based on XRF analysis, those heavy metals cannot be detected by SEM-EDX due to low concentration in the individual fly ash particle. **Figure 5.4** shows that Fe and Ti are precipitated in the groups. Overall, heavy metals included in almost every group. The concentration of Fe increases while CV values of Ca decreasing.

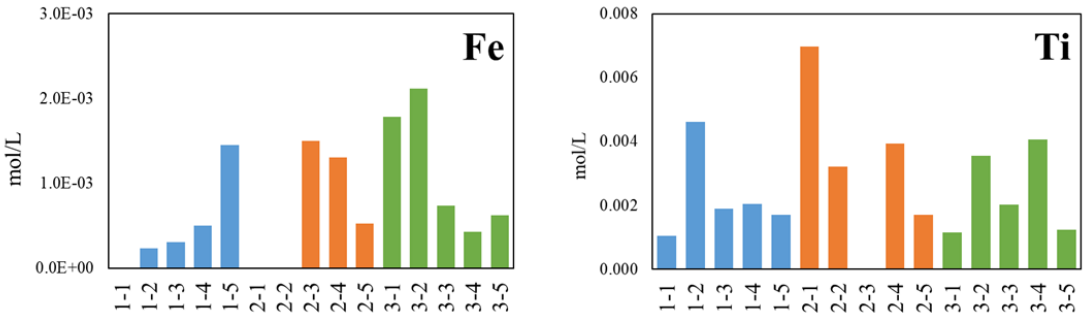

Figure 5.4 Heavy metal concentration in the solid phase after leaching

In contrast, Fe concentration is decreased while the CV value of Al and Si is also decreasing. Iron has a similar tendency with pH. Fe formed into a solid phase in high heterogeneity of Al and Si. In contrast, Fe remained in the low heterogeneity of Ca. It might imply the Fe-solid phase immobilized into the aluminosilicate domain in the fly ash particle. Leaching of iron in the MSWI fly ash mainly controlled by hematite (Fe_2O_3) and amorphous $Fe(OH)_3$ [13, 24].

Furthermore, another research found that Fe occurs in small amounts of Ca-nontronite and $FeCr_2O_4$ [28]. The potential presence of these solid phases can control the leaching potential of Fe. In the very acidic and basic conditions, leaching concentration increase into an effluent solution. In the simulation, Fe exists as solid-phase might explain the condition still possible for Fe precipitated into a solid phase. Hematite also observed in the XRD results; however, simulation result shows no hematite exist as the solid phase of iron. The iron occurs as celadonite and saponite. These minerals rarely observed in the mineralogical characteristic of MSWI fly ash.

Titanium had not simulated in heavy metal leachability in some research. Although titanium detected in the elemental composition and crystalline phase of MSWI fly ash, **Figure 5.4** shows no clear correlation between the CV value of Al, Ca, and Si with a concentration of Ti. Titanium in this fly ash sample exists as rutile. Furthermore, rutile as solid-phase deposition after leaching simulation. Perovskite not observed in the mineral simulation. Titanium preferred to entrap into Al-based than Ca-based materials in the fly ash, which influence Ti leaching behavior. Ti does not depend on the heterogeneity of Si. In summary, heavy metal formation into solid phase can be affected by elemental heterogeneity.

5.4 Conclusion

In Chapter 5, we tried to investigate the impact of heterogeneity on elemental leachability of the fly ash particle generated from a fluidized bed incinerator. The geochemical model was used to model solid-phase dissolution behavior in the total availability leaching test. The solid-phase identified with elemental heterogeneity from the surface of MSWI fly ash were input into the model with the aim that the simulation would insoluble solid phase remained after leaching and produce leachate of similar composition to experimental leachate. Using PHREEQC as geochemical modeling could model solid-phase controlling leaching behavior. Elemental heterogeneity proposed local pH in the individual level of fly ash particle. pH after leaching is in the range 11- 13, in the high alkaline pH range. Alkaline pH in most of the groups might be due to dissolution CaO as the main factor of alkalinity in the fly ash. Heterogeneity affecting solid-phase concentration that is formed after leaching. Heavy metals that are detected by SEM-EDS are Fe and Ti. Those metals are precipitated into the solid phase, which has dispersed concentration. It suggested elemental heterogeneity can be affected by the formation of elements in their solid phase. However, it is not affecting the leaching behavior of Ca and Al. Mostly these elements controlled by solubility, which highly pH-dependent. Elemental heterogeneity might have a negligible effect on heavy metal leachability. Further research of elemental heterogeneity combine with comprehensive analysis is necessary to lower the gap between heavy metal leachability in the model and experimental data.

5.5 References

1. Elomaa H, Seisko S, Lehtola J, Lundström M (2019) A study on selective leaching of heavy metals vs. iron from fly ash. J Mater Cycles Waste Manag 21:1004–1013. https://doi.org/10.1007/s10163-019-00858-w
2. Mukunoki T, Hoai TT, Fukushima D, et al. (2019) Physical and mechanical properties of municipal solid waste incineration residues with cement and coal fly ash using X-ray Computed Tomography scanners. Front Struct Civ Eng 13:640–652. https://doi.org/10.1007/s11709-018-0502-6
3. Quina MJ, Bontempi E, Bogush A, et al. (2018) Technologies for the management of MSW incineration ashes from gas cleaning: New perspectives on recovery of secondary raw materials and circular economy. Sci Total Environ 635:526–542. https://doi.org/10.1016/j.scitotenv.2018.04.150
4. Phua Z, Giannis A, Dong ZL, et al. (2019) Characteristics of incineration ash for sustainable treatment and reutilization. Environ Sci Pollut Res 26:16974–16997. https://doi.org/10.1007/s11356-019-05217-8
5. Zhao K, Hu Y, Wang Y, et al. (2019) Speciation and Risk Assessment of Heavy Metals in Municipal Solid Waste Incineration Fly Ash during Thermal Processing. Energy and Fuels. https://doi.org/10.1021/acs.energyfuels.9b02187
6. Czop M, Łázniewska-Piekarczyk B (2019) Evaluation of the leachability of contaminations of fly ash and bottom ash from the combustion of solid municipal waste before and after stabilization process. Sustain 11:1–16. https://doi.org/10.3390/su11195384
7. Lima AT, Ottosen LM, Pedersen AJ, Ribeiro AB (2008) Characterization of fly ash from bio and municipal waste. Biomass and Bioenergy 32:277–282. https://doi.org/10.1016/j.biombioe.2007.09.005
8. Ohbuchi A, Koike Y, Nakamura T (2019) Quantitative phase analysis of fly ash of municipal solid waste by X-ray powder diffractometry/Rietveld refinement. J Mater Cycles Waste Manag 21:829–837. https://doi.org/10.1007/s10163-019-00838-0
9. Tong L, Tang Y, Wang F, et al. (2019) Investigation of controlling factors on toxic metal

leaching behavior in municipal solid wastes incineration fly ash. Environ Sci Pollut Res 26:29316–29326. https://doi.org/10.1007/s11356-019-06123-9

10. Dou X, Ren F, Nguyen MQ, et al. (2017) Review of MSWI bottom ash utilization from perspectives of collective characterization, treatment and existing application. Renew. Sustain. Energy Rev. 79:24–38
11. Yin K, Dou X, Chan WP, Chang VWC (2019) Comparative leaching characteristics of fly/bottom ashes from municipal solid waste incineration under various environmental stresses. J Mater Cycles Waste Manag. https://doi.org/10.1007/s10163-019-00915-4
12. Luo H, Cheng Y, He D, Yang EH (2019) Review of leaching behavior of municipal solid waste incineration (MSWI) ash. Sci. Total Environ. 668:90–103
13. Qiu Q, Jiang X, Chen Z, et al. (2018) Leaching of heavy metals from MSWI fly ash: Experiments vs. simulation. Arch Environ Prot 44:55–61. https://doi.org/10.24425/119691
14. Hyks J, Astrup T, Christensen TH (2009) Long-term leaching from MSWI air-pollution-control residues: Leaching characterization and modeling. J Hazard Mater 162:80–91. https://doi.org/10.1016/j.jhazmat.2008.05.011
15. Allegrini E, Butera S, Kosson DS, et al. (2015) Life cycle assessment and residue leaching: The importance of parameter, scenario and leaching data selection. Waste Manag 38:474–485. https://doi.org/10.1016/j.wasman.2014.12.018
16. ZHANG Y, JIANG J, CHEN M (2008) MINTEQ modeling for evaluating the leaching behavior of heavy metals in MSWI fly ash. J Environ Sci 20:1398–1402. https://doi.org/10.1016/S1001-0742(08)62239-1
17. Astrup T, Dijkstra JJ, Comans RNJ, et al. (2006) Geochemical Modeling of Leaching from MSWI Air-Pollution-Control Residues. Environ Sci Technol 40:3551–3557. https://doi.org/10.1021/es052250r
18. Yin K, Chan WP, Dou X, et al. (2018) Co-complexation effects during incineration bottom ash leaching via comparison of measurements and geochemical modeling. J Clean Prod 189:155–168. https://doi.org/10.1016/j.jclepro.2018.03.320
19. Dahlan AV, Kitamura H, Tian Y, et al. (2020) Heterogeneities of fly ash particles generated

from a fluidized bed combustor of municipal solid waste incineration. J Mater Cycles Waste Manag. https://doi.org/10.1007/s10163-020-00973-z

20. Wang L, Jin Y, Nie Y (2010) Investigation of accelerated and natural carbonation of MSWI fly ash with a high content of Ca. J Hazard Mater 174:334–343. https://doi.org/10.1016/j.jhazmat.2009.09.055

21. Saffarzadeh A, Shimaoka T, Wei Y, et al. (2011) Impacts of natural weathering on the transformation/neoformation processes in landfilled MSWI bottom ash: A geoenvironmental perspective. Waste Manag 31:2440–2454. https://doi.org/10.1016/j.wasman.2011.07.017

22. Parkhurst DL AC (1999) User's guide to PHREEQC (version 2) - a computer program for speciation, batch-reaction, one-dimensional transport, and inverse geochemical calculations. US Geol Surv Water-Resources Investig Rep 99:312

23. Hu HY, Liu H, Shen WQ, et al. (2013) Comparison of CaO's effect on the fate of heavy metals during thermal treatment of two typical types of MSWI fly ashes in China. Chemosphere 93:590–596. https://doi.org/10.1016/j.chemosphere.2013.05.077

24. Komonweeraket K, Cetin B, Aydilek AH, et al. (2015) Effects of pH on the leaching mechanisms of elements from fly ash mixed soils. Fuel 140:788–802. https://doi.org/10.1016/j.fuel.2014.09.068

25. Van Herck P, Van Der Bruggen B, Vogels G, Vandecasteele C (2000) Application of computer modelling to predict the leaching behaviour of heavy metals from MSWI fly ash and comparison with a sequential extraction method. Waste Manag 20:203–210. https://doi.org/10.1016/S0956-053X(99)00321-9

26. Taylor Eighmy T, Dykstra Eusden J, Krzanowski JE, et al. (1995) Comprehensive Approach toward Understanding Element Speciation and Leaching Behavior in Municipal Solid Waste Incineration Electrostatic Precipitator Ash. Environ Sci Technol 29:629–646. https://doi.org/10.1021/es00003a010

27. Baciocchi R, Costa G, Di Bartolomeo E, et al. (2009) The effects of accelerated carbonation on CO2 uptake and metal release from incineration APC residues. Waste Manag 29:2994–3003. https://doi.org/10.1016/j.wasman.2009.07.012

28. Van Der Bruggen B, Vogels G, Van Herck P, Vandecasteele C (1998) Simulation of acid washing of municipal solid waste incineration fly ashes in order to remove heavy metals. J Hazard Mater 57:127–144. https://doi.org/10.1016/S0304-3894(97)00078-2

29. Wang L, Chen Q, Jamro IA, et al.. (2016) Geochemical modeling and assessment of leaching from carbonated municipal solid waste incinerator (MSWI) fly ash. Environ Sci Pollut Res 23:12107–12119. https://doi.org/10.1007/s11356-016-6320-2

30. Wang WX, Gao X, Li T, et al. (2018) Stabilization of heavy metals in fly ashes from municipal solid waste incineration via wet milling. Fuel 216:153–159. https://doi.org/10.1016/j.fuel.2017.11.045

31. Zhang Y, Cetin B, Likos WJ, Edil TB (2016) Impacts of pH on leaching potential of elements from MSW incineration fly ash. Fuel 184:815–825. https://doi.org/10.1016/j.fuel.2016.07.089

32. Garrels RM, Christ CL (1965) Solutions, minerals, and equilibria: Harper and Row, 450:65-66

33. Glynn PD (1991) MBSSAS: A code for the computation of Margules parameters and equilibrium relations in binary solid-solution aqueous-solution systems: Computers and Geosciences 17:907-966

34. Dzombak DA, Morel FM (1990) Surface complexation modeling—Hydrous ferric oxide: John Wiley 393

5.6 Supplementary materials

The geochemical simulation calculates chemical speciation in the aqueous system; besides that, it also calculates ion activity, precipitation, and surface complexation models [22]. Thermodynamic activities and mass-action equations describe the chemical speciation, ion exchange, and surface species by using a modified Newton-Raphson method to solve the simultaneous nonlinear equations.

Based on the Newton-Raphson method, mass-action can be express in a general way as:

$$K_i = a_i \prod_m^{M_{aq}} a_m^{-C_{m,i}} , \quad (1)$$

where K_i is a temperature-dependent equilibrium constant, M_{aq} is the total number of aqueous master species, and $c_{m,i}$ is the stoichiometric coefficient of master species *m* in species *i* that may be in a positive or negative value. The mass expression equation (2) can explain the total moles of an aqueous species *i*:

$$n_i = m_i W_{aq} = K_i W_{aq} \frac{\prod_m^{M_{aq}} a_m^{c_{m,i}}}{\gamma_i} , \quad (2)$$

where W_{aq} is the mass of solvent water in an aqueous solution. Davies equation is used to explained the activity coefficient of aqueous species as follow:

$$\log \gamma_i = -Az_i^2 \left(\frac{\sqrt{\mu}}{1+\sqrt{\mu}} - 0.3\mu \right), \quad (3)$$

where z_i is the ionic discharge of aqueous species *i*, A is constants dependent only on temperature, and μ is the ionic strength.

Based on Raoult's law [32], the activity of water is calculated from an approximation function as follow

$$f_{H_2O} = W_{aq}\left(a_{H_2O} - 1\right) + 0.0017 \sum_i^{N_{aq}} n_i . \quad (4)$$

Beside on activity of water, the function of ionic strength also defines as

$$\mu = \frac{1}{2} \sum_i^{N_{aq}} z_i^2 \frac{n_i}{W_{aq}}. \quad (5)$$

The function of ionic strength is defined as

$$f_\mu = W_{aq}\mu - \frac{1}{2}\sum_i^{N_{aq}} z_i^2 n_i . \quad (6)$$

Glynn et al. explained that the activity of component in solid solutions derived from solid solution on excess free energy, solid-phase activity coefficient, or distribution coefficient that can

be expressed by nondimensional Guggenheim parameters [33]. Therefore, the function used in the numerical method for solid solutions are

$$f_1 = \sum_m^{M_{aq}} c_{m,1} \ln a_m - \ln K_1 - \ln \frac{n_1}{n_1+n_2} - \ln \lambda_1 \text{ and} \quad (7)$$

$$f_2 = \sum_m^{M_{aq}} c_{m,2} \ln a_m - \ln K_2 - \ln \frac{n_2}{n_1+n_2} - \ln \lambda_2 , \quad (8)$$

where λ_1 and λ_2 are the activity coefficients of components 1 and 2.

The geochemical simulation uses the approach described by Dzombak and Morel [34] to relate the charge density on the surface, σ_s, with the potential at the surface, ψ_s. The surface-change density is the amount of charge per area of surface material, which can be calculated from the distribution of surface species:

$$\sigma_s = \frac{F}{A_{surf}} \sum_k^{K_s} \sum_{i_{(s_k)}}^{N_{s_k}} z_{i_{(s_k)}} n_{i_{(s_k)}}, \quad (9)$$

where σ_s is the charge density for surface s in coulombs per square meter (C/m^2), F is the Faraday constant in coulombs per mole, A_{surf} is the surface area of the material (m^2). The surface area is calculated by $A_{surf} = A_r n_r$, where A_r is the surface area per mole of pure phase or kinetic reactant (m^2/mol), and n_r is the moles of the pure phase or reactant. The charge-potential function is

$$f_{\psi_s} = (8000 \varepsilon \varepsilon_0 RT)^{\frac{1}{2}} \mu^{\frac{1}{2}} \sinh\left(\frac{F\psi_s}{2RT}\right) - \frac{F}{A_{surf}} \sum_k^{K_s} \sum_{i_{(s_k)}}^{N_{s_k}} z_{i_{(s_k)}} n_{i_{(s_k)}}. \quad (10)$$

Chemical speciation calculation requires calculating equilibrium between the aqueous phase and solid-solution assemblage that define to be present in a chemical system. The Newton-Raphson equations that can be included the equations $f_{m'}$, f_{H2O}, f_μ, f_{pss}, and f_{ψ_s}. These functions are equations for mole balance for elements or element valence states, the activity of water, ionic strength, solid solution, and implicit diffused-layer [22]. Mole-balance equations, $f_{m'}$, are included for total concentrations of elements, not individual valence states or combinations of individual valence states. Mole balance for elements is the total moles of an element in the system.

Chapter 6

Conclusion and recommendation

Abstract: In this chapter, significant results and findings of the study are summarized as a conclusion. Following the conclusion, recommendations for further work are suggested.

6.1 Conclusion

Heterogeneity characterization of MSWI fly ash from a fluidized bed incinerator was mainly focused on this research. The study investigated at a micro-scale level in the individual fly ash by using mainly SEM-EDX analysis to quantify heterogeneity characteristics. Fly ash particles likely consists of 3 main components; KCl/NaCl based aggregates on the surface, Al/Ca/Si-based semi-soluble component, and Al-rich, Ca-rich, or Si-rich insoluble core component. Fly ash components were observed by using three kinds of leaching experiments, which are using water, week acid, and strong acid. Therefore, this study modeled the components of fly ash particles to analyze their geochemical characteristics. Besides heterogeneity, other geochemical characteristics such as mineralogical and elemental components in the bulk samples were also observed in this study. The results obtained from this study allow us to draw the following major conclusion.

The mineralogical characteristic of fly ash from a fluidized bed shows a diversity of crystalline minerals. The crystalline phase in between each component in the fly ash particles is also diverse. The surface component mainly consists of quartz (SiO_2), sylvite (KCl), halite (NaCl), calcite ($CaCO_3$), gehlenite ($Ca_2Al_2SiO_7$), aluminum (Al), perovskite ($CaTiO_3$), and ferropericlase ($FeMg_8O$). The elemental composition resulting from XRF analysis consists of Ca, Cl, Si (>10 wt%), Fe, Al, K, Ti, Zn, Mg, S, Cu (>1 wt%), and other heavy metals (less than 1 wt%). Cl, Si (>10%), and Fe, Al, K, Ti, Zn, Mg, S, Cu (> wt%), and other heavy metals (less than 1 wt%).Other heavy metals are low detectable in the fly ash are Pb, Ba, Mn, Sn, Br, Sr, Sb, Zr, and Ni. Morphological characteristics of fly ash from the fluidized bed are similar shapes with stoker combustor fly ash. However, secondary mineral crystals like cubic and spicular shapes were not found, although they were observed in the stoker combustor fly ash.

Two types of heterogeneities, intra-particle heterogeneity, and inter-particle heterogeneity, of fly ash particles produced in a fluidized bed combustor, were evaluated quantitatively. Heterogeneities were measured in three components of fly ash particle bodies: surface, semi-soluble, and insoluble core components. Intra-particle heterogeneity is the heterogeneity inside each fly ash particle. Inter-particle heterogeneity is the heterogeneity among fly ash particles. The surface component of fly ash particles has more than 10% larger intra-particle heterogeneities than the semi-soluble and the insoluble core

components. In terms of inter-particle heterogeneity, the surface component has more than 5 % larger inter-particle heterogeneities then the semi-soluble component. The surface shows elemental heterogeneity due to more elemental composition such as chloride salts or oxide adsorb and become surface of fly ash particle. Besides, fly ash heterogeneity also gives insight into the fly ash formation process. The core of fluidized bed fly ash mostly consists of the Si-rich region. It formed mainly from flyable fine particles of silicate from silica sand and/or evaporated silicate. At the same time, heavy metal speciation was encapsulated inside the core. After the formation of the core component, Si-based aggregates formed a semi-soluble component around Si-core. Flyable silicate particles are still crucial in following the formation of lower semi-soluble components, but Ca adsorption becomes dominant in the formation of upper semi-soluble components. The possibility derived from Ca-based aggregates that aluminosilicate domain as part of the semi-soluble components. In the last stage of fly ash formation, salt chloride such as NaCl, KCl was randomly adsorbed around Ca-based aggregates with aluminosilicate included that generate hotspot in the surface of fly ash particle.

Different types of combustors can affect the characterization of fly ash. Fly ash from a fluidized bed has a more heterogeneous body. All components in the fly ash generated from the fluidized bed combustor have 4-760 % larger intra-particle heterogeneities than the stoker combustor fly ash. In terms of inter-particle heterogeneity, the semi-soluble and insoluble core components of the fluidized bed combustor fly ash have 30-72 % larger heterogeneity than the stoker fly ash. Two types of incinerators present different fly ash formation processes. The main difference is the formation of the insoluble core component of fly ash. The core component of the stoker combustor fly ash would be formed Al-, Ca- and Si-rich materials. However, the fly ash from a fluidized bed formed a Si-based insoluble core. Fly ash from both combustors contained Al/Ca/Si-based semi-soluble components. Fly ash from fluidized bed inclined to more Si-based semi-soluble component and stoker fly ash have more tendency to Ca-based semi-soluble components. On the surface of fly ash from both incinerators have random adsorption of soluble salts and Ca-based aggregates with aluminosilicate domains mainly observed on the surface of fly ash.

Besides heterogeneity analysis, possible metal speciation in the fluidized bed fly ash also investigated in this study. New possible heavy metals speciation was observed in all components of fly

ash. Dominant metal speciation and their bonding states with fly ash matrix are different in each fly ash particle. It suggested heterogeneity gives an impact on heavy metal speciation in the fly ash. Heavy metal speciation in the fly ash from a fluidized bed was detected mostly in the insoluble core. Metal oxides likely immobilize in the Al/Ca/Si-based matrix of fly ash. Heavy metal leachability might be controlled by not only metal oxide leachability but also the leachability of Al/Ca/Si-based matrix around metal oxides.

The impact on elemental heterogeneity in the elemental leachability is modeled by using geochemical simulation. In the individual-level, heterogeneity might give a slightly negligible effect on local pH, which can be affecting elemental solubility in the leaching of MSWI fly ash. Alkaline pH, after simulation in the range 11 – 13, in most of the groups might be due to dissolution CaO as the main factor of alkalinity in the fly ash. Moreover, elemental heterogeneity gives diverse solid-phase formation in the individual fly ash particle. Heavy metals that are detected by SEM-EDS are Fe and Ti. Those metals are precipitated into the solid phase, which has dispersed concentration. Elemental heterogeneity might have a negligible effect on heavy metal leachability and diverse formation on MSWI fly ash.

6.2 Recommendation

This present study observed heterogeneity characterization in the micro-scale level on MSWI fly ash particle, which can be considered in the comprehensive characteristic of fly ash. However, owing to limited samples of MSWI fly ash, this study might give specific results and conclusions. Although uncertainty owing to limited observations considered, this study concludes that fly ash has heterogeneous characteristics that should be considered in further research.

Proper and comprehensive characterization is needed for a more precise prediction of heavy metal leaching behavior. It is crucial for landfilling and/or utilizing MSWI fly ash in practice. Therefore, included heterogeneity in the characterization and/or one factor in the geochemical simulation for future research is better. Besides that, other characteristics, such as particle size, that there is a relation between particle size and leaching concentration, can be considered in further study. So, heterogeneity characterization could become more comprehensive. In this study, geochemical simulation focused on

major elements and primary heavy metals such as Fe and Ti leachability and solid-phase form after leaching. Further study can consider heterogeneity to predict other heavy metals such as Cr, Cu, Mn, and Zn leachability in the pH depending leaching model. Comprehensive heterogeneity characterization can lower the gap between geochemical simulation and experimental data.

Comparison between fluidized bed and stoker combustors where characteristics of waste combusted were assumes similar based on statistical analysis. Potentially non-negligible impact of waste difference should be taken into consideration. For future study, a comparison of MSWI fly ash from different combustors should be considered a similar waste stream and more samples to generalize the conclusion. Fly ash from fluidized bed incinerator more heterogeneous than stoker fly ash. Therefore, heavy metals in the fly ash from the fluidized bed not easily leached out than stokers. However, the amount of fluidized bed fly ash much higher than the stoker combustor.

In Chapter 4, heavy metal leachability might be controlled by the leachability of metal speciation and Al/Ca/Si-based matrix around metal speciation. Therefore, future treatment of MSWI fly ash based on aluminosilicate, which can give a negligible impact on heavy metal leachability. By using the geo-polymerization process, MSWI fly ash treatment into a geopolymer might be future treatment. Most studies of geopolymer using coal fly ash [1–3]. Some research has been investigated geopolymer from MSWI fly ash [4–6]. There is a potential utilization of MSWI fly ash by using the geo-polymerization process. Geopolymers can immobilize heavy metals by physical encapsulation and chemical bonding into their three-dimensional microstructure [7]. Therefore, it can develop more in the future to treat MSWI fly ash.

6.3 References

1. Sindhunata, Provis JL, Lukey GC, et al. (2008) Structural evolution of fly ash-based geopolymers in alkaline environments. Ind Eng Chem Res 47:2991–2999. https://doi.org/10.1021/ie0707671
2. Guo X, Huang J (2019) Effects of Cr3+, Cu2+, and Pb2+ on Fly Ash based Geopolymer. J Wuhan Univ Technol Mater Sci Ed 34:851–857. https://doi.org/10.1007/s11595-019-2128-5
3. Meftah M, Oueslati W, Chorfi N, Ben Haj Amara A (2016) Intrinsic parameters involved in the synthesis of metakaolin based geopolymer: Microstructure analysis. J Alloys Compd 688:946–956. https://doi.org/10.1016/j.jallcom.2016.07.297
4. Zhan X, Wang L, Hu C, et al. (2018) Co-disposal of MSWI fly ash and electrolytic manganese residue based on geopolymeric system. Waste Manag 82:62–70. https://doi.org/10.1016/j.wasman.2018.10.014
5. Jin M, Zheng Z, Sun Y, et al. (2016) Resistance of metakaolin-MSWI fly ash-based geopolymer to acid and alkaline environments. J Non-Cryst Solids 450:116–122. https://doi.org/10.1016/j.jnoncrysol.2016.07.036
6. Zheng L, Wang W, Shi Y (2010) The effects of alkaline dosage and Si/Al ratio on the immobilization of heavy metals in municipal solid waste incineration fly ash-based geopolymer. Chemosphere 79:665–671. https://doi.org/10.1016/j.chemosphere.2010.02.018
7. Vu TH, Gowripalan N (2018) Mechanisms of heavy metal immobilisation using geopolymerisation techniques – A review. J Adv Concr Technol 16:124–135. https://doi.org/10.3151/jact.16.124